Numerical solution of the sphaleron $\widehat{S}$ in $SU(3)$ Yang-Mills-Higgs theory

Zur Erlangung des akademischen Grades eines

DOKTORS DER NATURWISSENSCHAFTEN

von der Fakultät für Physik des
Karlsruher Instituts für Technologie (KIT)

genehmigte

DISSERTATION

von

Dipl.-Phys. Pascal Nagel
aus Siegen

Tag der mündlichen Prüfung: 21.07.2017

Referent: Prof. Dr. Frans R. Klinkhamer (Karlsruhe)
Korreferent: Prof. Dr. Yves Brihaye (Mons, Belgien)

Acknowledgements

First, I would like to thank my advisor Prof. F.R. Klinkhamer for giving me the opportunity to work on this fascinating topic. I am very grateful for all his contributions of time, ideas and funding, that have made this thesis possible. I would also like to express my gratitude to Prof. Y. Brihaye for assuming co-advisorship.

It has been a pleasure to have colleagues as the ones I've had at the ITP and TTP. In particular I would like to thank Drs. F. Loshaj, J. Diaz, R. Roth, V. Emelyanov, J. Queiruga, Y. Lu, C. Rahmede and S. Ertl, as well as S. Kast and C. Wiegand for always being open to questions and discussions.

Finally, my thanks goes to S. Kast for taking the time to proofread the draft.

Abstract

We solve numerically the reduced field equations of the sphaleron $\widehat{S}$ in $SU(3)$ Yang-Mills-Higgs theory with a single Higgs triplet and address some of the solution's properties. The energy barrier structure of the obtained configuration is of particular interest and motivates further research on the stability of the $\widehat{S}$. Furthermore, we solve the $\widehat{S}$ field equations in an extended $SU(3)$ Yang-Mills-Higgs theory with three Higgs triplets. This theory features a non-vanishing, equal mass for all eight gauge bosons and is intended to serve as a toy model of quantum chromodynamics, in which a mass scale arises from quantum effects (not from a fundamental scalar). The $\widehat{S}$ gauge fields are expected to contribute to the nonperturbative dynamics of quantum chromodynamics.

Zusammenfassung

In vorliegender Arbeit bestimmen wir die numerische Lösung der reduzierten Feldgleichungen des Sphalerons $\widehat{S}$ in der $SU(3)$ Yang-Mills-Higgs-Theorie mit einem aus einem einzigen Higgstriplett bestehenden Higgssektor und befassen uns mit den Eigenschaften dieser Lösung. Die gefundene, sphaleronuntypische Struktur der $\widehat{S}$-Energiebarriere stellt sich hierbei als besonders interessant heraus und gibt Anlass zur genaueren Untersuchung der Stabilität des $\widehat{S}$. Des Weiteren lösen wir die $\widehat{S}$-Feldgleichungen in einer auf drei Higgstripletts erweiterten $SU(3)$ Yang-Mills-Higgs-Theorie. Diese Theorie zeichnet sich durch acht identische Eichbosonmassen aus und soll auf gewisse Weise als effektives Modell der Quantenchromodynamik dienen, in welcher eine Massenskala dynamisch durch Quanteneffekte und nicht etwa durch ein fundamentales skalares Feld erzeugt wird. In dieser Theorie, mit ausschließlich massiven Eichbosonmoden, ändern sich fundamentale Eigenschaften des $\widehat{S}$. Wir beleuchten zudem phenomelogische Aspekte des Sphalerons $\widehat{S}$ und stellen die Vermutung an, dass die Eichfelder der $\widehat{S}$-Konfiguration maßgeblich zur nichtperturbativen Dynamik der Quantenchromodynamik beitragen.

Contents

CHAPTER 1

Introduction

The accuracy of predictions made from quantum chromodynamics (QCD) using perturbation theory is remarkable, yet we know comparatively little about crossing the bridge between theory and experiment in the nonperturbative regime of QCD. Solutions of classical field theory, most prominently the BPST instanton [1], have contributed significantly to our unstanding of nonperturbative QCD today [2].

The focus of this thesis is a solution of $SU(3)$ Yang-Mills-Higgs theory that has only recently been discovered, the sphaleron[1] $\widehat{S}$ [4]. It is well known, that the sphaleron S [3] (see also [5][6]) is closely linked to the Adler-Bell-Jackiw (triangle) anomaly [7][8]. In the electroweak sector of the Standard Model (an $SU(2)\times U(1)$ Yang-Mills-Higgs theory), this anomaly gives rise to $B+L$ nonconservation and may contribute to the baryon-antibaryon asymmetry we observe in the universe today. Similarly, the sphaleron S^* [9] is linked to the Witten anomaly [10]. Following this train of thought, the existence of the non-Abelian chiral gauge (Bardeen) anomaly [11] suggests the existence [12] of a new sphaleron, precicely the $\widehat{S}$ [4].

A question which may naturally arise at this point is: Why are we interested in $SU(3)$ Yang-Mills-Higgs theory, when we know that there is no fundamental scalar field in the QCD Lagrangian? Sphalerons do not exist in pure Yang-Mills theories. Unlike instantons, they do require a scale. They are by definition the top of a finite energy barrier [3]. At the same time, the existence of the QCD instanton entails the existence of a QCD sphaleron. In other words, if there is tunneling (described by the instanton) through an energy barrier, that barrier must also have a top (the sphaleron). It is also somewhat clear, that the energy scale that is required here originates from QCD quantum effects. The only question that remains is how do we introduce the scale, which originates from quantum effects, in a classical theory? In our case this is done by introducing a fundamental scalar field to the Lagrangian. In the course of this thesis we will discuss two of the many possible scalar sectors. The "basic" Yang-Mills-Higgs theory [4], with a single complex scalar triplet and the "extended" Yang-Mills-Higgs theory [13], with three triplets.

Sphalerons are a consequence of the non-trivial topology of the configuration space of fields

[1] Sphalerons are by definition static, unstable, finite-energy solutions of classical field equations [3].

[14]. Whenever two vacuum gauge-field configurations cannot be connected by a zero-energy path through configuration space, there exists a configuration (the sphaleron) on the path of minimal energy that has the largest energy. Accordingly, topological considerations aid with the construction of the sphaleron. More specifically, the sphaleron gauge and scalar field's boundary conditions at spatial infinity are linked to a map, which maps the smash product of the $\mathbb{S}^2_\infty$ at spatial infinity and an n-sphere in configuration space into the gauge group G, typically $SU(N)$. These maps can be classified into homotopy classes and will be discussed in detail in Chapter 2.

This thesis is structured as follows. In the remainder of Chapter 1 we introduce the two mentioned Yang-Mills-Higgs theories. Chapter 2 presents an explicit derivation and parametrization of generators of $\pi_n\left[SU(2)\right]$, which are not linked to the conducted analysis, but are relevant for the construction of so-called sphaleron-antisphaleron chains [15][16] [17] in $SU(2)$ Yang-Mills-Higgs theory. More importantly, this chapter features the map $\pi_5\left[SU(3)\right]$ [18] used for the construction of the $\widehat{S}$ and a novel parametrization thereof, which is important for the energy barrier analysis conducted in Chapter 7. In Chapter 3 we briefly address the $SU(2)$ sphaleron S and solve its reduced field equations. This serves to illustrate the general procedure of sphaleron construction and introduces the numerical methods used later on, using a relatively simple example. Chapter 4 outlines the employed numerical algorithms. Chapter 5 starts off the main analysis by recalling the $\widehat{S}$ *Ansatz* [4] in the basic $SU(3)$ Yang-Mills-Higgs theory, discussing the choice of gauge [19], solving the $\widehat{S}$ field equations analytically at the origin and finally applying two distinct numerical methods to obtain the $\widehat{S}$ field configuration. In Chapter 6 this analysis is more or less straightforwardly applied to the $\widehat{S}$ in the extended Yang-Mills-Higgs theory. Chapter 7 concerns itself with determining the energy of configurations on the non-contractible sphere (NCS), which connects the gauge-field vacuum with the $\widehat{S}$. This constitutes a first step in the stability analysis of the $\widehat{S}$. Finally, we present concluding remarks and propose future research in Chapter 8.

Appendix A gives the energy densities of the $\widehat{S}$ fields in radial gauge for the basic and extended Yang-Mills-Higgs theories. Appendix B features the reduced $\widehat{S}$ field equations, derived from the energy functionals of App. A by variation with respect to the profile functions of the *Ansatz*.

1.1 Basic $SU(N)$ Yang-Mills-Higgs theory

What we will refer to as basic $SU(N)$ Yang-Mills-Higgs theory[2], is a Yang-Mills-Higgs theory with a scalar sector comprised of a single complex doublet in the fundamental representation of the respective $SU(N)$. The classical action of $SU(N)$ Yang-Mills-Higgs theory is given by

$$S = \int_{\mathbb{R}^4} d^4x \left\{ \frac{1}{2}\mathrm{tr} F_{\mu\nu}F^{\mu\nu} + (D_\mu\Phi)^\dagger(D^\mu\Phi) - \lambda\left(\Phi^\dagger\Phi - \eta^2\right)^2 \right\} \tag{1.1}$$

with the $SU(N)$ Yang-Mills field strength tensor $F_{\mu\nu} = \partial_\mu A_\nu - \partial_\nu A_\mu + g[A_\mu, A_\nu]$, the covariant derivative $D_\mu = \partial_\mu + gA_\mu$ and the Yang-Mills gauge field $A_\mu(x) = A^a_\mu(x)\tau^a$, with SU(N) generators τ^a. In our case they are, for $SU(2)$, $\tau^a = \sigma^a/2i$, with the Pauli matrices

$$\sigma^1 = \begin{pmatrix} 0 & 1 \\ 1 & 0 \end{pmatrix}, \qquad \sigma^2 = \begin{pmatrix} 0 & -i \\ i & 0 \end{pmatrix}, \qquad \sigma^3 = \begin{pmatrix} 1 & 0 \\ 0 & -1 \end{pmatrix}, \tag{1.2}$$

[2]We also need to introduce $SU(2)$ Yang-Mills-Higgs theory for Chapter 3, hence we keep N in this section general.

and for $SU(3)$, $\tau^a = \lambda^a/2i$, with the Gell-Mann matrices

$$\lambda^1 = \begin{pmatrix} 0 & 1 & 0 \\ 1 & 0 & 0 \\ 0 & 0 & 0 \end{pmatrix}, \qquad \lambda^2 = \begin{pmatrix} 0 & -i & 0 \\ i & 0 & 0 \\ 0 & 0 & 0 \end{pmatrix}, \qquad \lambda^3 = \begin{pmatrix} 1 & 0 & 0 \\ 0 & -1 & 0 \\ 0 & 0 & 0 \end{pmatrix}, \tag{1.3}$$

$$\lambda^4 = \begin{pmatrix} 0 & 0 & 1 \\ 0 & 0 & 0 \\ 1 & 0 & 0 \end{pmatrix}, \qquad \lambda^5 = \begin{pmatrix} 0 & 0 & -i \\ 0 & 0 & 0 \\ i & 0 & 0 \end{pmatrix}, \qquad \lambda^6 = \begin{pmatrix} 0 & 0 & 0 \\ 0 & 0 & 1 \\ 0 & 1 & 0 \end{pmatrix},$$

$$\lambda^7 = \begin{pmatrix} 0 & 0 & 0 \\ 0 & 0 & -i \\ 0 & i & 0 \end{pmatrix}, \qquad \lambda^8 = \frac{1}{\sqrt{3}} \begin{pmatrix} 1 & 0 & 0 \\ 0 & 1 & 0 \\ 0 & 0 & -2 \end{pmatrix}.$$

As a result of the well-known "Mexican hat" shape of the scalar potential in the action (1.1), the scalar field acquires a vacuum expectation value. For our brief excursion to the sphaleron S of $SU(2)$ Yang-Mills-Higgs theory in Chapter 3, we take the scalar vacuum to be

$$\Phi = \begin{pmatrix} 0 \\ v/\sqrt{2} \end{pmatrix}, \tag{1.4}$$

giving mass to all three gauge fields and one scalar field mode. Turning to the $\widehat{S}$ and $SU(3)$ Yang-Mills-Higgs theory, we may choose the scalar vacuum field

$$\Phi = \begin{pmatrix} 0 \\ 0 \\ \eta \end{pmatrix}, \tag{1.5}$$

resulting in a mass for five of the gauge fields A^a_μ (for $a = 4, \ldots, 8$), leaving the remaining three massless. One of the scalar modes ($3 \times 2 - 5 = 1$) obtains a mass for $\lambda > 0$. Equivalent scalar vacua are obtained by multiplication with the following $SU(3)$ matrices

$$M_1 \equiv \begin{pmatrix} 1 & 0 & 0 \\ 0 & 0 & 1 \\ 0 & -1 & 0 \end{pmatrix}, \quad M_2 \equiv \begin{pmatrix} 0 & 0 & 1 \\ 0 & 1 & 0 \\ -1 & 0 & 0 \end{pmatrix}, \quad M_3 \equiv \begin{pmatrix} 0 & 1 & 0 \\ -1 & 0 & 0 \\ 0 & 0 & 1 \end{pmatrix}. \tag{1.6}$$

We will require all three of them for the $\widehat{S}$ *Ansatz* in the extended Yang-Mills-Higgs theory later on. For the basic theory, the following vacuum has been used [4]

$$\Phi = M_2 \cdot \begin{pmatrix} 0 \\ 0 \\ \eta \end{pmatrix} = \begin{pmatrix} \eta \\ 0 \\ 0 \end{pmatrix}. \tag{1.7}$$

Furthermore, we require the static bosonic energy of the action (1.1), given by

$$E[A,\Phi]=\int_{\mathbb{R}^3} d^3x\left\{-\frac{1}{2}\mathrm{tr}(F_{mn})^2+|D_m\Phi|^2+\lambda\left(|\Phi|^2-\frac{v^2}{2}\right)^2\right\}, \tag{1.8}$$

with spatial indices m and n running over $1,2,3$. For completeness, we also give the full Yang-Mills-Higgs field equations

$$\begin{aligned}[D_i,F_{ij}]&=g\left(\Phi^\dagger\tau^a\left(D_j\Phi\right)-\left(D_j\Phi\right)^\dagger\tau^a\Phi\right)\tau^a,\\ D_iD_i\Phi&=2\lambda\left(\Phi^\dagger\Phi-\frac{v^2}{2}\right)\Phi,\end{aligned} \tag{1.9}$$

which we intend to solve indirectly, by solving the reduced $\widehat{S}$ field equations.

1.2 Extended $SU(3)$ Yang-Mills-Higgs theory

The extended $SU(3)$ Yang-Mills-Higgs theory features an extension of the basic theory by two additional complex scalar triplets and their interactions. The classical action of the theory is given by

$$\begin{aligned}S &= \int_{\mathbb{R}^4} d^4x\left\{\frac{1}{2}\,\mathrm{tr}\,F_{\mu\nu}F^{\mu\nu}+\sum_{\alpha=1}^{3}\left[\left(D_\mu\Phi_\alpha\right)^\dagger\left(D^\mu\Phi_\alpha\right)-\lambda\left(\Phi_\alpha^\dagger\Phi_\alpha-\eta^2\right)^2\right]\right.\\ &\left.-\lambda\left(\Phi_1^\dagger\Phi_2\right)\left(\Phi_2^\dagger\Phi_1\right)-\lambda\left(\Phi_1^\dagger\Phi_3\right)\left(\Phi_3^\dagger\Phi_1\right)-\lambda\left(\Phi_2^\dagger\Phi_3\right)\left(\Phi_3^\dagger\Phi_2\right)\right\},\end{aligned} \tag{1.10}$$

with the three Higgs triplets Φ_α ($\alpha=1,2,3$). As indicated in the previous section, the scalar vacuum fields are chosen to be

$$\Phi_1=\begin{pmatrix}\eta\\0\\0\end{pmatrix},\quad \Phi_2=\begin{pmatrix}0\\\eta\\0\end{pmatrix},\quad \Phi_3=\begin{pmatrix}0\\0\\\eta\end{pmatrix}. \tag{1.11}$$

A nice feature of this particular scalar sector, is that all gauge fields acquire an equal mass, namely $m_A=g\eta$. Of the ten physical scalar modes nine aquire a mass for $\lambda>0$.

The energy functional of the extended Yang-Mills-Higgs theory is given by

$$\begin{aligned}E[A,\Phi] &= \int_{\mathbb{R}^3} d^3x\left\{-\frac{1}{2}\mathrm{tr}(F_{mn})^2+\sum_{\alpha=1}^{3}\left[|D_m\Phi_\alpha|^2+\lambda\left(\Phi_\alpha^\dagger\Phi_\alpha-\eta^2\right)^2\right]\right.\\ &\left.+\lambda\left(\Phi_1^\dagger\Phi_2\right)\left(\Phi_2^\dagger\Phi_1\right)+\lambda\left(\Phi_1^\dagger\Phi_3\right)\left(\Phi_3^\dagger\Phi_1\right)+\lambda\left(\Phi_2^\dagger\Phi_3\right)\left(\Phi_3^\dagger\Phi_2\right)\right\}.\end{aligned} \tag{1.12}$$

1.3 Notation and conventions

Finally, there are some notations and conventions we ought to fix. We will work in natural units $\hbar = c = 1$ and the form of the Minkowski space metric employed is $g_{\mu\nu}(x) = \text{diag}(+1, -1, -1, -1)$. Notationally, we use the convention of Latin letter indices starting from 1 and Greek letter indices running from 0 to 3, unless otherwise specified.

We will also commonly be using standard spherical coordinates r, θ and ϕ, as well as dimensionless and compactified radial coordinates $x \in [0, 1]$ for numerical analysis

$$x = \frac{\xi}{\chi + \xi} \,, \qquad \text{with} \;\; \xi = gvr. \tag{1.13}$$

CHAPTER 2

Topology

In this chapter we recall some of the topological considerations that are at the core of sphaleron construction. The derivation of the required maps is discussed in depth and explicit parametrizations are calculated and illustratively explained.

Finally, we iterate the construction method of [18] to obtain generators of $\pi_k[SU(2)]$ for $k > 4$ and identify them with the maps underlying the construction of a subset of sphaleron-antisphaleron chains [16].

2.1 Presentations of homotopy groups of unitary groups

Ever since the introduction of homotopy groups beyond the fundamental group [20] in 1932, homotopy groups have been of great interest in mathematics. They have found applications in physics, computer graphics and many other fields, as a tool for determining properties of topological spaces. Calculating homotopy groups however, is very challenging and so it was a tremendous advancement in the field, when in 1957 Raoul Bott found and proved a structure in the erratic landscape of homotopy groups. The Bott periodicity theorem [21] for homotopy groups of unitary groups states the isomorphisms

$$\pi_k[U(n)] = \pi_{k+2}[U(n)], \tag{2.1}$$

$$\pi_k[U(n)] = \pi_k[U(n+1)], \quad \text{for } k < 2n. \tag{2.2}$$

As a result of this, all of the so-called stable homotopy groups are isomorphic to either $\pi_1[U(1)] = \mathbb{Z}$ or $\pi_2[U(2)] = 0$. Unfortunately, the remaining unstable homotopy groups appear to bear no structure and must be determined, using for instance spectral sequences [22]. This has been done on a grand scale up to large values of k and n, especially for the groups $U(1)$ and $SU(2)$, as their homotopy groups are isomorphic to homotopy groups of spheres. A brief list of homotopy groups

of unitary groups [23] is given in Tab. 2.1.

	π_1	π_2	π_3	π_4	π_5	π_6	π_7
$U(1)$	$\mathbb{Z}$	0	0	0	0	0	0
$U(2)$	0	0	$\mathbb{Z}$	$\mathbb{Z}_2$	$\mathbb{Z}_2$	$\mathbb{Z}_{12}$	$\mathbb{Z}_2$
$U(3)$	0	0	$\mathbb{Z}$	0	$\mathbb{Z}$	$\mathbb{Z}_6$	0
$U(4)$	0	0	$\mathbb{Z}$	0	$\mathbb{Z}$	0	$\mathbb{Z}$

Table 2.1: Homotopy groups of unitary groups. Generators of these groups are required for the construction of the $SU(2)$ sphaleron S (red), the $SU(2)$ sphaleron S^* (blue) and the $SU(3)$ sphaleron $\widehat{S}$ (green).

However, there is a scarcity of (simple) presentations[1] of homotopy groups, i.e. explicit maps from k-spheres into e.g. n-spheres or U(n). Regrettably, these maps appear to be of little interest to most mathematicians. They are however of vital importance for applications such as ours, as they are the main ingredient in the construction of soliton and sphaleron gauge and Higgs fields.

In this section, we will compile known explicit generators of homotopy groups of the unitary groups of interest to us, from papers such as [18] and construct new maps to fill the gaps.

2.1.1 Stable homotopy groups

Following Ref. [18], we introduce the generators $\zeta_k : \mathbb{S}^{2k-1} \to U(2^{k-1})$ of groups $\pi_{2k-1}\left[U(2^{k-1})\right] = \mathbb{Z}$, linked by the Bott periodicity isomorphism (2.1). These can be obtained from the generator of $\pi_1\left[U(1)\right]$,

$$\zeta_1 : \mathbb{S}^1 \to U(1), \quad z_1 \to z_1, \tag{2.3}$$

by iteratively applying the following map

$$\begin{aligned}\zeta_{k+1} = B\left(\zeta_k\right) &= \begin{pmatrix} \mathbb{1} & 0 \\ 0 & \zeta_k(\hat{z}) \end{pmatrix} \begin{pmatrix} z_{k+1}\mathbb{1} & -|\vec{z}|\mathbb{1} \\ |\vec{z}|\mathbb{1} & \bar{z}_{k+1}\mathbb{1} \end{pmatrix} \begin{pmatrix} \mathbb{1} & 0 \\ 0 & \zeta_k^\dagger(\hat{z}) \end{pmatrix} \\ &= \begin{pmatrix} z_{k+1}\mathbb{1} & -|\vec{z}|\zeta_k^\dagger(\hat{z}) \\ |\vec{z}|\zeta_k(\hat{z}) & \bar{z}_{k+1}\mathbb{1} \end{pmatrix}. \end{aligned} \tag{2.4}$$

Here $\hat{z}$ denotes the complex-valued, k-dimensional unit vector $\frac{\vec{z}}{|\vec{z}|}$, composed of the $2k$ Cartesian coordinates[2], which parameterize the $\mathbb{S}^{2k-1}$ of the map ζ_k. The introduction of z_{k+1} extends $\hat{z}$ to parameterize the $\mathbb{S}^{2k+1}$ of ζ_{k+1}. For a detailed derivation of B, using two different approaches, the reader is referred to [24; 25] and [26], respectively.

[1] A group can be defined by a complete set of its generators and the relations among them. The combination of both is referred to as a presentation.

[2] As an example, a possible parametrization for $z_1 \in \mathbb{S}^1$ are the standard polar coordinates

$$\begin{pmatrix} x_1 \\ x_2 \end{pmatrix} = \begin{pmatrix} \cos\phi \\ \sin\phi \end{pmatrix}, \qquad z_1 = x_1 + ix_2 = e^{i\phi}.$$

We now iterate (2.4) to obtain the first elements of the sequence

$$\zeta_2 : \mathbb{S}^3 \to SU(2), \quad \begin{pmatrix} z_1 \\ z_2 \end{pmatrix} \to \begin{pmatrix} z_1 & -\bar{z}_2 \\ z_2 & \bar{z}_1 \end{pmatrix}, \tag{2.5}$$

$$\zeta_3 : \mathbb{S}^5 \to SU(4), \quad \begin{pmatrix} z_1 \\ z_2 \\ z_3 \end{pmatrix} \to \begin{pmatrix} z_1 & 0 & -\bar{z}_2 & -\bar{z}_3 \\ 0 & z_1 & z_3 & -z_2 \\ z_2 & -\bar{z}_3 & \bar{z}_1 & 0 \\ z_3 & \bar{z}_2 & 0 & \bar{z}_1 \end{pmatrix}, \tag{2.6}$$

with $\sum_k |z_k|^2 = 1$. This gives us the map ζ_2 required for the construction of the $SU(2)$ sphaleron S [3].

Going into the opposite direction, a generator of $\pi_5[SU(3)]$ can be obtained from the $\pi_5[SU(4)]$ generator (2.6), as shown in Ref. [18], by applying the deformation

$$\begin{pmatrix} A & b \\ c^\dagger & 0 \end{pmatrix} \to A - bc^\dagger, \qquad A \in \mathbb{C}^{3\times 3}, \quad b, c \in \mathbb{C}^3, \tag{2.7}$$

to map (2.6), yielding the map on which the $\widehat{S}$ is constructed

$$U : \mathbb{S}^5 \to SU(3), \quad \begin{pmatrix} z_1 \\ z_2 \\ z_3 \end{pmatrix} \to \begin{pmatrix} z_1^2 & z_1 z_2 - \bar{z}_3 & z_1 z_3 + \bar{z}_2 \\ z_1 z_2 + \bar{z}_3 & z_2^2 & z_2 z_3 - \bar{z}_1 \\ z_1 z_3 - \bar{z}_2 & z_2 z_3 + \bar{z}_1 & z_3^2 \end{pmatrix}. \tag{2.8}$$

A further reduction to a generator of $\pi_5[SU(2)]$ does not seem possible and so the $\widehat{S}$ appears to be non-existent in $SU(2)$ Yang-Mills-Higgs theory. We will also see later on, that $SU(2)$ is simply too small to generate the complex structure of the $\widehat{S}$ vector fields. Embedding the obtained map (2.8) into any $SU(N)$ for $N \geq 3$ is however possible and as a result the $\widehat{S}$ is expected to exist in the corresponding Yang-Mills-Higgs theories. Finding a good parametrization of the $\mathbb{S}^5$ of map (2.8) is a little tricky and will be addressed in Section 2.3.

2.1.2 Unstable homotopy groups

In addition to the few stable homotopy groups, there exist infinitely many non-trivial, unstable homotopy groups of each $SU(N)$. As we will see later in this section, the $SU(2)$ sphalerons corresponding to the unstable homotopy groups $\pi_k[SU(2)]$ ($k > 3$) are precisely the sphaleron-antisphaleron chains recently studied in detail by Kleihaus, Kunz and Leißner [16][3]. This identification gives additional topological support for the existence of a subset of these objects.

Our primary interest in the generators of these homotopy groups however lies in the fact, that they can also be embedded in larger unitary groups. For instance, the map which generates $\pi_5[SU(2)]$ can be embedded in $SU(3)$ to obtain a map $\mathbb{S}^5 \to SU(3)$. It would be interesting to

[3]The first object of this kind to be discovered and the only one with a name is the sphaleron S^* [9], which corresponds to the first unstable homotopy group of $SU(2)$.

compare the sphaleron corresponding to this map with the $\widehat{S}$, considering that they share the same homotopy class.

Following Ref. [18] once more, we start by constructing the generators of the first non-stable homotopy groups $\pi_{2n}\left[SU(n)\right] = \mathbb{Z}_{n!}$, i.e. of groups $\pi_4\left[SU(2)\right]$ and $\pi_6\left[SU(3)\right]$. This can be done by applying a map ϕ to a generator A of $\pi_{2n-1}\left[SU(n)\right]$

$$\phi : \left[0, \frac{2\pi}{n}\right] \times \mathbb{S}^{2n-1} \to SU(n), \quad \phi(t, A) = A \cdot \mathrm{diag}(e^{i(n-1)t}, e^{-it}, \ldots, e^{-it}) \cdot A^{-1}. \tag{2.9}$$

This expression can be simplified further, to make its application more feasible. Since global prefactors can be neglected, this can be done in the following way

$$\phi(t, A) = A \cdot e^{-it} \left(\mathbb{1} + \mathrm{diag}(e^{int} - 1, 0, \ldots, 0)\right) \cdot A^{-1} \tag{2.10}$$

$$= \mathbb{1} + (e^{-int} - 1) A \cdot \mathrm{diag}(1, 0, \ldots, 0) \cdot A^{-1}. \tag{2.11}$$

To now obtain a map $\phi : \mathbb{S}^{2n} \to SU(n)$ we apply the following inverse suspension

$$\left[0, \frac{2\pi}{n}\right] \times \mathbb{S}^{2n-1} \to \mathbb{S}^{2n}, \quad (t, \vec{z}) \to \left(\frac{tn}{\pi} - 1, \vec{z}\sqrt{1 - \left(\frac{tn}{\pi} - 1\right)^2}\right), \tag{2.12}$$

as well as the rational parametrization $\left(\frac{1+iy}{1-iy}\right)^2$ instead of the exponential parametrization $e^{i\pi y}$ of the complex unit circle, since trigonometric functions in the exponent are very inconvenient. The resulting map is

$$\mathbb{S}^{2n} \to SU(n), \quad (y, \vec{z}) \to \mathbb{1} - 2\frac{(1 - y^2)}{(1 - iy)^2} A \cdot \mathrm{diag}(1, 0, \ldots, 0) \cdot A^{\dagger}, \tag{2.13}$$

with the Cartesian coordinate $y = \frac{tn}{\pi} - 1$. For the special case of matrices A, whose first column is $\vec{z} \in \mathbb{S}^{2n-1}$, such as ζ_2, (2.13) simplifies to

$$\mathbb{S}^{2n} \to SU(n), \quad (y, z) \to \mathbb{1} - \frac{2}{(1 - iy)^2} z z^{\dagger}. \tag{2.14}$$

It has been proven in Ref. [27], that (2.14) in fact generates $\pi_{2n}\left[U(n)\right]$.

There appears to exist no publication with explicit forms of generators beyond $\pi_4\left[SU(2)\right]$ and so, we will attempt to construct them, simply by iterating over the map ϕ

$$\phi : [0, \pi] \times \mathbb{S}^m \to SU(2), \quad A_{m+1} = \phi(t, A_m) = A_m \cdot \mathrm{diag}(e^{it_{m+2}}, e^{-it_{m+2}}) \cdot A_m^{-1}, \tag{2.15}$$

for $m > 3$, starting with $A_3 = \zeta_2$, applying the inverse suspension (2.12) on every iteration. Employing the previously used simplifications we obtain the first elements of the sequence, A_4

being already given by (2.14),

$$A_5 = \mathbb{1} - 2\frac{(1-x_6^2)}{(1-ix_6)^2}\left(\mathbb{1} - \frac{2}{(1-ix_5)^2(1-x_6^2)}zz^\dagger\right)\begin{pmatrix}1&0\\0&0\end{pmatrix}\left(\mathbb{1} - \frac{2}{(1+ix_5)^2(1-x_6^2)}zz^\dagger\right) \tag{2.16}$$

and

$$\begin{aligned} A_6 = \mathbb{1} - a&\left[\left(\mathbb{1} - b\left(\mathbb{1} - czz^\dagger\right)\begin{pmatrix}1&0\\0&0\end{pmatrix}\left(\mathbb{1} - c^*zz^\dagger\right)\right)\right]\begin{pmatrix}1&0\\0&0\end{pmatrix} \\ &\times\left[\left(\mathbb{1} - b^*\left(\mathbb{1} - c^*zz^\dagger\right)\begin{pmatrix}1&0\\0&0\end{pmatrix}\left(\mathbb{1} - czz^\dagger\right)\right)\right], \end{aligned} \tag{2.17}$$

with

$$a = \frac{2(1-x_7^2)}{(1-ix_7)^2}, \quad b = \frac{2(1-x_6^2)}{(1-ix_6)^2}, \quad c = \frac{2}{(1-ix_5)^2(1-x_6^2)(1-x_7^2)}. \tag{2.18}$$

2.2 Parametrization of $\pi_n\left[SU(2)\right]$ generators

Now, we require an explicit and appropriate parametrization of the mapped n-spheres. For sphalerons in particular, the $\mathbb{S}^n$ is composed of the 2-sphere at spacial infinity, parametrized by $\theta \in [0,\pi]$ and $\phi \in [0,2\pi]$, and a $(n-2)$-sphere, via smash product[4]

$$\mathbb{S}^2_\infty \wedge \mathbb{S}^{n-2} \cong \mathbb{S}^n. \tag{2.19}$$

The angles of the $(n-2)$-sphere parametrize a subspace of configuration space, which by construction is the subspace, which connects topologically distinct vacua by a sphaleron transition.

The smash product at the core of such a parametrization requires the existence of two fixed points, i.e. fixing one of the $\mathbb{S}^2_\infty$ angles to a certain value must make the coordinate vector $\vec{x}$ independent of all $\mathbb{S}^{n-2}$ angles and fixing one of the $\mathbb{S}^{n-2}$ angles to a certain value must make the coordinate vector $\vec{x}$ independent of all $\mathbb{S}^2_\infty$ angles. Clearly, no matter how we identify the angles of standard spherical coordinates

[4]The smash product of two spaces X and Y is defined by the quotient of their product space with the one-point union of both spaces at fixed points x_0 and y_0: $X \wedge Y = (X \times Y)/(X \vee Y)$. A smash product of two spheres is homeomorphic to the sphere of their added dimensions: $\mathbb{S}^n \wedge \mathbb{S}^m \cong \mathbb{S}^{n+m}$.

$$
\begin{aligned}
x_1 &= \cos\phi_1, \\
x_2 &= \sin\phi_1 \cos\phi_2, \\
x_3 &= \sin\phi_1 \sin\phi_2 \cos\phi_3, \\
&\vdots \\
x_n &= \sin\phi_1 \ldots \sin\phi_{n-1} \cos\phi_n, \\
x_{n+1} &= \sin\phi_1 \ldots \sin\phi_{n-1} \sin\phi_n,
\end{aligned} \tag{2.20}
$$

with $\phi_1 \ldots \phi_{n-1} \in [0, \pi]$ and $\phi_n \in [0, 2\pi]$, describing a unit n-sphere in $(n+1)$-space in terms of $n-1$ polar and one azimuthal angle, there exists no such pair of fixed points. A way to construct a set of coordinates, which covers the n-sphere and displays such fixed points, is by rotating $\vec{x}$ of (2.20) using $SO(n+1)$ matrices and identifying the rotation angles with the ϕ_i in a specific manner. In practice we will see, that far smaller subgroups of $SO(n+1)$ are sufficient to arrive at such parameterizations.

Let us start with the $\mathbb{S}^3$ required for the sphaleron S, which is composed of the $\mathbb{S}^2_\infty$, parameterized by angles $\theta \in [0, \pi]$ and $\phi \in [0, 2\pi]$, and a loop, parameterized by $\mu \in [0, \pi]$. As demonstrated in Ref. [14], a feasible parameterization can be constructed by a single rotation R

$$
\vec{y} = R\vec{x} = \begin{pmatrix} \cos\alpha & -\sin\alpha & 0 & 0 \\ \sin\alpha & \cos\alpha & 0 & 0 \\ 0 & 0 & 1 & 0 \\ 0 & 0 & 0 & 1 \end{pmatrix} \begin{pmatrix} \cos\phi_1 \\ \sin\phi_1 \cos\phi_2 \\ \sin\phi_1 \sin\phi_2 \cos\phi_3 \\ \sin\phi_1 \sin\phi_2 \sin\phi_3 \end{pmatrix}. \tag{2.21}
$$

By choosing $\phi_1 = \mu$, $\phi_2 = \theta$ and $\phi_3 = \phi$, as well as $\alpha = -\mu$, we obtain

$$
\vec{y} = \begin{pmatrix} \cos\mu \sin\mu(\cos\theta - 1) \\ \cos^2\mu + \sin^2\mu \cos\theta \\ \sin\mu \sin\theta \cos\phi \\ \sin\mu \sin\theta \sin\phi \end{pmatrix}, \tag{2.22}
$$

which has the two coinciding fixed points

$$
\lim_{\theta\to 0} \vec{y} = \lim_{\mu\to 0} \vec{y} = (0, 1, 0, 0)^T. \tag{2.23}
$$

We may now arbitrarily assign the y_i to the real and imaginary parts of the complex coordinates

$$
z_1 = y_1 + iy_2, \quad z_2 = y_3 + iy_4, \tag{2.24}
$$

to arrive at the desired map

$$\zeta_2 = \begin{pmatrix} e^{i\mu}(i\cos\mu + \cos\theta\sin\mu) & -e^{-i\phi}\sin\mu\sin\theta \\ e^{i\phi}\sin\mu\sin\theta & e^{-i\mu}(\cos\theta\sin\mu - i\cos\mu) \end{pmatrix} \tag{2.25}$$

required for the construction of the Yang-Mills and Higgs fields of the sphaleron S.

For spheres of higher dimensions, we will employ a modified form of the $\mathbb{S}^5$ parameterization used in Ref. [4]

$$\vec{x} = \begin{pmatrix} 1 - \cos^2\frac{\theta}{2}(1-\cos\psi) \\ \cos\frac{\theta}{2}\sin\psi\cos\mu \\ \sin\frac{\theta}{2}\cos\frac{\theta}{2}(1-\cos\psi)\cos\phi \\ \sin\frac{\theta}{2}\cos\frac{\theta}{2}(1-\cos\psi)\sin\phi \\ \cos\frac{\theta}{2}\sin\psi\sin\mu\sin\alpha \\ \cos\frac{\theta}{2}\sin\psi\sin\mu\cos\alpha \end{pmatrix}. \tag{2.26}$$

This parameterization, with the fixed points

$$\lim_{\psi\to 0}\vec{x} = \lim_{\theta\to\pi}\vec{x} = (1,0,0,0,0,0)^T, \tag{2.27}$$

has the strongly simplifying property of being independent of all other NCS angles for $\psi = \pi$, which we will later see is the mid-point on the NCS between the topologically distinct vacua. From (2.26), due to this symmetry, we can now easily construct parameterizations for the $\mathbb{S}^4$

$$\vec{x} = \begin{pmatrix} 1 - \cos^2\frac{\theta}{2}(1-\cos\psi) \\ \cos\frac{\theta}{2}\sin\psi\cos\mu \\ \sin\frac{\theta}{2}\cos\frac{\theta}{2}(1-\cos\psi)\cos\phi \\ \sin\frac{\theta}{2}\cos\frac{\theta}{2}(1-\cos\psi)\sin\phi \\ \cos\frac{\theta}{2}\sin\psi\sin\mu \end{pmatrix}, \tag{2.28}$$

the $\mathbb{S}^6$

$$\vec{x} = \begin{pmatrix} 1 - \cos^2\frac{\theta}{2}(1-\cos\psi) \\ \cos\frac{\theta}{2}\sin\psi\cos\mu \\ \sin\frac{\theta}{2}\cos\frac{\theta}{2}(1-\cos\psi)\cos\phi \\ \sin\frac{\theta}{2}\cos\frac{\theta}{2}(1-\cos\psi)\sin\phi \\ \cos\frac{\theta}{2}\sin\psi\sin\mu\sin\alpha\cos\beta \\ \cos\frac{\theta}{2}\sin\psi\sin\mu\cos\alpha \\ \cos\frac{\theta}{2}\sin\psi\sin\mu\sin\alpha\sin\beta \end{pmatrix}, \tag{2.29}$$

and so on. We will not give the fully parametrized maps, obtained simply by plugging these parametrizations into the maps derived in Section 2.1.2, as they are far too extensive and there

is no additional insight to be gained from their explicit form. It is however interesting to take a look at the first few parameterized $SU(2)$ maps at the mid-way point ($\psi = \pi$)

$$\zeta_2\big|_{\psi=\pi} = \begin{pmatrix} -\cos\theta & e^{-i\phi}\sin\theta \\ e^{i\phi}\sin\theta & \cos\theta \end{pmatrix}, \tag{2.30}$$

$$A_4\big|_{\psi=\pi} = \begin{pmatrix} -\cos 2\theta & e^{-i\phi}\sin 2\theta \\ e^{i\phi}\sin 2\theta & \cos 2\theta \end{pmatrix}, \tag{2.31}$$

$$A_5\big|_{\psi=\pi} = \begin{pmatrix} -\cos 4\theta & e^{-i\phi}\sin 4\theta \\ e^{i\phi}\sin 4\theta & \cos 4\theta \end{pmatrix}, \tag{2.32}$$

$$A_6\big|_{\psi=\pi} = \begin{pmatrix} -\cos 8\theta & e^{-i\phi}\sin 8\theta \\ e^{i\phi}\sin 8\theta & \cos 8\theta \end{pmatrix}, \tag{2.33}$$

which appear to be part of a sequence. For $n \geq 3$ we conjecture this sequence to be

$$A_n\big|_{\psi=\pi} = \begin{pmatrix} -\cos\left(2^{n-3}\theta\right) & e^{-i\phi}\sin\left(2^{n-3}\theta\right) \\ e^{i\phi}\sin\left(2^{n-3}\theta\right) & \cos\left(2^{n-3}\theta\right) \end{pmatrix}, \tag{2.34}$$

and have explicitly verified this for $n \leq 8$.

We can now identify these maps with the sphaleron-antisphaleron chain maps [16], which have an arbitrary positive integer θ-pre-factor $m \in \mathbb{N}$

$$U = \begin{pmatrix} -\cos m\theta & e^{-i\phi}\sin m\theta \\ e^{i\phi}\sin m\theta & \cos m\theta \end{pmatrix}. \tag{2.35}$$

The interpretation of the objects obtained from these maps as sphaleron-antisphaleron chains is based on their Chern-Simons number [17]

$$N_{CS} = \frac{(1-(-1)^m)}{4}, \tag{2.36}$$

as well as their energy, energy density distribution and the number of $|\phi|^2$ nodes. These properties indicate, that a step-wise increase of m alternately adds a sphaleron S or an antisphaleron $\bar{S}$ to the configuration. This way we can give a further topological motivation for the existence of configurations consisting of two sphaleron-antisphaleron pairs (A_5), four sphaleron-antisphaleron pairs (A_6), and so on.

An alternative construction method of higher homotopy group generators of $SU(2)$ iterates the suspension map procedure featured in Ref. [28], which is how the generator of $\pi_4\left[SU(2)\right]$ used in the original S^* sphaleron paper [9] was constructed. Despite being much simpler, this method does not replace the former derivation, since it is not immediately clear from this method, that the obtained map is in fact a generator of $\pi_n\left[SU(2)\right]$. As before, we start off with the generator ζ_2 of $\pi_3\left[SU(2)\right]$ and apply the following suspension

$$\tilde{A}_4 = ie^{i\frac{\pi}{2}\sigma_3}\left(e^{i\nu\sigma_3}\zeta_2 e^{-i\nu\sigma_3}\right)\zeta_2^\dagger, \tag{2.37}$$

with the new angle $\nu \in [0, \pi]$, to obtain $\tilde{A}_4$, a generator of $\pi_4 SU(2)$. Since for the hedgehog structured map ζ_2 a unitary transformation is equivalent to a rotation, we could alternatively write the transformation generated by $e^{i\nu\sigma_3}$ by a rotation of the ζ_2 parameterization around the x_1-axis by -2ν.

To construct higher homotopy group generators, we can now simply repeat this procedure

$$\tilde{A}_{n+1} = ie^{i\frac{\pi}{2}\sigma_3}\left(e^{i\nu_{n+1}\sigma_3}\tilde{A}_n e^{-i\nu_{n+1}\sigma_3}\right)\tilde{A}_n^\dagger, \tag{2.38}$$

yielding generators of $\pi_{n+1}[SU(2)]$. Choosing the antipode ($\mu = \pi/2$, $\nu_i = \pi/2$) of the fixed point yields precisely the maps (2.34) from before. Better yet, we can easily prove our previous conjecture (2.34) for all n, using induction

$$\begin{aligned}
\tilde{A}_{n+1}\Big|_{\mu=\nu_i=\frac{\pi}{2}} &= ie^{i\pi\sigma_3}\tilde{A}_n e^{-i\frac{\pi}{2}\sigma_3}\tilde{A}_n^\dagger\Big|_{\mu=\nu_i=\frac{\pi}{2}} \\
&= i\begin{pmatrix} -1 & 0 \\ 0 & -1 \end{pmatrix}\begin{pmatrix} -\cos\left(2^{n-3}\theta\right) & e^{-i\phi}\sin\left(2^{n-3}\theta\right) \\ e^{i\phi}\sin\left(2^{n-3}\theta\right) & \cos\left(2^{n-3}\theta\right) \end{pmatrix}\begin{pmatrix} i & 0 \\ 0 & -i \end{pmatrix} \\
&\quad\times\begin{pmatrix} -\cos\left(2^{n-3}\theta\right) & e^{-i\phi}\sin\left(2^{n-3}\theta\right) \\ e^{i\phi}\sin\left(2^{n-3}\theta\right) & \cos\left(2^{n-3}\theta\right) \end{pmatrix} \\
&= \begin{pmatrix} -\cos\left(2^{(n+1)-3}\theta\right) & e^{-i\phi}\sin\left(2^{(n+1)-3}\theta\right) \\ e^{i\phi}\sin\left(2^{(n+1)-3}\theta\right) & \cos\left(2^{(n+1)-3}\theta\right) \end{pmatrix} \quad \blacksquare
\end{aligned} \tag{2.39}$$

2.3 Parametrization of the $\widehat{S}$ map

For the construction of the $\widehat{S}$, we use the following map

$$U : S^5 \to SU(3), \quad \begin{pmatrix} z_1 \\ z_2 \\ z_3 \end{pmatrix} \to \begin{pmatrix} z_1^2 & z_1 z_2 - \bar{z}_3 & z_1 z_3 + \bar{z}_2 \\ z_1 z_2 + \bar{z}_3 & z_2^2 & z_2 z_3 - \bar{z}_1 \\ z_1 z_3 - \bar{z}_2 & z_2 z_3 + \bar{z}_1 & z_3^2 \end{pmatrix}, \tag{2.40}$$

with $z_1, z_2, z_3 \in \mathbb{C}$, $|z_1|^2 + |z_2|^2 + |z_3|^2 = 1$, which was originally constructed in Ref. [18]. This is the same map used by Klinkhamer and Rupp in the original $\widehat{S}$ paper [4].

We will however not employ the parameterization used in Ref. [4]:

$$\begin{pmatrix} z_1 \\ z_2 \\ z_3 \end{pmatrix} = \begin{pmatrix} 1 - \cos^2\frac{\theta}{2}(1 - \cos\tilde{\psi}) + i\ \cos\frac{\theta}{2}\sin\tilde{\psi}\cos\tilde{\mu} \\ e^{i\phi}\sin\frac{\theta}{2}\cos\frac{\theta}{2}(1 - \cos\tilde{\psi}) \\ \cos\frac{\theta}{2}\sin\tilde{\psi}\sin\tilde{\mu}(\sin\tilde{\alpha} + i\cos\tilde{\alpha}) \end{pmatrix}, \tag{2.41}$$

with $\tilde{\psi}, \tilde{\mu}, \theta \in [0, \pi]$ and $\tilde{\alpha}, \phi \in [0, 2\pi]$, since we are not only interested in the configuration at the "top" of the NCS, i.e. the $\widehat{S}$ configuration, but also in the energy barrier structure.

Parameterization (2.41) is independent of the two NCS angles $\tilde{\mu}$ and $\tilde{\alpha}$ at the pole $\tilde{\psi} = \pi$ and as a consequence so is the map and ultimately the energy. Hence, two out of the three eigenvalues of the energy Hessian matrix at the "top" vanish. We wish to find a parametrization which allows us to construct three slices through the NCS, that are orthogonal at the poles, giving a much better insight into the energy barrier structure around the $\widehat{S}$. One such parameterization is obtained if we consider, that our non-contractible 3-sphere is homeomorphic to the smash product of three 1-spheres

$$S^3 \simeq S^1 \wedge S^1 \wedge S^1 \tag{2.42}$$

and rewrite our 3-sphere parameterization in terms of the three 1-sphere angles. In these coordinates, the smash product's necessary fixed point is now the only point on the sphere, which does not depend on all NCS angles and will correspond to the vacuum configuration. In total there will be fixed points for four out of the five 5-sphere angles, namely all three NCS angles ψ, μ and α, as well as the S^2_∞ angle θ.

In the following, we will combine the steps of constructing the 3-sphere parameterization in terms of the three 1-sphere angles and smashing it with the 2-sphere at spatial infinity into a single coordinate transformation. We start off with a standard $\mathbb{S}^5$ parameterization:

$$\begin{aligned}
x_1 &= \cos\mu, \\
x_2 &= \sin\mu\cos\psi, \\
x_3 &= \sin\mu\sin\psi\cos\alpha, \\
x_4 &= \sin\mu\sin\psi\sin\alpha\cos\theta, \\
x_5 &= \sin\mu\sin\psi\sin\alpha\sin\theta\cos\phi, \\
x_6 &= \sin\mu\sin\psi\sin\alpha\sin\theta\sin\phi,
\end{aligned} \tag{2.43}$$

with $\psi, \mu, \alpha, \theta \in [0, \pi]$ and $\phi \in [0, 2\pi]$. Now we rotate

$$\vec{x}' = R\vec{x}, \tag{2.44}$$

using a $SO(4)$ subgroup representation of $SO(6)$, which we write explicitly by decomposition into left- and right-isoclinic rotations

$$R = \begin{pmatrix} a & -b & -c & -d & 0 & 0 \\ b & a & -d & c & 0 & 0 \\ c & d & a & -b & 0 & 0 \\ d & -c & b & a & 0 & 0 \\ 0 & 0 & 0 & 0 & 1 & 0 \\ 0 & 0 & 0 & 0 & 0 & 1 \end{pmatrix} \begin{pmatrix} p & -q & -r & -s & 0 & 0 \\ q & p & s & -r & 0 & 0 \\ r & -s & p & q & 0 & 0 \\ s & r & -q & p & 0 & 0 \\ 0 & 0 & 0 & 0 & 1 & 0 \\ 0 & 0 & 0 & 0 & 0 & 1 \end{pmatrix}, \tag{2.45}$$

with $a^2 + b^2 + c^2 + d^2 = 1$ and $p^2 + q^2 + r^2 + s^2 = 1$. The parameterization of this rotation may

be taken as follows

$$\begin{aligned} a &= \cos\gamma_1, & p &= \cos\gamma_4, \\ b &= \sin\gamma_1\cos\gamma_2, & q &= \sin\gamma_4\cos\gamma_5, \\ c &= \sin\gamma_1\sin\gamma_2\cos\gamma_3, & r &= \sin\gamma_4\sin\gamma_5\cos\gamma_6, \\ d &= \sin\gamma_1\sin\gamma_2\sin\gamma_3, & s &= \sin\gamma_4\sin\gamma_5\sin\gamma_6. \end{aligned} \tag{2.46}$$

By making the choice $\gamma_1 = -\mu$, $\gamma_2 = \psi$, $\gamma_3 = \alpha$, $\gamma_4 = 0$, $\gamma_5 = \pi$ and $\gamma_6 = 0$, we obtain the following parameterization

$$\begin{aligned} x_1' &= \cos^2\mu + \sin^2\mu\left(\cos^2\psi + \sin^2\psi\left(\cos^2\alpha + \cos\theta\sin^2\alpha\right)\right), \\ x_2' &= \cos\alpha\left(1-\cos\theta\right)\sin\alpha\sin^2\mu\sin^2\psi, \\ x_3' &= \cos\psi\left(\cos\theta - 1\right)\sin\alpha\sin^2\mu\sin\psi, \\ x_4' &= \cos\mu\left(\cos\theta - 1\right)\sin\alpha\sin\mu\sin\psi, \\ x_5' &= \cos\phi\sin\alpha\sin\mu\sin\psi\sin\theta, \\ x_6' &= \sin\alpha\sin\mu\sin\psi\sin\phi\sin\theta \end{aligned} \tag{2.47}$$

and find the four desired fixed points

$$\lim_{\theta\to 0}\vec{x}' = \lim_{\mu\to 0}\vec{x}' = \lim_{\psi\to 0}\vec{x}' = \lim_{\alpha\to 0}\vec{x}' = (1,0,0,0,0,0)^T. \tag{2.48}$$

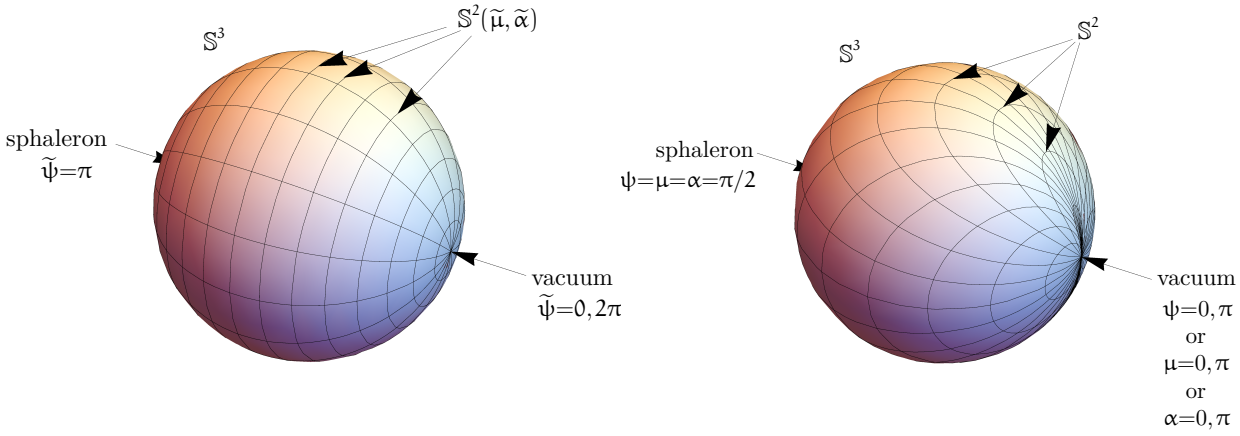

(a) Coordinates used by Klinkhamer and Rupp [4] and here given by Eq. (2.41).

(b) New coordinates given by Eq. (2.49).

Figure 2.1: Non-contractible 3-sphere coordinate choices, illustratively compared.

With the parameter ranges $\psi, \mu, \alpha, \theta \in [0, \pi]$ and $\phi \in [0, 2\pi]$ this parameterization covers the $\mathbb{S}^5$ exactly once. For each point on the NCS we obtain an unstable S^2_∞, which shrinks to a point (at the smash product fixed point) along either of the three NCS angles, as opposed to just along $\tilde{\psi}$ in (2.41). The "top", i.e. the point, where the S^2_∞ volume is largest, given by $\tilde{\psi} = \pi$ in the coordinates (2.41), is now at $\psi = \mu = \alpha = \pi/2$ in our new coordinates. Illustratively, what we have done here is pull together the poles of our S^3 to a single point, the smash product fixed point (see Fig. 2.1b).

Now we can choose the real and imaginary parts of the complex valued parameters z_i of map (2.40) arbitrarily from the set of unit vector elements x'_i

$$\begin{pmatrix} z_1 \\ z_2 \\ z_3 \end{pmatrix} = \begin{pmatrix} -x'_1 + ix'_2 \\ x'_5 + ix'_6 \\ x'_3 + ix'_4 \end{pmatrix} = \begin{pmatrix} -\cos^2\mu - \sin^2\mu\left(\cos^2\psi + e^{-i\alpha}\left(\cos\alpha + i\cos\theta\sin\alpha\right)\sin^2\psi\right) \\ e^{i\phi}\sin\alpha\sin\mu\sin\psi\sin\theta \\ \left(\cos\theta - 1\right)\sin\alpha\sin\mu\sin\psi\left(\cos\psi\sin\mu + i\cos\mu\right) \end{pmatrix}. \tag{2.49}$$

We chose this particular combination, since it yields precisely the $\widehat{S}$ map W of Ref. [4] for $\psi = \mu = \alpha = \pi/2$.

CHAPTER 3

$SU(2)$ sphaleron S

Now that we have introduced the required maps from coordinate space and configuration subspace into the group spaces $SU(2)$ and $SU(3)$, let us jump straight into a basic example, the $SU(2)$ sphaleron S. The $SU(2)$ solution was first found numerically by Dashen, Hasslacher and Neveu [5] and later by Boguta [29], but was ultimately rediscovered and given its physical interpretation and name by Klinkhamer and Manton [3]. We will discuss here the spherically symmetric S in pure $SU(2)$ Yang-Mills theory with a single Higgs doublet, i.e. the Weinberg-Salam model in the limit of vanishing weak mixing angle θ_w. It was shown in Refs. [3][30][31], that the sphaleron energy for physical values of θ_w only changes by a few percent.

3.1 *Ansatz*

The S-sphaleron *Ansatz* is constructed from a generator of $\pi_3\left[SU(2)\right]$. Demanding finite energy of the field configuration, we require the Yang-Mills field to be pure gauge at infinity

$$\lim_{r\to\infty} A_\mu(r,\theta,\phi) = \lim_{r\to\infty} A^a_\mu(r,\theta,\phi)\tau^a = -\frac{1}{g}\partial_\mu U(\theta,\phi)U^{-1}(\theta,\phi), \tag{3.1}$$

as well as the Higgs field to obtain its vacuum expectation value

$$\lim_{r\to\infty} \Phi(r,\theta,\phi) = \frac{v}{\sqrt{2}} U(\theta,\phi)\begin{pmatrix}0\\1\end{pmatrix} \tag{3.2}$$

there, with the weak coupling constant g, the Higgs vev $v/\sqrt{2}$ and U being the afore mentioned map at the critical point $\mu = \pi/2$:

$$U(\theta,\phi) = \zeta_2(\mu,\theta,\phi)\big|_{\mu=\pi/2} = \begin{pmatrix} -\cos\theta & \sin\theta e^{-i\phi} \\ \sin\theta e^{i\phi} & \cos\theta \end{pmatrix}. \tag{3.3}$$

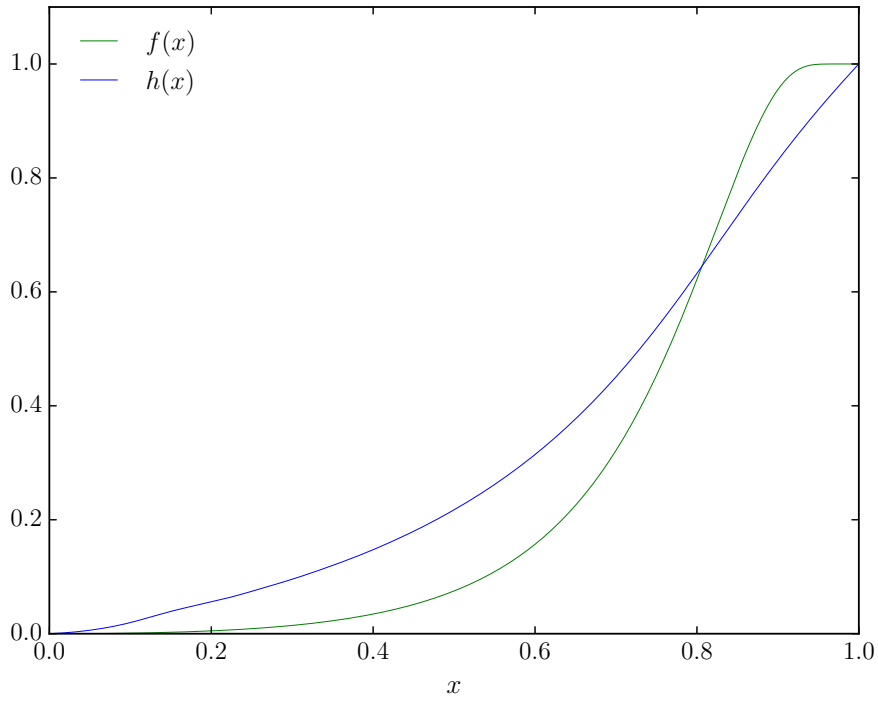

Figure 3.1: Numerical approximation of profile functions $f(x)$ and $h(x)$ of the sphaleron S for vanishing Higgs self-coupling ($\lambda = 0$) and electro-weak mixing angle ($\theta_w = 0$).

In contrast to all other sphalerons, there is a tremendously simplifying spherical symmetry present here. Clearly the field A_μ is not left unchanged after varying θ or ϕ, however the original field can be obtained from the rotated one by a unitary gauge transformation. Hence what we mean by spherical symmetry, is that the physical fields E and B are left invariant under rotations. As a result also the energy must be independent of θ and ϕ. Due to this, a simple radial *Ansatz* can be made for the gauge and Higgs fields

$$gA_\mu(r,\theta,\phi) = -f(r)\partial_\mu U(\theta,\phi)U^{-1}(\theta,\phi), \tag{3.4}$$

$$\phi(r,\theta,\phi) = h(r)\frac{v}{\sqrt{2}}U(\theta,\phi)\begin{pmatrix}0\\1\end{pmatrix}, \tag{3.5}$$

with boundary conditions

$$f(0) = h(0) = 0, \qquad \lim_{r\to\infty} f(r) = \lim_{r\to\infty} h(r) = 1, \tag{3.6}$$

as a necessary requirement for regularity and finite energy, respectively. With this, the static

energy (1.8) in compactified coordinates (1.13) becomes

$$E = 4\pi \int_0^1 dx \left\{ 4(x-1)^2 f'^2 + \frac{8}{x^2}(f(1-f))^2 + \frac{1}{2}x^2 h'^2 \right. \\ \left. + \frac{1}{(x-1)^2}(h(1-f))^2 + \frac{\lambda}{4}\frac{x^2}{(x-1)^4}(h^2-1)^2 \right\}. \tag{3.7}$$

3.2 Numerical solution

Minimizing the energy over profile functions $f(x)$ and $h(x)$ for $\lambda = 0$, using the numerical methods described later on, yields a good approximation of the field equation's solution. The obtained profile functions, given in Fig. 3.1, match the established results [3] well. The corresponding energy is

$$E_S = 1.520244 \pm 0.000010 \left[\frac{4\pi v}{g}\right], \tag{3.8}$$

where the numerical error has been approximated by considering the rate of convergence for varying grid sizes in x, as well as increasing orders in the orthogonal function expansion. The details of this procedure are given in the following chapters. The numerical approximation here was obtained using a mesh of 50000 grid points in x and Legendre polynomials up to order 90. The possibility of a non-global minimum can never be ruled out entirely, however identical results have been obtained for other sets of initial values. The numerical value of $E_S = 1.52$ $[4\pi v/g]$ is given in the original paper [3].

CHAPTER 4

Numerical methods

We wish to determine the $\widehat{S}$ Yang-Mills and Higgs fields, the corresponding energy and the energy barrier structure. Since no sphaleron has analytically solvable reduced field equations, we must turn to numerical methods. As has been previously remarked in Section 3, our problem of finding solutions to the field equations can be formulated in two ways: Either as an *optimization* problem, where one attempts to find the minimum of the action or as a set of coupled differential equations (ODEs or PDEs), the *equations of motion*, obtained from the action through variational methods, i.e. the Euler-Lagrange equations

$$\frac{\partial \mathcal{L}(\phi, \partial\phi/\partial x^i_\mu)}{\partial \phi} - \sum_i \frac{\partial}{\partial x^i_\mu} \frac{\partial \mathcal{L}(\phi, \partial\phi/\partial x^i_\mu)}{\partial \left(\partial\phi/\partial x^i_\mu\right)} = 0. \tag{4.1}$$

This chapter features a basic introduction to some well established numerical methods, commonly used to tackle both classes of problems, as well as our particular approach.

4.1 Optimization

Optimization algorithms are designed to find the local or global optimum of a scalar objective function of one or multiple variables $f(x_1, \ldots, x_n)$. The problem at hand however requires us to minimize a functional, a scalar function of multiple profile functions, which in many cases depend on multiple variables themselves.
We could naively approach this by discretizing the profile functions and rewriting the functional as a function of all grid point values as variables. However, this is not a good choice for several reasons. First, this approach leads to a highly non-convex function of a vast amount of variables, easily of the order 10^5. Finding the global minimum or even a decent approximation of it within reasonable computation times seems entirely unfeasible. Second, most importantly, we would need to employ some sort of additional constraints to ensure the profile functions' continuity.
To get a handle on this, we choose a semi-analytical approach, which has been shown to be

effective [19][32][33]. This approach expands the profile functions in nested orthogonal functions (Legendre polynomials) and uses the expansion coefficients as variables. An explicit example of this is shown in the following chapter.

Despite the seeming elegance of this approach, we will still have to minimize a function over several hundred, in some cases more than a thousand parameters. To do so we first employ Simulated Annealing (SA), a randomized global minimizer, to give us the best possible set of initial values (within feasible run-time) for our second step, in which we apply a quadratically convergent local minimizer based on the Sequential Least-Squares Quadratic Programming (SLSQP) method. Both algorithms are outlined in Sections 4.1.1 and 4.1.2, respectively.

4.1.1 Global Minimization with Simulated Annealing

Simulated annealing (SA) [34] is a randomized optimization algorithm, commonly used to approximate solutions of global optimization problems in high-dimensional parameter spaces. A popular problem of this kind is that of the traveling salesman, who would like to take the optimal route (by length) connecting all of his destinations on a given day. Solving this problem for just 50 destinations combinatorially would take even the fastest computer more than the salesman's lifetime to solve. Using SA however, a route very close to the optimal one can be found almost instantaneously.

The algorithm begins by evaluating the function value $f(\vec{x})$ of the set of passed initial values $\vec{x}$. It then randomly generates $\vec{x}_{\text{prop}}$ in the proximity of $\vec{x}$ and evaluates the corresponding function value $f(\vec{x}_{\text{prop}})$. If the new function value is below the previous one ($f(\vec{x}_{\text{prop}}) < f(\vec{x})$), $\vec{x}$ is replaced by $\vec{x}_{\text{prop}}$, in other words the proposed step is accepted and a new proposal is generated. The unique characteristic of SA is that it also accepts some steps which increase the function value, based on the Metropolis criterion [35]:

$$p_{\text{accept}} = \exp\left(-\frac{f(x_{\text{prop}}) - f(x)}{T}\right), \tag{4.2}$$

with the "temperature" T (by analogy with the annealing of solids), which controls the rate of acceptance.

The procedure of generating a new proposal and then accepting or declining it is repeated N_S times for a given initial temperature. Subsequently the temperature is lowered, decreasing the likelihood of acceptance, and another N_S iterations are made. The temperature is lowered a total of N_T times, until the rate of acceptance (or the step size) becomes negligibly small and the algorithm converges. How the temperature is lowered after each set of N_S iterations may be freely chosen, however we have found the so-called exponential cooling schedule, i.e. the multiplication of the temperature T with a constant factor[1] $\chi \in (0, 1)$ after each set of N_S iterations, to be most effective. It is this schedule which most closely resembles the natural cooling of a solid.

Finally, we must decide on a step length, i.e. how close the proposal $\vec{x}_{\text{prop}}$ should be to $\vec{x}$ on average. This parameter is fixed dynamically to maintain a fixed ratio of accepted steps over total steps, ideally $r \sim 0.5$. This is an improvement upon the basic SA algorithm, however it is vital for its efficiency. In practice, whenever the step ratio r falls below l or rises above u the following

[1] We have tried out different values of χ and found $\chi = 0.85$ to work well.

adjustments are made:

$$\begin{aligned} r &\to r\left(1 + c\,\frac{r-u}{l}\right) && \text{if } r > u, \\ r &\to r\left(1 - c\,\frac{r-l}{l}\right)^{-1} && \text{if } r < l, \end{aligned} \tag{4.3}$$

with a fixed parameter[2] $c \in \mathbb{R}^+$.

4.1.2 Local Minimization with SLSQP

Sequential Least-Squares Quadratic Programming (SLSQP) is a gradient-based, non-linearly constrained local minimizer, first devised and implemented by Dieter Kraft [36].
If we don't focus on its ability to handle constraints for now, the algorithm is essentially a Broyden-Fletcher-Goldfarb-Shanno (BFGS) algorithm [37][38][39][40], which optimizes second-order objective function approximations. So let us outline the BFGS algorithm.

The BFGS algorithm iteratively improves a set of variables $\vec{x}$ to find the optimum of a given nonlinear optimization problem. There are two important values required for each iteration i, the search direction $\vec{p}_i$ and the step-size α_i, in order to make a parameter update

$$\vec{x}_{i+1} = \vec{x}_i + \alpha_i \vec{p}_i. \tag{4.4}$$

For the commonly known Newton method the correction factor $\vec{s}_i = \alpha_i \vec{p}_i$ is simply

$$H^{-1}(\vec{x}_i)\nabla f(\vec{x}_i), \tag{4.5}$$

with the Hessian H of the objective function f. Similarly to the quasi-Newton method, the BFGS algorithm uses an approximated Hessian B_i, which is updated on each iteration

$$B_{i+1} = B_i + U_i + V_i = B_i + \frac{\vec{y}_i \vec{y}_i^T}{\vec{y}_i^T \vec{s}_i} - \frac{B_i \vec{s}_i \vec{s}_i^T B_i}{\vec{s}_i^T B_i \vec{s}_i}, \tag{4.6}$$

with $\vec{y}_i = \nabla f\left(\vec{x}_{i+1}\right) - f\left(\vec{x}_i\right)$.
The search direction $\vec{p}_i$ is determined upon each iteration by solving the equation

$$B_i \vec{p}_i = -\nabla f\left(\vec{x}_i\right), \tag{4.7}$$

for example by LU decomposition. A feasible step-size α_i is then found by doing a line search in the determined direction and a parameter update is made.

The constraints, which can be either equalities or inequalities are then simply combined with Karush-Kuhn-Tucker multipliers and added to the objective function. We used here the SLSQP implementation of the Python library SciPy [41].

[2] Choosing $c = 2.0$ worked well for our applications.

4.2 Collocation

The method we have found to best solve the coupled ODE boundary value problems, that are the reduced field equations[3], is the collocation method[4]. We will here sketch the algorithm behind this remarkably stable boundary-value solver.

The idea behind solving a system of N coupled ODEs is to approximate the involved functions with orthogonal polynomials of order M and solving the obtained equations at M points between the boundaries, the so called collocation points. From inserting the polynomials of degree M and writing down each ODE for each collocation point, we obtain a system of $N \times M$ non-linear equations of the expansion coefficients. The boundary conditions are easily fixed in this method, simply by fixing two expansion coefficients of each function. One can now attempt to simultaneously minimize the residual of each equation. The implementation we use, MATLABs BVP4C, does this using the Levenberg-Marquardt algorithm [43]. The grid size (= expansion order) is gradually increased, until the residual falls below the desired error tolerance.

Non-convergence can of course occur, if the residual sum as a function of the expansion coefficients is fluctuating too wildly and one gets stuck in a local minimum. In such cases the use of a stochastic based global minimization method could perhaps be the solution. In our case however, this was not necessary and the algorithm converged nicely for a wide range of randomly chosen initial values. The two methods outlined in this Chapter are meant to check each other, hence it is crucial, that they can reach convergence without using the results of the other as initial values.

[3] In case of the PDE field equations we encounter later on, we will use the method of lines [42] (MOL) to reduce the PDE system to a larger ODE system.

[4] Since our ODEs are volatile towards the boundaries, methods such as the shooting method are not of much use here.

CHAPTER 5

$\widehat{S}$ in the basic $SU(3)$ Yang-Mills-Higgs theory

As for the sphaleron S, we demand finite energy of the field configuration and hence pure gauge for the Yang-Mills field at infinity

$$\lim_{r\to\infty} A_\mu(r,\theta,\phi) = \lim_{r\to\infty} A^a_\mu(r,\theta,\phi)\tau^a = -\frac{1}{g}\partial_\mu W(\theta,\phi)W^{-1}(\theta,\phi), \tag{5.1}$$

and a Higgs field, which obtains its vacuum expectation value there

$$\lim_{r\to\infty} \Phi(r,\theta,\phi) = \frac{v}{\sqrt{2}} W(\theta,\phi) \begin{pmatrix} 1 \\ 0 \\ 0 \end{pmatrix}, \tag{5.2}$$

with the strong coupling constant g, the Higgs vacuum expectation value

$$\eta \equiv \frac{v}{\sqrt{2}} \tag{5.3}$$

and $W(\theta,\phi)$ being the map $U(\psi,\mu,\alpha,\theta,\phi)$ given by Eq. (2.40) with our new parameterization (2.49) at the critical point $\psi = \mu = \alpha = \pi/2$:

$$W(\theta,\phi) = \begin{pmatrix} \cos^2\theta & -\cos\theta\sin\theta\ e^{i\phi} & \sin\theta\ e^{-i\phi} \\ -\cos\theta\sin\theta\ e^{i\phi} & \sin^2\theta\ e^{2i\phi} & \cos\theta \\ -\sin\theta\ e^{-i\phi} & -\cos\theta & 0 \end{pmatrix}. \tag{5.4}$$

The map W is equivalent to the map of the same notation in Ref. [4].

Unlike the sphaleron S however, the Yang-Mills and Higgs fields are not spherically symmetric (up to a gauge transformation, as discussed for the sphaleron S) and as a result a radial *Ansatz* does not solve the equations of motion consistently. Nevertheless, the energy obtained from such an *Ansatz* is easily minimized and gives a solid upper bound for the $\widehat{S}$ energy.

5.1 Spherically symmetric approximation

Following Ref. [4] the Yang-Mills and Higgs fields are defined as follows:

$$gA_\mu(r,\theta,\phi) = -f(r)\partial_\mu W(\theta,\phi)W^{-1}(\theta,\phi), \tag{5.5}$$

$$\phi(r,\theta,\phi) = h(r)\frac{v}{\sqrt{2}}W(\theta,\phi)\begin{pmatrix}1\\0\\0\end{pmatrix}, \tag{5.6}$$

with boundary conditions

$$f(0) = h(0) = 0, \qquad \lim_{r\to\infty} f(r) = \lim_{r\to\infty} h(r) = 1. \tag{5.7}$$

To introduce the reader to the way the numerical methods outlined in Chapter 4 are applied to approximate solutions throughout this thesis, including more complex *Ansätze* later on, we will go into some detail here.[1]

The first of the two methods discussed in Chapter 4 is the direct minimization of the energy functional (using the compactified, dimensionless coordinate x, given by Eq. (1.13))

$$\begin{aligned} E = 4\pi\int_0^1 dx\Big\{&\frac{28}{3}(x-1)^2 f'^2 + \frac{80}{3x^2}\left(f(1-f)\right)^2 + \frac{1}{2}x^2 h'^2 \\ &+\frac{4}{3}\frac{1}{(x-1)^2}\left(h(1-f)\right)^2 + \frac{\lambda}{4g^2}\frac{x^2}{(x-1)^4}(h^2-1)^2\Big\} \end{aligned} \tag{5.8}$$

over the two profile functions $f(x)$ and $h(x)$. This is done by making an expansion of both profile functions in orthogonal functions, in our case Legendre polynomials $P_m(x)$:

$$f(x) = \sum_{m=0}^{M} a_m P_m(x) \tag{5.9}$$

$$h(x) = \sum_{m=0}^{M} b_m P_m(x) \tag{5.10}$$

and consequently approximating the energy functional with an energy function of the expansion coefficients a_m and b_m. The profile function derivatives can conveniently be evaluated analytically,

[1] The same methods were used to determine the profile functions and energy of the sphaleron S in Chapter 3.

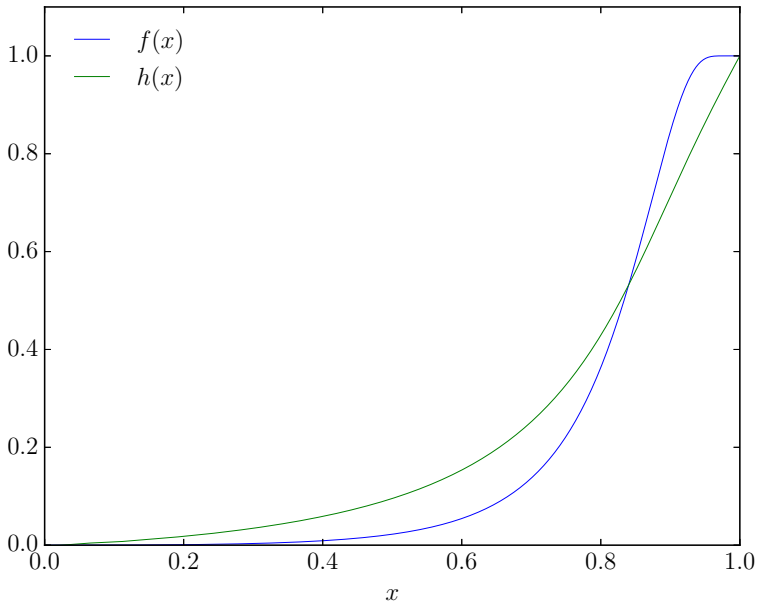

Figure 5.1: Numerical approximation of profile functions $f(x)$ and $h(x)$ of the $\widehat{S}$ configuration with vanishing Higgs self-coupling ($\lambda = 0$) in the approximate radial *Ansatz*

using standard Legendre polynomial relations.

The profile function boundary conditions at the origin and towards infinity are enforced by adjusting the first and third respective expansion coefficients a_0, b_0, a_2 and b_2 on each energy evaluation, to satisfy

$$\sum_{m=0}^{M} a_m = 1, \qquad \sum_{m=0}^{M} b_m = 1, \qquad \sum_{m=0}^{M} a_m P_m(0) = 0, \qquad \sum_{m=0}^{M} b_m P_m(0) = 0. \tag{5.11}$$

The integration over the radial coordinate $x \in [0, 1]$ is done, using the composite Simpson's rule over a mesh, given by the nodes of a Chebyshev polynomial of degree 5000, i.e. 5000 grid points[2]. Considering, that in this case, the number of grid points far exceeds the degree M of the approximating polynomial, Runge's phenomenon [44] is barely existent and we could just as well use an equidistant grid. In the context of solving more complex *Ansätze* later on, we will however encounter significantly higher evaluation times of the energy density, forcing us to reduce the grid size. Employing Chebyshev node grid spacing, when solving these problems, reduces the computational power required to reach the desired error bounds by a fair amount.

We now minimize the present energy function over $2M = 176$ expansion coefficients, for $\chi = 1$ and $\lambda/g^2 = 0$. Our first step is to apply Simulated Annealing, to obtain a good set of initial values for the local minimizer. This has been done using $N_S = 2000$ steps per temperature and

[2]The Chebyshev nodes are clustered in the proximity of the boundaries and have been shown to minimize polynomial fitting errors caused by Runge's phenomenon.

the following exponential cooling schedule and parameters

Initial temperature:	2.0
Final temperature:	1.0×10^{-8}
Temperature reduction factor (χ):	0.85
Lower step ratio boundary (l):	0.47
Upper step ratio boundary (u):	0.53
Number of steps before step size adjustment:	10
Step size adjustment factor (c):	2.0

Details regarding the SA parameters will be omitted in the following, as they are not changed. They have been determined by trial and error and appear to work well enough for all present problems. The only parameter, that is changed is N_S, in order to maintain reasonable run times for growing evaluation times of the energy.

The obtained coefficients a_m and b_m are then used as initial values for the SLSQP based local solver, which converges to the set of coefficients corresponding to the profile functions shown in Fig. 5.1. The corresponding energy, which has been obtained from the coefficients a_m and b_m by integration of the energy density over a grid of size 50000 is

$$E_{\widehat{S}_{approx}} = 2.596341 \pm 0.000010 \left[\frac{4\pi v}{g}\right] = (1.707845 \pm 0.000018) E_S, \tag{5.12}$$

where the error has been approximated conservatively through variation of mesh size and orthogonal expansion order M. Since the methods of error estimation remain largely unchanged for all problems of this type, let us go into a bit more detail:
Fig. 5.2 shows the absolute energy difference between the best (lowest) obtained value (5.12) and those obtained for varying mesh size and orthogonal expansion order M

$$\Delta E = \left\| E(\text{mesh size}, M) - E_{\widehat{S}_{approx}} \right\| \left[\frac{4\pi v}{g}\right]. \tag{5.13}$$

by evaluating the energy from the obtained expansion coefficients using a far larger grid (50000 equidistant points) post-minimization, to ensure the integration error is negligible. All tolerances, e.g. of the SLSQP termination, have been set far below the presented errors.

As in most complex numerical problems, we can of course not provide any kind of rigorous proof of convergence, however, we can observe an exponential error decay along both axes up to the 10^{-5} scale, at which other sources of uncertainty come into play. Since reducing the grid size used to obtain our best result by a factor of 10 and halving the radial expansion order M still leaves us well inside the 10^{-5} error contour, we have chosen this as a conservative upper error bound for (5.12). Fig. 5.2 also serves nicely to demonstrate the dramatic error increase in the "overfitting region" (bottom right corner) and how effectively the choice of a Chebyshev node grid reduces such effects.

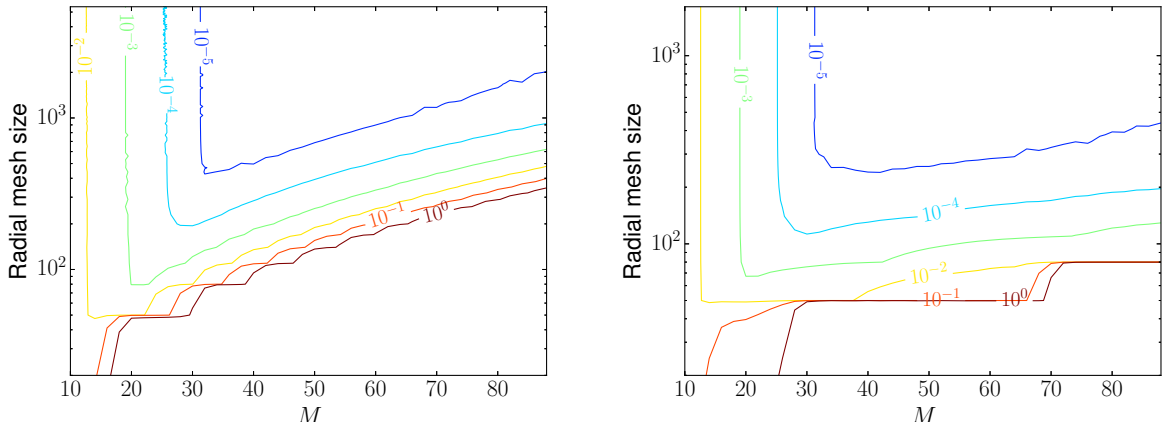

(a) Equidistant grid (b) Chebyshev node grid

Figure 5.2: Presented here is $\Delta E\left[\frac{4\pi v}{g}\right]$ as defined by Eq. (5.13) for varying radial expansion order M and grid size, for two different choices of grid spacing.

The second method outlined in Chapter 4 consists of solving the reduced field equations, obtained from the action by applying the Euler-Lagrange equations. Varying with respect to both profile functions, we obtain the following set of coupled, second order ODEs

$$\begin{aligned} 7(x-1)x^2(2f'+(x-1)f'') &= (f-1)\left(20(2f-1)f+\frac{x^2h^2}{(x-1)^2}\right), \\ (x-1)^2x(2h'+xh'') &= \frac{8}{3}(f-1)^2h+x^2\frac{\lambda}{g^2}\frac{h^2-1}{(x-1)^2}h. \end{aligned} \tag{5.14}$$

To get them into the required form for the collocation based BVP4C ODE solver, we define

$$\begin{aligned} f_a(x) &= f(x), \qquad & h_a(x) &= h(x), \\ f_b(x) &= f'(x), \qquad & h_b(x) &= h'(x) \end{aligned} \tag{5.15}$$

and obtain a system of four first order ODEs, for $\vec{y}=(f_a(x),f_b(x),h_a(x),h_b(x))^T$, with boundary conditions $f_a(0)=0$, $f_a(1)=1$, $h_a(0)=0$ and $h_a(1)=1$, which we then solve to obtain the form

$$\vec{y}'(x)=\vec{f}(\vec{y},x), \tag{5.16}$$

the right hand side of which is then passed to the solver.

Since the present ODEs are singular at both boundaries and to a high degree towards $x=1$, any ODE solver, even the highly robust collocation based one used here, becomes numerically unstable when approaching either boundary. This is the case here below $x=0.0001$ and above $x=0.995$. As a result we are forced to solve the boundary value problem in the range $x\in[0.0001,0.995]$ and redefine both boundary conditions. Potentially this can lead to rather poor

results, which we will see later on. Here however this approximation only results in a small error ($< 1\%$), as the profile functions both converge rather quickly towards infinity (which is not given for all higher order profile functions, as we will see in the following). The magnitude of the error can be roughly assessed by varying both bounds slightly[3].

Profile functions obtained in this fashion are barely distinguishable from those presented in Fig. 5.1. The corresponding energy

$$E_{\widehat{S}_{\text{approx}}} = (2.6188 \pm 0.0358) \left[\frac{4\pi v}{g}\right] = (1.7226 \pm 0.0235)\, E_S, \tag{5.17}$$

with E_S from (3.8), deviates slightly upwards from (5.12), but agrees well within the errors. Due to the instability at the boundaries, achieving an accuracy comparable to the minimization method is not possible and so this method serves more as a cross-check and less as a tool to obtain high precision energy values and configurations.

5.2 *Ansatz*

We will now introduce an *Ansatz* for the $\widehat{S}$ Yang-Mills and Higgs fields, as was done in Ref. [4], which is general enough to consistently solve the field equations. Fortunately, the map $W(\theta, \phi)$ has some simplifying symmetries, which strongly constrain the *Ansatz*, starting with

$$\partial_\phi W + \frac{i}{2}\left(\lambda_3 - \sqrt{3}\lambda_8\right) W + \frac{i}{2} W \left(\lambda_3 - \sqrt{3}\lambda_8\right) = 0. \tag{5.18}$$

As can be seen from (5.18) the $\widehat{S}$ fields are axially symmetric, i.e. a rotation around the z-axis can be compensated by a gauge transformation and hence all physical quantities (e.g. the energy) are invariant under this rotation.
Consequently, we can find a basis such as $\{T_\phi, T_\rho, V_\phi, V_\rho, U_\phi, U_\rho, \lambda_3/(2i), \lambda_8/(2i)\}$, with matrices

$$\begin{aligned}
T_\phi &= \sin\phi\frac{\lambda_1}{2i} + \cos\phi\frac{\lambda_2}{2i}, & T_\rho &= \cos\phi\frac{\lambda_1}{2i} - \sin\phi\frac{\lambda_2}{2i},\\
V_\phi &= -\sin\phi\frac{\lambda_4}{2i} + \cos\phi\frac{\lambda_5}{2i}, & V_\rho &= \cos\phi\frac{\lambda_4}{2i} + \sin\phi\frac{\lambda_5}{2i},\\
U_\phi &= -\sin(2\phi)\frac{\lambda_6}{2i} + \cos(2\phi)\frac{\lambda_7}{2i}, & U_\rho &= \cos(2\phi)\frac{\lambda_6}{2i} + \sin(2\phi)\frac{\lambda_7}{2i},
\end{aligned} \tag{5.19}$$

the λ_i being the Gell-Mann matrices (1.3), in which all fields components are ϕ independent. An elegant *Ansatz* requiring only eight instead of sixteen generators was found in Ref. [4] using this

[3] All other errors are negligible by comparison to this truncation error.

$\mathfrak{su}(3)$ basis. This *Ansatz* for the Yang-Mills fields in temporal gauge is given by

$$\begin{aligned} gA_0(r,\theta,\phi) &= 0, \\ gA_\phi(r,\theta,\phi) &= \alpha_1(r,\theta)\cos\theta T_\rho + \alpha_2(r,\theta)V_\rho + \alpha_3(r,\theta)\cos\theta U_\rho + \alpha_4(r,\theta)\frac{\lambda_3}{2i} + \alpha_5(r,\theta)\frac{\lambda_8}{2i}, \\ gA_\theta(r,\theta,\phi) &= \alpha_6(r,\theta)\ T_\phi + \alpha_7(r,\theta)\cos\theta V_\phi + \alpha_8(r,\theta)U_\phi, \\ gA_r(r,\theta,\phi) &= \alpha_9(r,\theta)\cos\theta\ T_\phi + \alpha_{10}(r,\theta)V_\phi + \alpha_{11}(r,\theta)\cos\theta U_\phi, \end{aligned} \tag{5.20}$$

with real profile functions $\alpha_i(r,\theta)$ and boundary conditions

$$\alpha_i(0,\theta) = 0, \qquad \lim_{r\to\infty} \begin{pmatrix} \alpha_1(r,\theta) \\ \alpha_2(r,\theta) \\ \alpha_3(r,\theta) \\ \alpha_4(r,\theta) \\ \alpha_5(r,\theta) \\ \alpha_6(r,\theta) \\ \alpha_7(r,\theta) \\ \alpha_8(r,\theta) \\ \alpha_9(r,\theta) \\ \alpha_{10}(r,\theta) \\ \alpha_{11}(r,\theta) \end{pmatrix} = \begin{pmatrix} -2\sin\theta(1+\sin^2\theta) \\ 2\sin\theta\cos^2\theta \\ -2\sin^2\theta \\ -\sin^2\theta(1+2\sin^2\theta) \\ \sqrt{3}\sin^2\theta \\ 2 \\ 2 \\ -2\sin\theta \\ 0 \\ 0 \\ 0 \end{pmatrix}, \tag{5.21}$$

as a consequence of demanding regularity at the origin and the pure gauge configuration (5.1) at infinity. Another symmetry is the reflection symmetry

$$\begin{pmatrix} -1 & 0 & 0 \\ 0 & 1 & 0 \\ 0 & 0 & -1 \end{pmatrix} W(\theta,\phi) \begin{pmatrix} -1 & 0 & 0 \\ 0 & 1 & 0 \\ 0 & 0 & -1 \end{pmatrix} = W(\pi-\theta,\phi), \tag{5.22}$$

which leaves our fields invariant under the reflection on the equatorial plane up to a gauge transformation. In conjunction with axial symmetry, this induces positive parity of gauge invariant quantities, such as the energy density. In light of this, the *Ansatz* has been constructed to require positive parity profile functions

$$\alpha_i(r,\pi-\theta) = \alpha_i(r,\theta). \tag{5.23}$$

Furthermore, due to this symmetry, we need only integrate the energy density over half the polar angle θ, which halves our numerical run time.

Similarly for the Higgs triplet, the axial symmetry of W (5.18) leads to the axial symmetry

$$\partial_\phi \Phi + \frac{\sqrt{3}\lambda_8 - \lambda_3}{2i}\Phi = 0. \tag{5.24}$$

The most general *Ansatz* [4], which fulfills this symmetry is then

$$\Phi(r,\theta,\phi) = \frac{v}{\sqrt{2}}\left[\beta_1(r,\theta)\lambda_3 + \beta_2(r,\theta)\cos\theta 2iT_\rho + \beta_3(r,\theta)2iV_\rho\right]\begin{pmatrix}1\\0\\0\end{pmatrix}, \tag{5.25}$$

with real profile functions $\beta_j(r,\theta)$, which must also have positive parity, under reflection on the equator

$$\beta_j(r,\pi-\theta) = \beta_j(r,\theta), \tag{5.26}$$

and boundary conditions

$$\beta_j(0,\theta) = 0, \quad \text{for } j = 1,2,3, \qquad \lim_{r\to\infty}\begin{pmatrix}\beta_1(r,\theta)\\ \beta_2(r,\theta)\\ \beta_3(r,\theta)\end{pmatrix} = \begin{pmatrix}\cos^2\theta\\ -\sin\theta\\ -\sin\theta\end{pmatrix}. \tag{5.27}$$

Now we can calculate the energy functional in terms of the α_i and β_j profile functions, by inserting the above *Ansatz* into the energy functional (1.8), yielding the following form

$$E\left[\widehat{A},\,\widehat{\Phi}\right] = 4\pi\int_0^\infty \mathrm{d}r\ \int_0^{\pi/2}\mathrm{d}\theta\ r^2\sin\theta\ \widehat{e}(r,\,\theta)\,. \tag{5.28}$$

Integration over $\theta \in [0,\pi/2]$ is sufficient due to the previously mentioned reflection symmetry

$$\widehat{e}(r,\,\theta) = \widehat{e}(r,\,\pi-\theta)\,. \tag{5.29}$$

The total energy density $\widehat{e}(r,\theta)$ has contributions from the Yang-Mills, the kinetic Higgs and the the Higgs potential terms

$$\widehat{e}(r,\,\theta) = \widehat{e}_{\mathrm{YM}}(r,\,\theta) + \widehat{e}_{\mathrm{Hkin}}(r,\,\theta) + \widehat{e}_{\mathrm{Hpot}}(r,\,\theta) \tag{5.30}$$

and is given explicitly in App. A for the radial gauge ($A_r = 0$). Inspecting the product of energy density and integral measure, we can see, that it is not finite on the symmetry axis ($\theta = 0,\pi$) for an arbitrary choice of non-singular profile functions. Since the solution we are looking for is however certainly of finite energy, one can determine the following constraints, given in Ref. [4]

for $\bar{\theta} = 0, \pi$:

$$\begin{aligned}
\alpha_j(r,\bar{\theta}) &= \bar{\alpha}_j(r)\sin\theta\big|_{\theta=\bar{\theta}} && \text{for } j = 1,2,9,10,\\
\alpha_j(r,\bar{\theta}) &= \bar{\alpha}_j(r)\sin^2\theta\big|_{\theta=\bar{\theta}} && \text{for } j = 3,4,5,11,\\
\alpha_j(r,\bar{\theta}) &= (-)^{j-5}\cos\theta\partial_\theta\alpha_{j-5}(r,\theta)\big|_{\theta=\bar{\theta}} && \text{for } j = 6,7,\\
\alpha_j(r,\bar{\theta}) &= \frac{1}{2}\cos\theta\partial_\theta\alpha_{j-5}(r,\theta)\big|_{\theta=\bar{\theta}} && \text{for } j = 8,\\
\partial_\theta\beta_1(r,\bar{\theta})\big|_{\theta=\bar{\theta}} = 0, \quad \beta_j(r,\bar{\theta}) &= \bar{\beta}_j(r)\sin\theta\big|_{\theta=\bar{\theta}} && \text{for } j = 2,3,
\end{aligned} \tag{5.31}$$

which are of course in agreement with origin and infinity boundary conditions.

Applying the Euler-Lagrange equations (4.1) to the energy functional yields 14 PDEs. These reduced field equations are equivalent to the 14 PDEs left over after inserting the *Ansatz* given by Eqs. (5.20) and (5.25) into the full field equations (1.9). All other components of the field equations are directly fulfilled by the *Ansatz*. Hence, solving the obtained PDEs will also consistently solve the full Yang-Mills-Higgs equations. The PDEs in radial gauge ($A_r = 0$) are given explicitly in App. B and we will tackle them directly using the Method of Lines (MOL) approach in Section 5.5.

There exist a range of profile function behaviors close to the origin, which lead to a singular or irregular energy density there. The suggestion is, therefore, to solve the PDEs near the origin analytically, by expanding the profile functions in a Taylor series around $r = 0$ and solving the reduced PDEs in leading order. The obtained behavior of the *Ansatz* functions is [13]

$$r \to 0: \quad \begin{pmatrix} \alpha_1(r,\theta) \\ \alpha_2(r,\theta) \\ \alpha_3(r,\theta) \\ \alpha_4(r,\theta) \\ \alpha_5(r,\theta) \\ \alpha_6(r,\theta) \\ \cos^2\theta\,\alpha_7(r,\theta) \\ \alpha_8(r,\theta) \end{pmatrix} \sim \begin{pmatrix} c_1 r^2\sin\theta \\ c_2 r^2\sin\theta|\cos\theta| \\ c_3 r^3\sin^2\theta \\ c_4 r^2\sin^2\theta \\ c_5 r^2\sin^2\theta \\ -c_1 r^2 \\ c_2 r^2|\cos\theta| \\ c_3 r^3\sin\theta \end{pmatrix},$$

$$r \to 0: \quad \begin{pmatrix} \beta_1(r,\theta) \\ \beta_2(r,\theta) \\ \beta_3(r,\theta) \end{pmatrix} \sim \begin{pmatrix} c_6 r|\cos\theta| \\ c_7 r^2\sin\theta \\ c_8 r\sin\theta \end{pmatrix}, \tag{5.32}$$

with constants c_i for $i = 1, \ldots, 8$.

5.3 Choice of gauge

The fields given by the *Ansatz* (5.20) and (5.25), have already been fixed to temporal gauge, however they are still invariant under an $SO(3)$ gauge transformation

$$gA'_n = \Omega\left(gA_n + \partial_n\right)\Omega^{-1}, \qquad \Phi' = \Omega\Phi, \tag{5.33}$$

with

$$\Omega(r,\theta,\phi) = \exp\left[\omega_T(r,\theta)T_\phi + \omega_V(r,\theta)V_\phi + \omega_U(r,\theta)U_\phi\right]. \tag{5.34}$$

Unlike most gauge fixing scenarios, where the choice of gauge is merely decided upon to ease technical aspects of computation, a bad choice of gauge for the $\widehat{S}$ *Ansatz* may lead to irregular or singular fields. To give an example, it has been explicitly shown for the $SU(2)\times U(1)$ sphaleron with finite mixing angle θ_w [45], where the only known gauge with well behaved solutions is the Coulomb gauge, that gauge transformations from Coulomb gauge to a wide range of commonly used gauges (radial gauge, background gauge, hedgehog gauge, ...) are all irregular at the origin.

5.3.1 Radial gauge

Previous work on the $\widehat{S}$ [19][33] has been conducted exclusively in the radial gauge

$$gA_r = 0: \quad \alpha_9(r,\theta) = \alpha_{10}(r,\theta) = \alpha_{11}(r,\theta) = 0, \tag{5.35}$$

primarily out of technical convenience, since it reduces the number of PDEs by three[4] and reduces the remaining equations' complexity significantly. It can also easily be seen, that this gauge is in agreement with all boundary conditions. Nevertheless, it is not clear a priori if solutions obtained in this gauge lead to a regular energy density and we must verify this explicitly.

We will conduct all of our numerical calculations in this gauge.

5.3.2 Coulomb gauge

Given the usefulness of this gauge for finding regular solutions of axially symmetric $SU(2)\times U(1)$ sphalerons, we will quickly discuss the Coulomb gauge, as was done before by [19]. The gauge conditions

$$\begin{aligned} \nabla\cdot\vec{A} = 0: \qquad & \partial_\theta\alpha_6 + r\cos\theta\partial_r\alpha_9 = 0, \\ & \partial_\theta\left(\cos\theta\alpha_7\right) + r\partial_r\alpha_{10} = 0, \\ & \partial_\theta\alpha_8 + r\cos\theta\partial_r\alpha_{11} = 0, \end{aligned} \tag{5.36}$$

are obtained by expanding the matrix constraint equation into the generators T_ϕ, V_ϕ and U_ϕ. For the $\widehat{S}$ this appears to be a bad choice of gauge, since the gauge conditions are in conflict with the

[4] Using gauge conditions to entirely eliminate PDEs is far more difficult for other gauges and most of the time makes their solution even more difficult, e.g. yielding integro-differential equations for the remaining equations.

boundary conditions at infinity, e.g.

$$r \to \infty : \quad \partial_\theta \left(\cos\theta \alpha_7\right) + r\partial_r \alpha_{10} = -2\sin\theta \neq 0. \tag{5.37}$$

5.3.3 Modified Coulomb gauge

As shown in Ref. [19], a minor modification of the Coulomb gauge fixes the conflict at infinity

$$\begin{aligned} \nabla \cdot \vec{A} = -\frac{2}{r^2} f(r) \left(\sin\theta V_\phi + \cos\theta U_\phi\right) : \quad & \partial_\theta \alpha_6 + r\cos\theta \partial_r \alpha_9 = 0, \\ & \partial_\theta \left(\cos\theta \alpha_7\right) + r\partial_r \alpha_{10} + 2f(r)\sin\theta = 0, \\ & \partial_\theta \alpha_8 + r\partial_r \alpha_{11} + 2f(r)\cos\theta = 0, \end{aligned} \tag{5.38}$$

with

$$f(0) = 0, \quad f(\infty) = 1. \tag{5.39}$$

Inspecting the symmetry axis boundary conditions (5.31), we find, that the gauge function $f(r)$ may not be freely chosen, but is

$$f(r) = -\frac{1}{2} \partial_\theta \alpha_8(r,\theta)\big|_{\theta\to 0}. \tag{5.40}$$

5.4 Numerical minimization of the energy functional

We will now expand the profile functions $\alpha_i(x,\theta)$ and $\beta_j(x,\theta)$ in nested orthogonal functions. Cutting off these expansions, in essence, approximates the energy functional (5.28) with an energy function of expansion coefficients, allowing us to apply our numerical minimization methods. Similar approaches to the minimization of the $\widehat{S}$ energy functional have previously been tested [19; 33].

Once again, we will employ the convenient compactified coordinates

$$x = \frac{gvr}{\chi + gvr}, \quad x \in [0,1], \quad \chi \in \mathbb{R}^+. \tag{5.41}$$

With the origin behavior (5.32) and the boundary conditions towards spatial infinity (5.21) and (5.27) in mind, we redefine the *Ansatz* profile functions as follows [13]:

$$\begin{pmatrix} \overline{\alpha}_1(x,\theta) \\ \overline{\alpha}_2(x,\theta) \\ \overline{\alpha}_3(x,\theta) \\ \overline{\alpha}_4(x,\theta) \\ \overline{\alpha}_5(x,\theta) \\ \overline{\alpha}_6(x,\theta) \\ \overline{\alpha}_7(x,\theta) \\ \overline{\alpha}_8(x,\theta) \end{pmatrix} = \begin{pmatrix} \alpha_1(x,\theta)/[-4x^2\sin\theta] \\ \alpha_2(x,\theta)/[2x^2\sin\theta] \\ \alpha_3(x,\theta)/[-2x^3\sin^2\theta] \\ \alpha_4(x,\theta)/[-3x^2\sin^2\theta] \\ \alpha_5(x,\theta)/[\sqrt{3}x^2\sin^2\theta] \\ \alpha_6(x,\theta)/[2x^2] \\ \alpha_7(x,\theta)/[2x^2] \\ \alpha_8(x,\theta)/[-2x^3\sin\theta] \end{pmatrix}, \tag{5.42a}$$

$$\begin{pmatrix} \overline{\beta}_1(x,\theta) \\ \overline{\beta}_2(x,\theta) \\ \overline{\beta}_3(x,\theta) \end{pmatrix} = \begin{pmatrix} \beta_1(x,\theta)/x \\ \beta_2(x,\theta)/[-x^2\sin\theta] \\ \beta_3(x,\theta)/[-x\sin\theta] \end{pmatrix}. \tag{5.42b}$$

This redefinition naturally fulfills several boundary conditions on the symmetry axis, given by Eq. (5.31). The remaining four conditions for ($\overline{\theta} = 0, \pi$) are:

$$\overline{\alpha}_6(x,\overline{\theta}) = 2\cos\theta\partial_\theta\big[\sin\theta\,\overline{\alpha}_1(x,\theta)\big]\Big|_{\theta=\overline{\theta}}, \tag{5.43a}$$

$$\overline{\alpha}_7(x,\overline{\theta}) = \cos\theta\partial_\theta\big[\sin\theta\,\overline{\alpha}_2(x,\theta)\big]\Big|_{\theta=\overline{\theta}}, \tag{5.43b}$$

$$\overline{\alpha}_8(x,\overline{\theta}) = \left(\cos^2\theta\,\overline{\alpha}_3 + \frac{1}{2}\sin\theta\cos\theta\partial_\theta\overline{\alpha}_3\right)\Big|_{\theta=\overline{\theta}}, \tag{5.43c}$$

$$\partial_\theta\overline{\beta}_1(x,\theta)\Big|_{\theta=\overline{\theta}} = 0. \tag{5.43d}$$

Note, that the *Ansatz* functions have been redefined to take values between $[0,1]$ as they approach $x = 1$:

$$\lim_{x\to 1}\begin{pmatrix}\overline{\alpha}_1(x,\theta)\\ \overline{\alpha}_2(x,\theta)\\ \overline{\alpha}_3(x,\theta)\\ \overline{\alpha}_4(x,\theta)\\ \overline{\alpha}_5(x,\theta)\\ \overline{\alpha}_6(x,\theta)\\ \overline{\alpha}_7(x,\theta)\\ \overline{\alpha}_8(x,\theta)\end{pmatrix} = \begin{pmatrix}(1+\sin^2\theta)/2\\ \cos^2\theta\\ 1\\ (1+2\sin^2\theta)/3\\ 1\\ 1\\ 1\\ 1\end{pmatrix}, \tag{5.44a}$$

$$\lim_{x\to 1}\begin{pmatrix}\overline{\beta}_1(x,\theta)\\ \overline{\beta}_2(x,\theta)\\ \overline{\beta}_3(x,\theta)\end{pmatrix} = \begin{pmatrix}\cos^2\theta\\ 1\\ 1\end{pmatrix}. \tag{5.44b}$$

We may now introduce the θ expansion of the redefined *Ansatz* functions. It is given by

$$\begin{aligned}\overline{\alpha}_i(x,\theta) = \frac{f_{i0}(x)}{2} &+ \sum_{n=1}^{N}\Big[f_{in}(x)\cos(2n\theta) + p_{in}(x)\sin((2n-1)\theta)\Big]\\ &+ \begin{cases}p_{20}(x)\,|\cos\theta|, & \text{for } i=2,\\ p_{70}(x)/|\cos\theta|, & \text{for } i=7,\\ 0, & \text{for } i=1,3,4,5,6,8,\end{cases}\end{aligned} \tag{5.45a}$$

$$\begin{aligned}\overline{\beta}_j(x,\theta) = \frac{h_{j0}(x)}{2} &+ \sum_{n=1}^{N}\Big[h_{jn}(x)\cos(2n\theta) + q_{jn}(x)\sin((2n-1)\theta)\Big]\\ &+ \begin{cases}q_{10}(x)\,|\cos\theta|, & \text{for } j=1,\\ 0, & \text{for } j=2,3.\end{cases}\end{aligned} \tag{5.45b}$$

If we choose the origin boundary conditions of the introduced radial functions in the following way

$$f_{i0}(0) = 0, \quad \text{for } i=2,7, \tag{5.46a}$$

$$h_{10}(0) = 0, \tag{5.46b}$$

$$f_{in}(0) = p_{in}(0) = h_{jn}(0) = q_{jn}(0) = 0, \quad \forall i,j \text{ and } n>0, \tag{5.46c}$$

the expansion (5.45) meets the desired origin behavior (5.32) precisely. Upon insertion of the expansion (5.45) into the boundary conditions on the symmetry axis (5.43), we find that they are

only met, if we fix

$$p_{70}(x) := p_{20}(x). \tag{5.47}$$

Furthermore, we find that the following boundary conditions are required to match the redefined profile functions' boundary conditions towards infinity (5.44):

$$f_{in}(1) = \begin{pmatrix} \frac{3}{2} & 1 & 2 & \frac{4}{3} & 2 & 2 & 2 & 2 \\ -\frac{1}{4} & \frac{1}{2} & 0 & -\frac{1}{3} & 0 & 0 & 0 & 0 \end{pmatrix}, \quad \text{for } n \in [0,1], \tag{5.48a}$$

$$h_{jn}(1) = \begin{pmatrix} 1 & 2 & 2 \\ \frac{1}{2} & 0 & 0 \end{pmatrix}, \quad \text{for } n \in [0,1], \tag{5.48b}$$

$$f_{in}(1) = h_{jn}(1) = 0, \quad \text{for } n > 1 \tag{5.48c}$$

$$p_{in}(1) = q_{jn}(1) = 0, \quad \forall n. \tag{5.48d}$$

Finally, the conditions obtained from inserting the expansion (5.45) into the boundary conditions on the symmetry axis (5.43), specifically

$$\frac{f_{60} - 2f_{10}}{2} + \sum_{n=1}^{N} [f_{6n} - 2f_{1n}] = 0, \tag{5.49a}$$

$$\frac{f_{i,0} - f_{i-5,0}}{2} + \sum_{n=1}^{N} [f_{i,n} - f_{i-5,n}] = 0, \quad \text{for } i = 7, 8, \tag{5.49b}$$

$$\sum_{n=1}^{N} (2n-1) q_{1n} = 0, \tag{5.49c}$$

are enforced by fixing f_{60}, f_{70}, f_{80} and q_{11}.

In a second step, we expand the radial functions in Legendre polynomials[5] $P_m(2x-1)$:

$$f_{in}(x) = x^2 \sum_{m=0}^{M} a_{inm} P_m(2x-1) + \begin{cases} 2e_i, & \text{for } i = 1,3,4,5 \text{ and } n = 0, \\ 2e_{i-5}, & \text{for } i = 6,8 \text{ and } n = 0, \\ 0, & \text{for } i = 2,7 \text{ or } n > 0, \end{cases} \tag{5.50a}$$

$$h_{jn}(x) = x^2 \sum_{m=0}^{M} b_{jnm} P_m(2x-1) + \begin{cases} 2e_{j+5}, & \text{for } j = 2,3, \text{ and } n = 0, \\ 0, & \text{for } j = 1 \text{ or } n > 0, \end{cases} \tag{5.50b}$$

$$p_{in}(x) = x^2 \sum_{m=0}^{M} c_{inm} P_m(2x-1) + \begin{cases} e_2, & \text{for } i = 2 \text{ and } n = 0, \\ 0, & \text{for } n > 0, \end{cases} \tag{5.50c}$$

$$q_{jn}(x) = x^2 \sum_{m=0}^{M} d_{jnm} P_m(2x-1) + \begin{cases} e_6, & \text{for } j = 1, \text{ and } n = 0, \\ 0, & \text{for } n > 0, \end{cases} \tag{5.50d}$$

with the eight coefficients e_k, which are proportional to the coefficients c_k introduced in the origin behavior (5.32). By multiplying the respective first summands of the expansion (5.50) with a pre-factor x^2, we are guaranteed to obtain the desired origin behavior and suppress any other behavior close to the origin, making the solution there more stable. To satisfy the radial function boundary conditions (5.48) at $x = 1$, we adjust one expansion coefficient for each i/j and n in the following conditions

$$\sum_{m=0}^{M} a_{inm} = f_{in}(1) - \begin{cases} 2e_i, & \text{for } i = 1,3,4,5 \text{ and } n = 0, \\ 2e_{i-5}, & \text{for } i = 6,8 \text{ and } n = 0, \\ 0, & \text{for } i = 2,7 \text{ or } n > 0, \end{cases} \tag{5.51a}$$

$$\sum_{m=0}^{M} b_{jnm} = h_{jn}(1) - \begin{cases} 2e_{j+5}, & \text{for } j = 2,3, \text{ and } n = 0, \\ 0, & \text{for } j = 1 \text{ or } n > 0, \end{cases} \tag{5.51b}$$

$$\sum_{m=0}^{M} c_{inm} = p_{in}(1) - \begin{cases} e_2, & \text{for } i = 2 \text{ and } n = 0, \\ 0, & \text{for } n > 0, \end{cases} \tag{5.51c}$$

$$\sum_{m=0}^{M} d_{jnm} = q_{jn}(1) - \begin{cases} e_6, & \text{for } j = 1, \text{ and } n = 0, \\ 0, & \text{for } n > 0. \end{cases} \tag{5.51d}$$

Considering the trade-off between runtime and numerical precision, we may now choose to cut off the angular expansion at a given N and the radial expansion at a given M, yielding an energy function to minimize over numerically, using the previously outlined method.

[5] These Legendre polynomials are normalized to $P_m(1) = 1$ and orthogonal on $x \in [0,1]$.

To be precise, the minimization is carried out over the following expansion coefficients:

- a_{imn} and b_{jmn} for $n \in [0, N]$ and $m \in [1, M]$ ($m = 0$ coefficients are fixed to satisfy the boundary conditions at $x = 1$), excluding a_{60m}, a_{70m} and a_{80m} (fixed for all m to satisfy the symmetry axis boundary conditions)
- c_{imn} and d_{jmn} for $n \in [1, N]$ and $m \in [1, M]$ (same reason as for a and b), excluding d_{11m} (same reason as for a and b)
- c_{20m} and d_{10m}
- e_k

The total number coefficients is

$$N_{\text{coeff}} = 8 + \Big[11(2N+1) - 2\Big]M \xrightarrow{N,M\to\infty} 22NM. \tag{5.52}$$

5.4.1 Numerical solution

We present in this section the results obtained from minimization of the energy function for $\lambda/g^2 = 0$, employing the expansion in nested orthogonal functions, as outlined in the previous section. However, we must first obtain the energy function from the energy functional with a cut-off expansion inserted, by integration over $x \in [0, 1]$ and $\theta \in [0, \pi/2]$. For anything but small expansion order cut-offs (M, N), the energy functional is very sizable. As a result its analytic integration is unfeasible and the integral has to be carried out numerically during run-time. Nevertheless, we will start off with the minimization of a low-order energy function, that has been obtained through analytic integration using Mathematica, in order to verify our numerical integration.

We find, that for large expansion order cut-offs the number of terms to be handled grows like N^4M^4, quickly becoming too large for our simple symbolic calculation set-up. To gain a rough idea of the complexity of the symbolic calculations at each expansion order cut-off, we estimate the number of terms in the final energy function, which depends only on the expansion coefficients and numeric pre-factors:

$$N_{\text{terms}} \leq 14 \times 5^2 \times (2N+1)^4 M^4. \tag{5.53}$$

We give this upper bound for the number of terms in Tab. 5.1, for a range of relevant expansion order cut-offs. For those cut-offs for which we were able to carry out the calculation, the given numbers appear to be a good index of the complexity of a given evaluation and the associated run-time.

Since this minimization involves evaluating huge expressions on each function call (up to 20 MB of code), we have outsourced the energy function to a C++ compiled python module and gained a significant speed-up. Since any calculation beyond $(M, N) = (3, 1)$ would have required developing a different approach to many aspects of the procedure and perhaps even switching to a different infrastructure, we stopped at this point. Besides the bottlenecks of the symbolic

	$M=1$	$M=2$	$M=3$	$M=4$	$M=5$
$N=0$	0.35	5.6	28	90	219
$N=1$	28	454	2 296	7 258	17 719
$N=2$	219	3 500	17 719	56 000	136 719
$N=3$	840	13 446	68 068	215 130	525 219

Table 5.1: Rough estimate of the number of summands in units of [1000], involved in the expanded energy, obtained from analytic integration. This serves as an index of the complexity of the corresponding symbolic calculation. The shaded cells above the dashed line indicate the expansion cut-offs, for which we were able to carry out the analytic integration, as well as compile and run the corresponding minimization programs.

calculation, the size of the source file and its compilation time also grow to become a considerable obstacle[6].

M	N	$E\,[4\pi v/g]$	E/E_S
1	1	2.09925	1.38086
1	2	2.07619	1.36568
2	1	1.63636	1.07637
3	1	1.52004	0.99985

Table 5.2: Energy of configurations obtained from minimization of the energy function (from analytic integration) at various expansion cut-offs (M,N), using $\chi = 2.4$ and $\lambda/g^2 = 0$. The energy E_S of the $SU(2)$ sphaleron S embedded in $SU(3)$ Yang-Mills-Higgs theory is taken to be $E_S = 1.52024[4\pi v/g]$.

The obtained values for the energy at various expansion order cut-offs are given in Tab. 5.2 and are in agreement with the results using numerical integration. We do not show the obtained profile functions, as they match those obtained using numerical integration well.

We now move on to minimizing the energy functional at various expansion order cut-offs (M,N), carrying out the two-dimensional integral numerically during minimization. The energies of the configurations obtained at various expansion order cut-offs (M,N), using $\chi = 5$, are given in Tab. 5.3. From there we gain the following value of the $\widehat{S}$ energy

$$E_{\widehat{S}}^{\text{basic YMHth, } \lambda/g^2=0} = (1.35 \pm 0.03)\,[4\pi v/g]\,. \tag{5.54}$$

The error has been estimated by variation of expansion order cut-offs and grid sizes, similar to the detailed error discussion in Section 5.1. This energy is remarkably low, e.g. by comparison with the $SU(2)$ sphaleron S embedded in $SU(3)$ Yang-Mills-Higgs theory, perhaps due the fact, that the azimuthal and polar gauge fields of the *Ansatz* are distributed evenly over the Lie algebra [13]. In order to compare with the analytic results of Tab. 5.2, we also give the energy obtained with numerical integration at $(M,N) = (3,1)$ and using $\chi = 2.4$: $E = 1.51118\,[4\pi v/g]$.

[6] Already for the expansion order cut-off $(M,N) = (3,1)$, several steps had to be taken to compile in reasonable time, with acceptable memory consumption.

Figs. 5.3 and 5.4 show the $(M, N) = (11, 3)$ configuration's profile functions, normalized as follows:

$$\begin{pmatrix} \widehat{\alpha}_1(x,\theta) \\ \widehat{\alpha}_2(x,\theta) \\ \widehat{\alpha}_3(x,\theta) \\ \widehat{\alpha}_4(x,\theta) \\ \widehat{\alpha}_5(x,\theta) \\ \widehat{\alpha}_6(x,\theta) \\ \widehat{\alpha}_7(x,\theta) \\ \widehat{\alpha}_8(x,\theta) \end{pmatrix} = \begin{pmatrix} \alpha_1(x,\theta)/[-2\sin\theta(1+\sin^2\theta)] \\ \alpha_2(x,\theta)/[2\sin\theta] \\ \alpha_3(x,\theta)/[-2\sin^2\theta] \\ \alpha_4(x,\theta)/[-\sin^2\theta(1+2\sin^2\theta)] \\ \alpha_5(x,\theta)/[\sqrt{3}\sin^2\theta] \\ \alpha_6(x,\theta)/2 \\ \alpha_7(x,\theta)/2 \\ \alpha_8(x,\theta)/[-2\sin\theta] \end{pmatrix}, \tag{5.55a}$$

$$\begin{pmatrix} \widehat{\beta}_1(x,\theta) \\ \widehat{\beta}_2(x,\theta) \\ \widehat{\beta}_3(x,\theta) \end{pmatrix} = \begin{pmatrix} \beta_1(x,\theta) \\ \beta_2(x,\theta)/[-\sin\theta] \\ \beta_3(x,\theta)/[-\sin\theta] \end{pmatrix}, \tag{5.55b}$$

to increase readability. We notice a large gradient of the profile functions $\widehat{\alpha}_i$ close to $x = 1$ (note that the profile functions are plotted for $\chi = 25$, as $\chi = 5$ is already not readable). In other words, these profile functions tend to their asymptotic value at $r \to \infty$ very slowly, most likely caused by the massless gauge-field modes. For increasing expansion order cut-offs (M, N) this behavior becomes worse, as a large part of the profile function gradient gets pushed out further and further towards infinity, where their contribution to the total energy is lowest. Most likely an energy minimization based method is simply not a good choice to determine such a tricky far-field behavior. Nevertheless, we observe clear signs of convergence for the near-field behavior, the energy and the energy density.

M	N	$E\,[4\pi v/g]$	E/E_S
6	1	1.468	0.965
6	2	1.433	0.953
11	2	1.371	0.902
11	3	1.360	0.895
18	3	1.345	0.885

Table 5.3: Energy of configurations obtained from minimization at various expansion cut-offs (M, N), using $\chi = 5.0$ and $\lambda/g^2 = 0$. The energy E_S of the $SU(2)$ sphaleron S embedded in $SU(3)$ Yang-Mills-Higgs theory is taken to be $E_S = 1.52024[4\pi v/g]$.

Finally, the energy density corresponding to the $(M, N) = (18, 3)$ configuration is shown for slices of various θ in Fig. 5.6 and as a contour plot in Euclidean space for $y = 0$ in Fig. 5.5. We notice a slightly prolate energy density distribution for $1 \leq gvr \leq 2$ and a non-trivial core structure. Further out the energy density becomes spherically symmetric, as to be expected. The energy density slices depicted in Fig. 5.6 display the expected exponential fall-off towards large gvr and a regular behavior at the origin. However, this figure also shows fluctuations close to the

origin, probably caused by numerical inaccuracies, as they are unlikely to be physical.

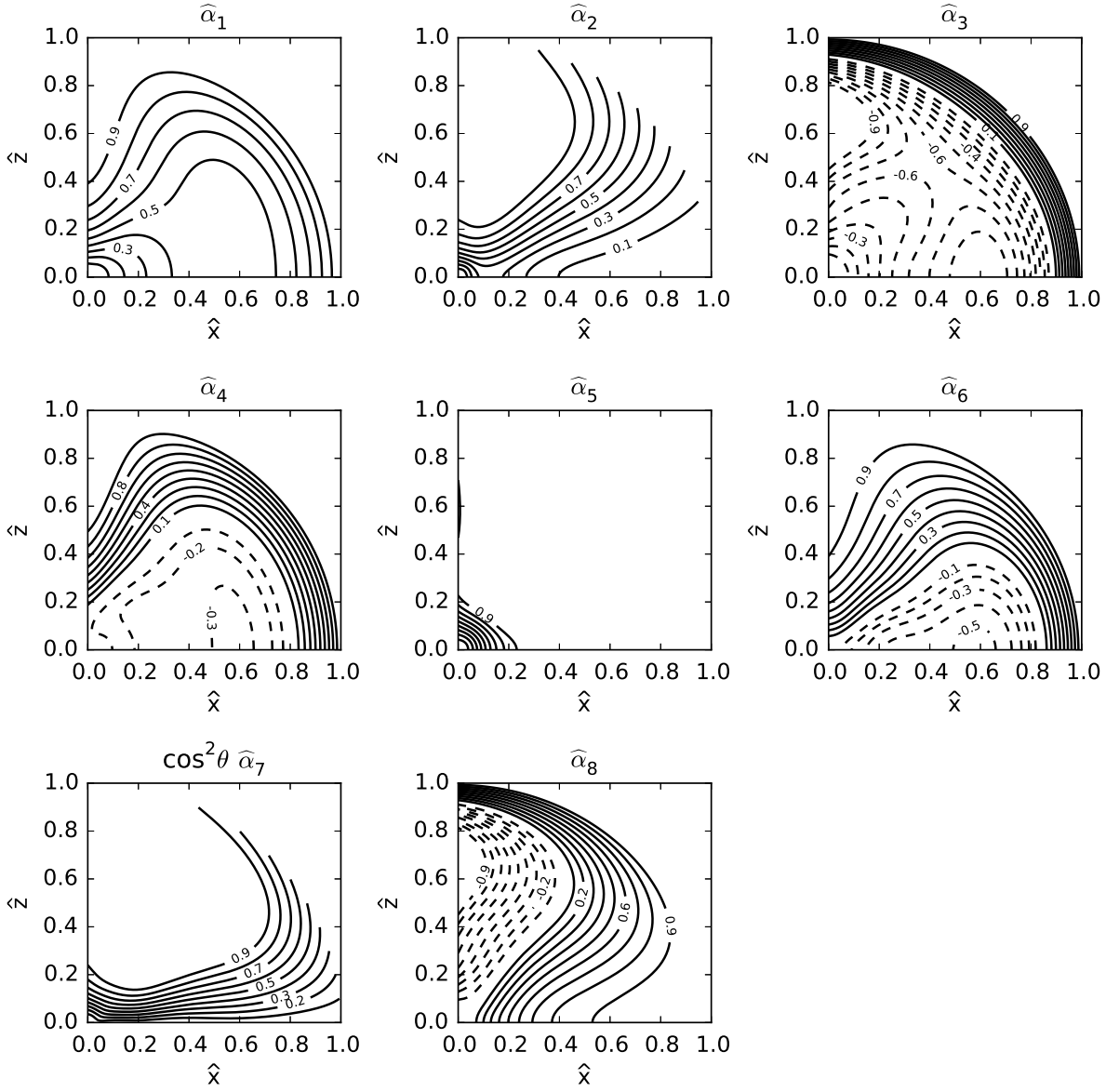

Figure 5.3: Equidistant contour-plots of the re-scaled profile functions $\widehat{\alpha}_i$ of the configuration obtained from minimization of the energy functional at $(M, N) = (11, 3)$ for $\lambda/g^2 = 0$ and $\chi = 5.0$. The two shown compactified Cartesian coordinates are given by $\widehat{x} = gvr/(gvr + 25)\ \sin\theta$ and $\widehat{z} = gvr/(gvr + 25)\ \cos\theta$.

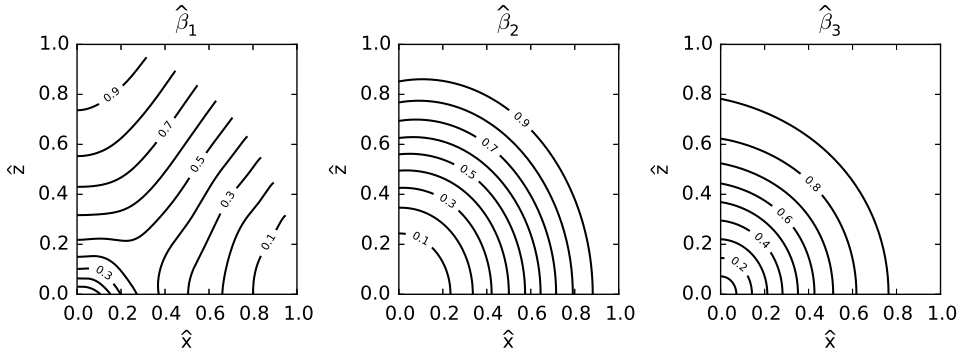

Figure 5.4: Same as Fig. 5.3, but for the normalized profile functions $\widehat{\beta}_j$ and using coordinates $\widehat{x} = gvr/(gvr + 5)\ \sin\theta$ and $\widehat{z} = gvr/(gvr + 5)\ \cos\theta$.

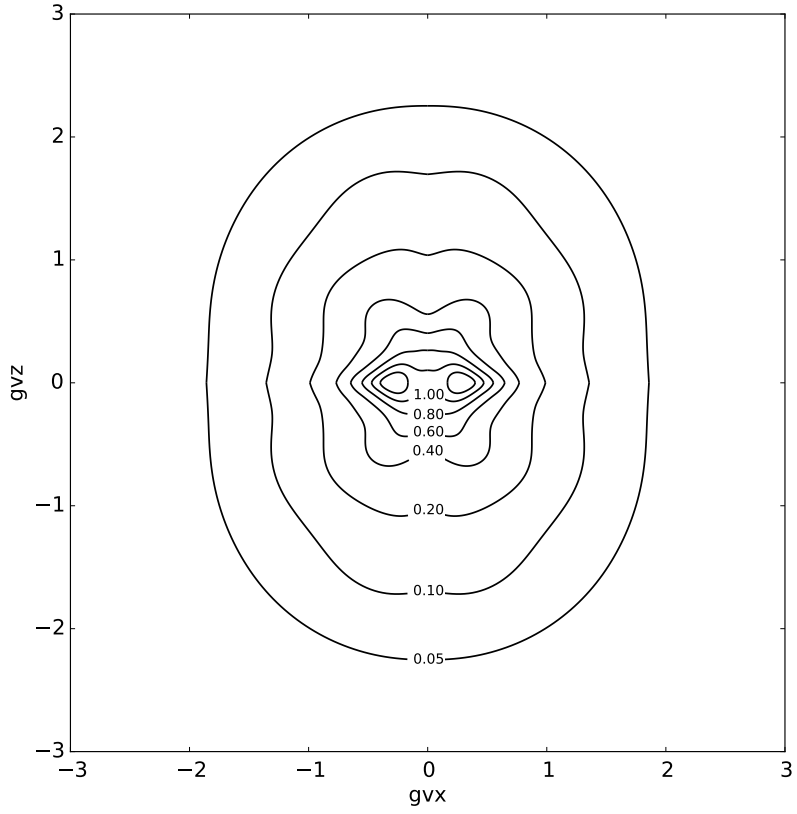

Figure 5.5: Energy density contours of the configuration obtained from minimization of the basic Yang-Mills-Higgs theory energy functional with $(M, N) = (13, 3)$, for $\lambda/g^2 = 0$ and $\chi = 5.0$. The slice is in Euclidean space for $gvy = 0$. The two contours around $(gvx, gvz) = (\pm 0.3, 0)$ have the value $1.20\,[(4\pi g/g)(gv)^3]$.

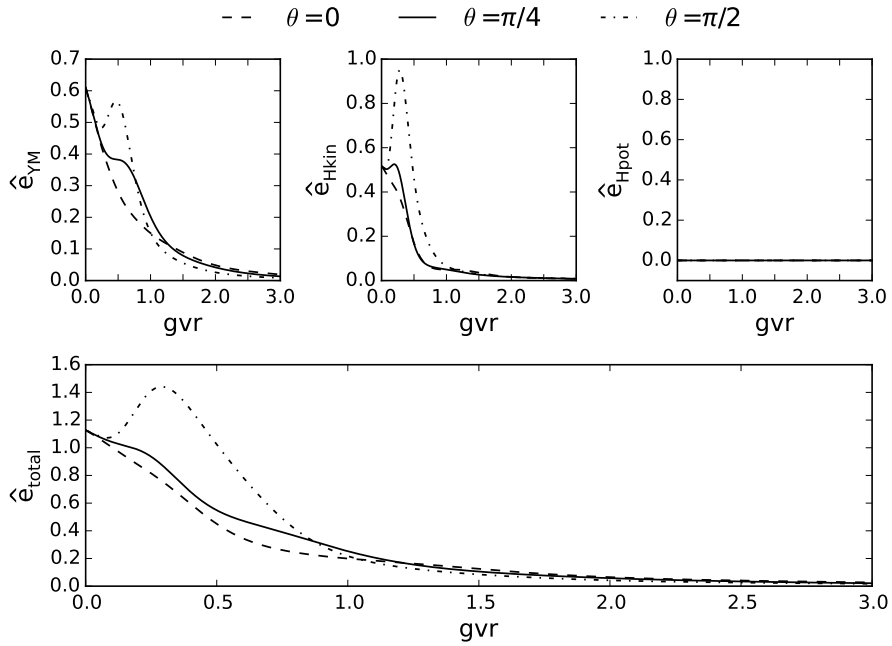

Figure 5.6: Slices of energy density constituents for the configuration obtained from minimization of the basic Yang-Mills-Higgs theory energy functional with $(M, N) = (18, 3)$, for $\lambda/g^2 = 0$ and $\chi = 5.0$.

5.5 Solving the reduced field equations

Now, let us apply an entirely different numerical method to the problem: solving the reduced field equations in radial gauge, given in App. B, directly. It should be mentioned at this point, that this method is nowhere near as robust and the obtained results are not as reliable as those obtained from minimization. However, they are in agreement and hence, this method serves to support the minimization results, using a completely distinct method.

The given PDE boundary value problem consists of 11 PDEs in gvr and θ and we will approach these by using the method of lines [42] (MOL). This involves discretizing the angular grid into p lines and replacing all θ derivatives with central differences. By doing so, we obtain a large set of $11p$ second order ODEs. After fixing the lines on the symmetry axis to the boundary conditions (5.31), we can solve the ODE system with the BVP4C solver, as previously done for the smaller system of 2 ODEs of the spherically symmetric approximation in Section 5.1. The large memory consumption of the solver for such a large system limits us to a maximum angular grid size of $p = 30$[7].

There was a lot of fine tuning necessary to get the solver to converge. In particular it was necessary to iteratively solve the ODEs for radial ranges of increasing size, starting off with $gvr \in [0.1, 50]$ and increasing step by step to $gvr \in [0.003, 800]$. Attempts to solve the ODEs on a greater range have not been successful, neither have attempts to use a compactified radial grid, as used for minimization.

Nevertheless, the obtained configurations' profile functions resemble those obtained from minimization. The lowest energy obtained with this method is

$$E_{MOL} = (1.31 \pm 0.10)\,[4\pi v/g]\,, \tag{5.56}$$

with a falling tendency (on a near perfect hyperbola) for higher upper range bounds. Even though the obtained energy value is lower than the one obtained from minimization, there is likely a significant numerical error from θ integration of the energy functional. Furthermore, inspection of the obtained profile functions suggests, that the corresponding configuration is nowhere near as close to the solution as the one obtained from minimization. The obtained energy values for various upper range bounds are presented in Fig. 5.7.

[7] Solving the 660 first order ODEs consumed close to all of the 64GB of memory available to us on our best machine.

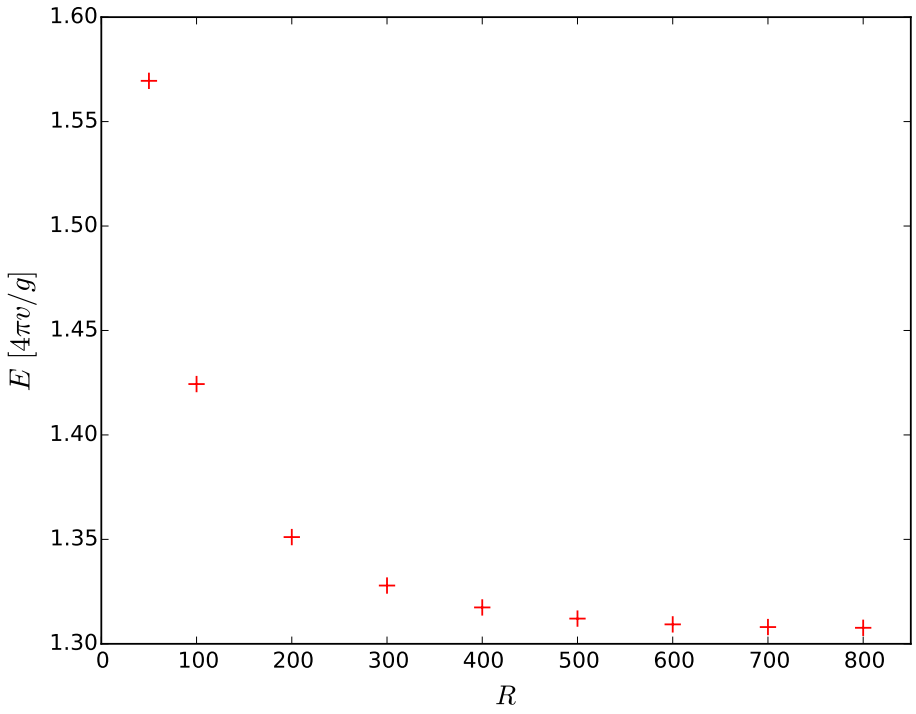

Figure 5.7: Energy of the $\widehat{S}$ configurations obtained by applying the MOL with the BVP4C ODE solver. The solutions are obtained by fixing the profile functions to their infinity boundary conditions at $gvr = R$, as well as to their origin boundary conditions at $gvr = 0.003$ and solving the lines ODEs in the range $gvr \in [0.003, R]$, using $p = 30$ lines.

CHAPTER 6

$\widehat{S}$ in the extended $SU(3)$ Yang-Mills-Higgs theory

The gauge fields of the $\widehat{S}$ configuration in the extended Yang-Mills-Higgs theory (1.10) are constructed in precisely the same way as those in the basic Yang-Mills-Higgs theory. The gauge-field *Ansatz* is given by Eq. (5.20) and will not be repeated here. In case of the three scalar triplet fields, the *Ansatz* must match the following boundary conditions towards infinity

$$\lim_{r\to\infty} \Phi_1(r,\theta,\phi) = \eta\, W(\theta,\phi) \begin{pmatrix} 1 \\ 0 \\ 0 \end{pmatrix}, \tag{6.1a}$$

$$\lim_{r\to\infty} \Phi_2(r,\theta,\phi) = \eta\, W(\theta,\phi) \begin{pmatrix} 0 \\ 0 \\ -1 \end{pmatrix}, \tag{6.1b}$$

$$\lim_{r\to\infty} \Phi_3(r,\theta,\phi) = \eta\, W(\theta,\phi) \begin{pmatrix} 0 \\ 1 \\ 0 \end{pmatrix}, \tag{6.1c}$$

with the $SU(3)$ matrix W defined by Eq. (5.4).

6.1 Extension of the *Ansatz*

In light of the boundary conditions (6.1) of the scalar fields and similar to the *Ansatz* (5.25) made for the single scalar triplet of the basic Yang-Mills-Higgs theory, the following radial-gauge *Ansatz* can be made [13]:

$$\widehat{\Phi}_1(r,\theta,\phi) = \eta \begin{pmatrix} \beta_1(r,\,\theta) \\ \cos\theta\,\beta_2(r,\,\theta)\,e^{i\phi} \\ \beta_3(r,\,\theta)\,e^{-i\phi} \end{pmatrix}, \tag{6.2a}$$

$$\widehat{\Phi}_2(r,\theta,\phi) = \eta \begin{pmatrix} \beta_4(r,\,\theta)\,e^{-i\phi} \\ \cos\theta\,\beta_5(r,\,\theta) \\ \beta_6(r,\,\theta) \end{pmatrix}, \tag{6.2b}$$

$$\widehat{\Phi}_3(r,\theta,\phi) = \eta \begin{pmatrix} \cos\theta\,\beta_7(r,\,\theta)\,e^{i\phi} \\ \beta_8(r,\,\theta)\,e^{2i\phi} \\ \cos\theta\,\beta_9(r,\,\theta) \end{pmatrix}, \tag{6.2c}$$

with real profile functions $\beta_k(r,\,\theta)$. As for the $\widehat{S}$ in the basic theory, these profile functions have even parity

$$\beta_k(r,\pi-\theta) = +\beta_k(r,\,\theta)\,, \quad \text{for } k = 1,\,\ldots\,,9\,. \tag{6.3}$$

Comparing this *Ansatz* with Eq. (6.1) yields the following boundary conditions towards infinity

$$\lim_{r\to\infty} \begin{pmatrix} \beta_1(r,\,\theta) \\ \beta_2(r,\,\theta) \\ \beta_3(r,\,\theta) \\ \beta_4(r,\,\theta) \\ \beta_5(r,\,\theta) \\ \beta_6(r,\,\theta) \\ \beta_7(r,\,\theta) \\ \beta_8(r,\,\theta) \\ \beta_9(r,\,\theta) \end{pmatrix} = \begin{pmatrix} \cos^2\theta \\ -\sin\theta \\ -\sin\theta \\ -\sin\theta \\ -1 \\ 0 \\ -\sin\theta \\ \sin^2\theta \\ -1 \end{pmatrix}. \tag{6.4}$$

Regularily of the solution at the origin requires

$$\beta_k(0,\theta) = 0, \quad \text{for } k = 1,\ldots,9. \tag{6.5}$$

Finally we find the following boundary conditions on the symmetry axis ($\bar{\theta} = 0, \pi$):

$$\partial_\theta\,\beta_1(r,\,\theta)\,\big|_{\theta=\bar{\theta}} = 0\,, \qquad \text{for } k = 1,\,5,\,6,\,9\,, \tag{6.6a}$$

$$\beta_k(r,\,\theta)\,\big|_{\theta=\bar{\theta}} = \bar{\beta}_k(r)\,\sin\theta\,\big|_{\theta=\bar{\theta}}\,, \quad \text{for } k = 2,\,3,\,4,\,7\,, \tag{6.6b}$$

$$\beta_8(r,\,\theta)\,\big|_{\theta=\bar{\theta}} = \bar{\beta}_8(r)\,\sin^2\theta\,\big|_{\theta=\bar{\theta}}\,. \tag{6.6c}$$

To summarize, the $\widehat{S}$ *Ansatz* in the extended Yang-Mills-Higgs theory has been extended by six profile functions $\beta_k(r,\theta)$ for $k = 4,\ldots,9$, giving a total of 17 profile functions. We can now insert

the above Ansatz into the energy functional (1.12) to obtain the energy density given in App. A.2 and the corresponding reduced field equations, given in App. B.

Solving these reduced field equations close to the origin, as done for the basic Yang-Mills-Higgs theory, yields the following behavior of the profile functions close to the origin

$$\begin{pmatrix} \beta_4(r,\theta) \\ \beta_5(r,\theta) \\ \beta_6(r,\theta) \\ \beta_7(r,\theta) \\ \beta_8(r,\theta) \\ \beta_9(r,\theta) \end{pmatrix} \sim \begin{pmatrix} c_9 r \sin\theta \\ c_{10} r \\ c_{11} r |\cos\theta| \\ c_{12} r^2 \sin\theta \\ c_{13} r^2 \sin^2\theta \\ c_{14} r \end{pmatrix}. \tag{6.7}$$

6.2 Numerical minimization of the energy functional

We now extend the numerical set-up to include the additional fields of the extended Yang-Mills-Higgs theory's *Ansatz*. The profile functions α_i and β_j for $j = 1, 2, 3$ are defined and will be treated numerically as described in Section 5.4. In analogy to Eq. (5.42), we redefine our profile functions under consideration of the profile function behavior at the origin (6.7), towards $x = 1$ (6.4) and on the symmetry axis (6.6) to

$$\begin{pmatrix} \overline{\beta}_4(x,\theta) \\ \overline{\beta}_5(x,\theta) \\ \overline{\beta}_6(x,\theta) \\ \overline{\beta}_7(x,\theta) \\ \overline{\beta}_8(x,\theta) \\ \overline{\beta}_9(x,\theta) \end{pmatrix} = \begin{pmatrix} \beta_4(x,\theta)/[-x\sin\theta] \\ \beta_5(x,\theta)/[-x] \\ \beta_6(x,\theta)/x \\ \beta_7(x,\theta)/[-x^2\sin\theta] \\ \beta_8(x,\theta)/[x^2\sin^2\theta] \\ \beta_9(x,\theta)/[-x] \end{pmatrix}. \tag{6.8}$$

The three remaining boundary conditions on the symmetry axis, which are not directly fulfilled by this redefinition are, for ($\overline{\theta} = 0, \pi$):

$$\partial_\theta \overline{\beta}_j(x,\theta)\Big|_{\theta=\overline{\theta}} = 0 \quad \text{for } j = 5, 6, 9. \tag{6.9}$$

The boundary conditions of the redefined *Ansatz* functions at $x = 1$ are then:

$$\lim_{x\to 1} \begin{pmatrix} \overline{\beta}_4(x,\theta) \\ \overline{\beta}_5(x,\theta) \\ \overline{\beta}_6(x,\theta) \\ \overline{\beta}_7(x,\theta) \\ \overline{\beta}_8(x,\theta) \\ \overline{\beta}_9(x,\theta) \end{pmatrix} = \begin{pmatrix} 1 \\ 1 \\ 0 \\ 1 \\ 1 \\ 1 \end{pmatrix}. \tag{6.10}$$

By analogy with Eq. (5.45), we chose the angular expansion of the redefined *Ansatz* functions as follows

$$\begin{aligned}\overline{\beta}_j(x,\theta) = \frac{h_{j0}(x)}{2} + \sum_{n=1}^{N}\Big[h_{jn}(x)\cos(2n\theta) + q_{jn}(x)\sin((2n-1)\theta)\Big] \\ + \begin{cases} q_{60}(x)\,|\cos\theta|, & \text{for } j=6, \\ 0, & \text{for } j=4,5,7,8,9. \end{cases}\end{aligned} \tag{6.11}$$

Together with boundary conditions at the origin, given by

$$h_{60}(0) = 0, \tag{6.12a}$$

$$h_{jn}(0) = q_{jn}(0) = 0, \quad \text{for } n>0, \tag{6.12b}$$

the profile functions behave precisely as (6.7) close to the origin. The boundary conditions (6.10) at $x=1$ demand the following asymptotic behavior of the radial functions $h(x)$ and $q(x)$

$$h_{jn}(1) = \begin{pmatrix} 2 & 2 & 0 & 2 & 2 & 2 \\ 0 & 0 & 0 & 0 & 0 & 0 \end{pmatrix}, \quad \text{for } j=4,\ldots,9 \text{ and } n\in[0,1], \tag{6.13a}$$

$$h_{jn}(1) = 0, \qquad \text{for } n>1, \tag{6.13b}$$

$$q_{jn}(1) = 0, \qquad \text{for } n\geq 0. \tag{6.13c}$$

Finally, the symmetry axis boundary conditions (6.9) are enforced by fixing the radial profile functions q_{51}, q_{61} and q_{91} to satisfy the following equations

$$\sum_{n=1}^{N}(2n-1)q_{jn} = 0, \qquad \text{for } j=5,6,9. \tag{6.14}$$

Turning to the radial approximation, we now expand the radial functions in Legendre polynomials $P_m(2x-1)$:

$$h_{jn}(x) = x^2\sum_{m=0}^{M} b_{jnm}P_m(2x-1) + \begin{cases} 2e_{j+5}, & \text{for } j=4,5,7,8,9 \text{ and } n=0, \\ 0, & \text{for } j=6 \text{ or } n>0, \end{cases} \tag{6.15a}$$

$$q_{jn}(x) = x^2\sum_{m=0}^{M} d_{jnm}P_m(2x-1) + \begin{cases} e_{11}, & \text{for } j=6 \text{ and } n=0, \\ 0, & \text{for } n>0, \end{cases} \tag{6.15b}$$

with x^2 pre-factors, that ensure the origin behavior, as before. The boundary conditions (6.13) at $x=1$ are now fixed by adjusting, for each radial function expansion, one expansion coefficient,

to satisfy

$$\sum_{m=0}^{M} b_{jnm} = h_{jn}(1) - \begin{cases} 2e_{j+5}, & \text{for } j = 4,5,7,8,9 \text{ and } n = 0, \\ 0, & \text{for } j = 6 \text{ or } n > 0, \end{cases} \tag{6.16a}$$

$$\sum_{m=0}^{M} d_{jnm} = q_{jn}(1) - \begin{cases} e_{11}, & \text{for } j = 6, \text{ and } n = 0, \\ 0, & \text{for } n > 0. \end{cases} \tag{6.16b}$$

The total number of coefficients to minimize over at a given radial (M) and angular (N) expansion cut-off increases to

$$N_{\text{coeff}} = 14 + \Big[17(2N+1) - 5\Big]M \xrightarrow{N,M\to\infty} 34NM. \tag{6.17}$$

6.2.1 Numerical results

This section gives details on the obtained results from numeric minimization of the energy functional of the extended Yang-Mills-Higgs theory. Using $\chi = 1.5$ and $\lambda/g^2 = 1$, we obtain the energy values given in Tab. 6.1 for various expansion order cut-offs. From this table we take the value of the $\widehat{S}$ energy in the extended Yang-Mills-Higgs theory

$$E_{\widehat{S}}^{\text{ext. SU(3) YMHth, } \lambda/g^2=1} = (8.50 \pm 0.03) \left[\frac{4\pi\eta}{g}\right]. \tag{6.18}$$

Similar to the $\widehat{S}$ in the basic Yang-Mills-Higgs theory, the error is estimated by variation of grid size and expansion order. Furthermore, we give the total energy contribution of the $(M,N) = (11,3)$ configuration up to various radii gvR in Table 6.2, the largest contribution coming from around $gvr = 1.5$. Among the energy density constituents as listed in App. A.2, the total energy is distributed as follows: $E_{\text{YM}} : E_{\text{Hkin}} : E_{\text{Hpot}} \approx 0.532 : 0.384 : 0.084$.

M	N	$E\,[4\pi\eta/g]$
3	1	8.627
6	1	8.527
6	2	8.526
11	2	8.506
11	3	8.503

Table 6.1: Energy of configurations obtained from minimization at various expansion cut-offs (M,N), using $\chi = 1.5$ and $\lambda/g^2 = 1$.

gvR	E_R/E_∞
0.3	0.0125
0.6	0.0719
0.9	0.1923
1.2	0.3574
1.5	0.5252
1.8	0.6785
2.1	0.7840
2.4	0.8649
2.7	0.9120
3.0	0.9449
4.0	0.9870
5.0	0.9958
6.0	0.9979

Table 6.2: Total energy contribution up to a radius gvR, of the numerical $\widehat{S}$ solution in the extended $SU(3)$ Yang-Mills-Higgs theory for $\lambda/g^2 = 1$ and $v = \sqrt{2}\eta$, obtained from minimization with expansion cutoffs $N = 3$ and $M = 11$ using $\chi = 3/2$. We give the contribution as a quotient with the total energy E_∞ (given in Tab. 6.1), with $E_R = \int_0^R dr \int_0^{\pi/2} d\theta \; r^2 \sin\theta \; \widehat{e}(r,\theta)$.

Figs. 6.1 and 6.2 show the re-scaled profile functions, defined by Eq. (5.55) and extended by the following:

$$\begin{pmatrix} \widehat{\beta}_4(x,\theta) \\ \widehat{\beta}_5(x,\theta) \\ \widehat{\beta}_6(x,\theta) \\ \widehat{\beta}_7(x,\theta) \\ \widehat{\beta}_8(x,\theta) \\ \widehat{\beta}_9(x,\theta) \end{pmatrix} = \begin{pmatrix} \beta_4(x,\theta)/[-\sin\theta] \\ -\beta_5(x,\theta) \\ \beta_6(x,\theta) \\ \beta_7(x,\theta)/[-\sin\theta] \\ \beta_8(x,\theta)/[\sin^2\theta] \\ -\beta_9(x,\theta) \end{pmatrix}, \tag{6.19}$$

for the configuration obtained at $(M, N) = (11, 3)$. With all Yang-Mills modes massive, these profile functions appear to have converged very well, also in the far-field. The obtained solution for $\widehat{\beta}_6$ is almost zero and indeed, it has been shown [13], that $\beta_6 = 0$ does solve the variational equations given in App. B.

The energy density corresponding to the $(M, N) = (11, 3)$ configuration is shown for slices of various θ in Fig. 6.4 and as a contour plot in Euclidean space for $y = 0$ in Fig. 6.3.

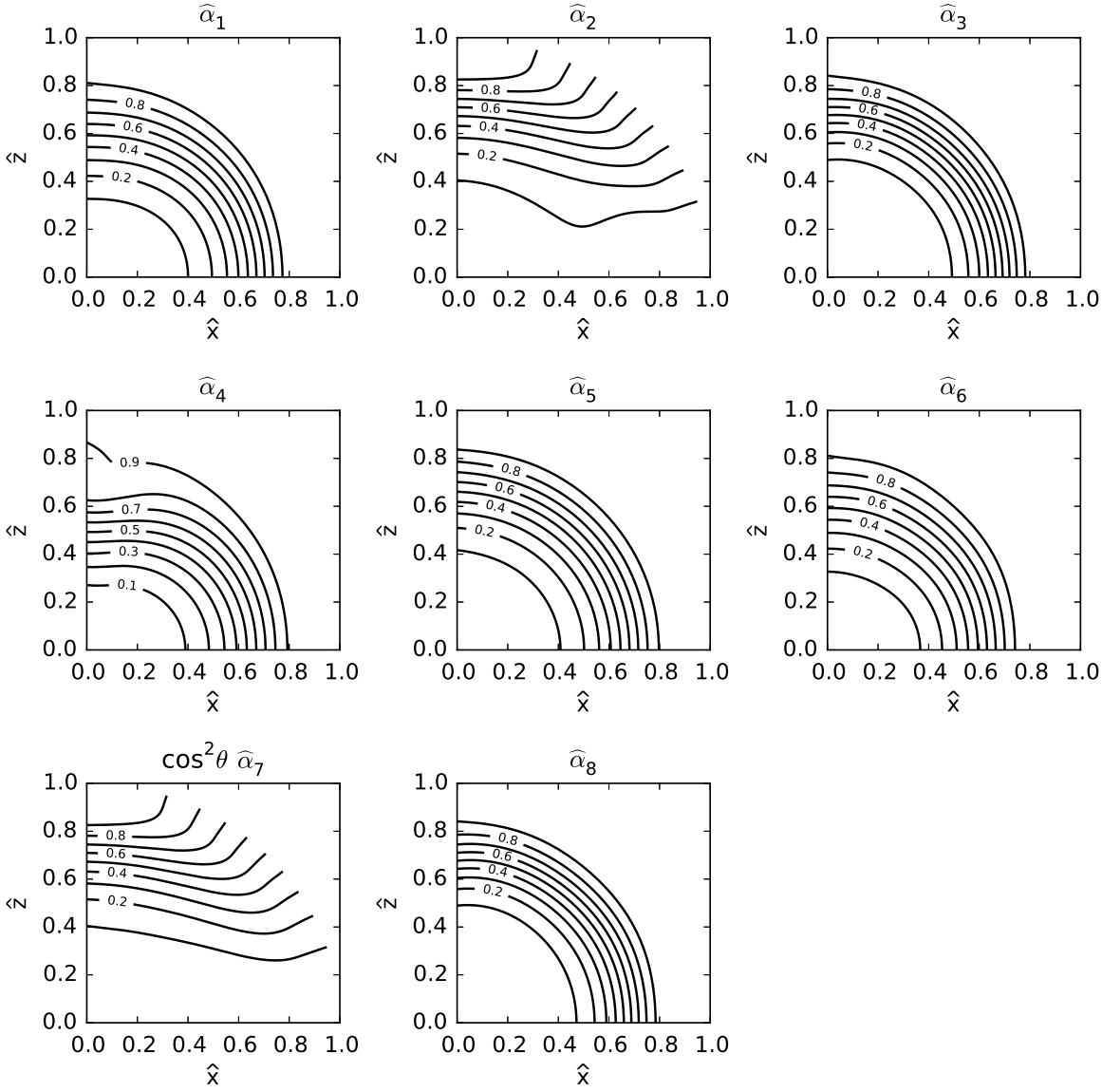

Figure 6.1: Equidistant contour-plots of the re-scaled profile functions $\widehat{\alpha}_i$ of the configuration obtained from minimization of the extended Yang-Mills-Higgs theory energy functional at $(M, N) = (11, 3)$ for $\lambda/g^2 = 1$ and $\chi = 1.5$. The two coordinates are given by $\widehat{x} = gvr/(gvr + 1.5)\ \sin\theta$ and $\widehat{z} = gvr/(gvr + 1.5)\ \cos\theta$.

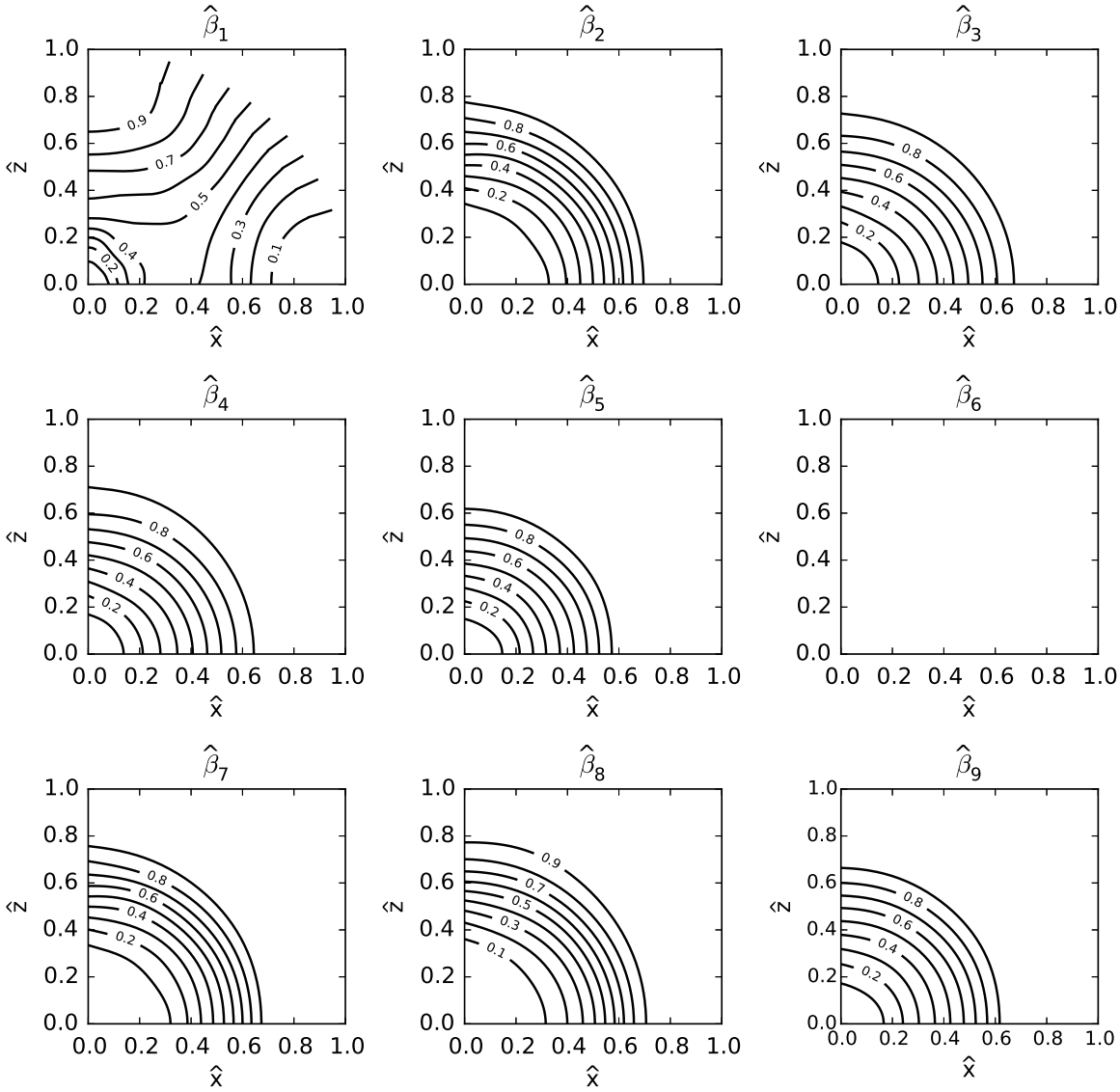

Figure 6.2: Same as Fig. 6.1, but for profile functions $\widehat{\beta}_k(x, \theta)$. The obtained numerical result for $\widehat{\beta}_6$ is almost zero ($|\widehat{\beta}_6| \leq 3 \times 10^{-4}$).

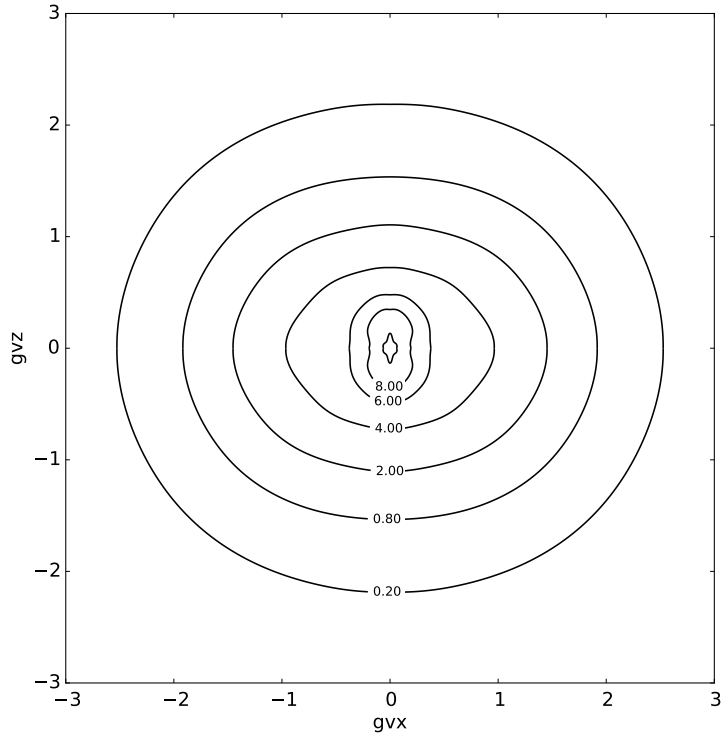

Figure 6.3: Energy density contours of the configuration obtained from $(M, N) = (11, 3)$ minimization of the extended Yang-Mills-Higgs theory energy functional, for $\lambda/g^2 = 1$, $v = \sqrt{2} \times \eta$ and $\chi = 2.5$. The slice is in Euclidean space for $gvy = 0$. The contour around $(gvx, gvz) = (0, 0)$ has the value $8.00\,[(4\pi g/g)(gv)^3]$.

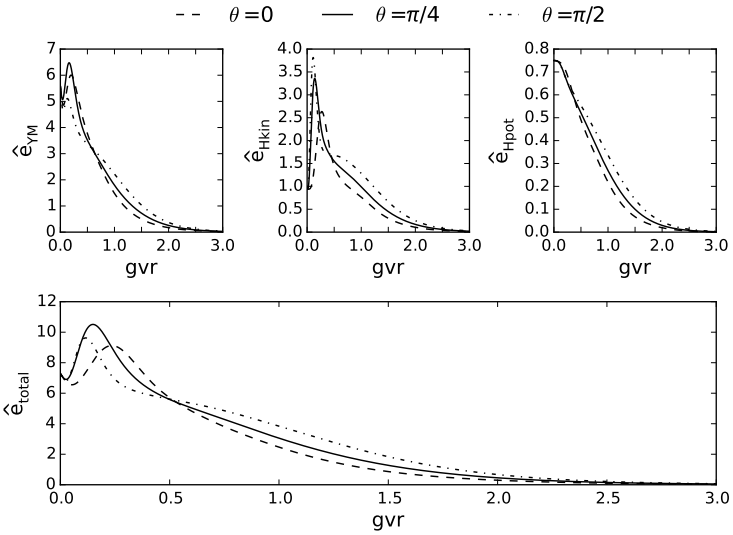

Figure 6.4: Slices of energy density constituents for the configuration obtained from $(M, N) = (11, 3)$ minimization of the extended Yang-Mills-Higgs theory energy functional, for $\lambda/g^2 = 1$ and $\chi = 1.5$.

CHAPTER 7

$\hat{S}$ energy barrier structure

We will now take a first step towards determining the stability of the $\widehat{S}$, by evaluating the energy of field configurations along paths on the non-contractible sphere (NCS), connecting the gauge-field vacuum and the $\widehat{S}$. Ultimately, a stability analysis is focused on determining if there exists a path from the $\widehat{S}$ configuration to the vacuum, crossing only configurations of energy below $E_{\widehat{S}}$. If such a path exists, the $\widehat{S}$ is unstable. The much harder task of showing (meta-)stability is to prove, that no such path exists. This last task can not be done by mere inspection of the $\widehat{S}$ energy barrier, since the path one is trying to rule out need not be on the NCS, but could be located in a different sector of configuration space entirely. Hence, the energy barrier analysis conducted in this chapter can give us conclusive evidence of instability, if a path of instability happens to lie on the NCS, but can only give hints at a possible (meta-)stability of the $\widehat{S}$.

To determine the energy of any configuration on the NCS, let us start by recalling that Yang-Mills fields on the NCS must approach the following pure-gauge toward spatial infinity:

$$\lim_{r\to\infty} A_i(r,\theta,\phi) = -\frac{1}{g}\partial_i U(\psi,\mu,\alpha,\theta,\phi)\; U^{-1}(\psi,\mu,\alpha,\theta,\phi), \tag{7.1}$$

where the map U, given by Eq. (2.8) with parametrization (2.49), is now not fixed to $\psi = \mu = \alpha = \pi/2$ as before, but is left completely free. To avoid confusion regarding the NCS angles ψ, μ and α, let us recall that these are not the angles of the same notation used in Ref. [4] (which are in this work referred to as $\tilde{\psi}$, $\tilde{\mu}$ and $\tilde{\alpha}$), but the coordinates introduced in Section 2.3. These angles are all on equal footing, in the sense that choosing either one of them to be zero yields the map at the "bottom" of the NCS and to obtain the map at the "top" of the NCS all angles need to be $\pi/2$. Similarly, the Higgs fields on the NCS must feature the asymptotic behavior

$$\lim_{r\to\infty} \Phi(r,\theta,\phi) = \frac{v}{\sqrt{2}}\, U(\psi,\mu,\alpha,\theta,\phi) \begin{pmatrix} 1 \\ 0 \\ 0 \end{pmatrix}, \tag{7.2}$$

in the basic Yang-Mills-Higgs theory and the behavior given by

$$\lim_{r\to\infty} \Phi_1(r,\theta,\phi) = \eta\, U(\psi,\mu,\alpha,\theta,\phi) \begin{pmatrix} 1 \\ 0 \\ 0 \end{pmatrix}, \tag{7.3a}$$

$$\lim_{r\to\infty} \Phi_2(r,\theta,\phi) = \eta\, U(\psi,\mu,\alpha,\theta,\phi) \begin{pmatrix} 0 \\ 0 \\ -1 \end{pmatrix}, \tag{7.3b}$$

$$\lim_{r\to\infty} \Phi_3(r,\theta,\phi) = \eta\, U(\psi,\mu,\alpha,\theta,\phi) \begin{pmatrix} 0 \\ 1 \\ 0 \end{pmatrix}, \tag{7.3c}$$

in the extended Yang-Mills-Higgs theory.

At this moment it should be pointed out, that configurations on the NCS in general have fewer symmetries than the $\widehat{S}$ configuration:
First of all, the reflection symmetry (5.22) of the *Ansatz* is lost. Thus we will have to numerically integrate over the full polar angle $\theta \in [0,\pi]$. As a further consequence of this, the fields are no longer necessarily of positive parity and a general expansion for the profile functions would have to use the complete Fourier basis (even and odd basis functions).
Second, the fields can (for most of the NCS) no longer be constructed with just a subset of $SU(3)$ generators. We need all eight generators for each component of A_i, resulting in sixteen instead of eight α_i profile functions for a fixed gauge.
Third and by far the most dramatic is the loss of axial symmetry (5.18). A general *Ansatz* for fields on the NCS would therefore contain profile functions depending also on the azimuthal angle ϕ. There exists one exceptional path on the NCS however, along which axial symmetry remains intact. It is parametrized by varying $\alpha \in [0,\pi]$, while fixing $\psi = \mu = \pi/2$ and can be attributed to the following symmetry:

$$\left[\partial_\phi U(\psi,\mu,\alpha,\theta,\phi) + \frac{i}{2} \left\{ \lambda_3 - \sqrt{3}\lambda_8 \,,\; U(\psi,\mu,\alpha,\theta,\phi) \right\} \right]_{\psi=\mu=\pi/2} = 0. \tag{7.4}$$

On the other hand, we manage to find a new simplifying symmetry, namely the following reflection symmetry of the energy density

$$\widehat{e}(\psi,\mu,\alpha) = \widehat{e}(\pi-\psi,\mu,\alpha) = \widehat{e}(\psi,\pi-\mu,\alpha) = \widehat{e}(\psi,\mu,\pi-\alpha) \tag{7.5}$$

on planes intersecting vacuum and $\widehat{S}$ on the NCS, obtained by fixing two of the three NCS angles to $\pi/2$. We did not manage to explain this symmetry in the context of a simple constant unitary transformation such as (5.22), however, the structure functions of the generalized *Ansatz*, which we will introduce shortly, are invariant under this symmetry and so it is clear, that the energy density must be as well.

We will now make a generalized *Ansatz* for the Yang-Mills fields on the NCS, which features the extension to eight $SU(3)$ generators for each field component. This is necessary to match the required aymptotic behavior at spatial infinity. We are not interested in making this *Ansatz* as

general as possible, merely in having it be general enough to construct a finite energy vacuum-vacuum path on the NCS through the $\widehat{S}$ configuration obtained in Section 5.4. The following *Ansatz* does precicely that, it yields finite energy field configurations anywhere on the NCS and reduces to the *Ansatz* of [4], given by Eq. 5.20 for $\psi = \mu = \alpha = \pi/2$:

$$g\widehat{A}_0(r,\omega) = g\hat{A}_r(r,\omega) = 0 \tag{7.6a}$$

$$\begin{aligned} g\widehat{A}_\phi(r,\omega) &= \alpha_{12}(r,\theta)\,\Gamma_{A_\phi,1}(\omega)T_\phi + \alpha_1(r,\theta)\,\Gamma_{A_\phi,2}(\omega)T_\rho + \alpha_{13}(r,\theta)\,\Gamma_{A_\phi,3}(\omega)V_\phi \\ &+ \alpha_2(r,\theta)\,\Gamma_{A_\phi,4}(\omega)V_\rho + \alpha_{14}(r,\theta)\,\Gamma_{A_\phi,5}(\omega)U_\phi + \alpha_3(r,\theta)\,\Gamma_{A_\phi,6}(\omega)U_\rho \\ &+ \alpha_4(r,\theta)\,\Gamma_{A_\phi,7}(\omega)\frac{\lambda_3}{2i} + \alpha_5(r,\theta)\,\Gamma_{A_\phi,8}(\omega)\frac{\lambda_8}{2i}, \end{aligned} \tag{7.6b}$$

$$\begin{aligned} g\widehat{A}_\theta(r,\omega) &= \alpha_6(r,\theta)\,\Gamma_{A_\theta,1}(\omega)T_\phi + \alpha_{15}(r,\theta)\,\Gamma_{A_\theta,2}(\omega)T_\rho + \alpha_7(r,\theta)\,\Gamma_{A_\theta,3}(\omega)V_\phi \\ &+ \alpha_{16}(r,\theta)\,\Gamma_{A_\theta,4}(\omega)V_\rho + \alpha_8(r,\theta)\,\Gamma_{A_\theta,5}(\omega)U_\phi + \alpha_{17}(r,\theta)\,\Gamma_{A_\theta,6}(\omega)U_\rho \\ &+ \alpha_{18}(r,\theta)\,\Gamma_{A_\theta,7}(\omega)\frac{\lambda_3}{2i} + \alpha_{19}(r,\theta)\,\Gamma_{A_\theta,8}(\omega)\frac{\lambda_8}{2i}, \end{aligned} \tag{7.6c}$$

with matrices T_ϕ, T_ρ, V_ϕ, V_ρ, U_ϕ and U_ρ given by (5.19). We used here the short-hand notation $\omega = \{\psi, \mu, \alpha, \theta, \phi\}$. The real valued structure functions $\Gamma_{A_\phi,i}(\omega)$ and $\Gamma_{A_\theta,i}(\omega)$, for $i = 1, \ldots, 8$, are determined by matching the field *Ansatz* (7.6) at spatial infinity to the pure gauge fields (7.1). These structure functions are very lengthly and are not given explicitly at this point (see App. C for more details on their derivation).

The newly introduced profile functions α_i, for $i = 12, \ldots, 19$, can be chosen arbitrarily, since the sphaleron configuration is independent of them[1]. They have the following boundary conditions

$$\alpha_i(0,\theta) = 0, \quad \lim_{r\to\infty} \alpha_i(r,\theta) = 1, \qquad \text{for } i = 12, \ldots, 19, \tag{7.7}$$

and we will simply choose them to be

$$\alpha_i(r,\theta) = \left(\frac{r}{1+r}\right)^2, \qquad \text{for } i = 12, \ldots, 19. \tag{7.8}$$

There is one technical detail, which stops us from using the profile functions α_i ($i = 1, \ldots, 8$) of the (e.g. $(M, N) = (18, 3)$) configurations obtained from minimization of the basic and extended Yang-Mills-Higgs theory energy functionals in Sections 5.4 and 6.2, respectively. Finiteness of energy requires an additional boundary condition on two of the profile functions for configurations away from the NCS poles, namely:

$$\alpha_2(r,\theta)\big|_{\theta=\pi/2} = \beta_1(r,\theta)\big|_{\theta=\pi/2} = 0. \tag{7.9}$$

Hence, we need to repeat the minimization procedures detailed in Section 5.4 for the basic Yang-

[1] The corresponding structure functions vanish at the NCS poles.

Mills-Higgs theory and in Section 6.2 for the extended Yang-Mills-Higgs theory, with these conditions in place. We enforce them by pulling out a $\cos^2\theta$ pre-factor in the expansion for these two profile functions, removing said factor from their boundary conditions at infinity[2].

For the basic Yang-Mills-Higgs theory, as expected from a more constrained profile function expansion, the energy of $E_{\widehat{S}} \approx 1.81\ [4\pi v/g]$, obtained from minimization at $(M, N) = (11, 3)$, is larger than the value obtained in Section 5.4 at the same cut-off.

For the extended Yang-Mills-Higgs theory, we obtain a value of $E_{\widehat{S}} \approx 6.0\ [4\pi v/g]$ for $(M, N) = (11, 3)$, using $\lambda/g^2 = 1$, which is only a minor increase.

We will now split up our analysis into basic and extended Yang-Mills-Higgs theory, in order to generalize their respective Higgs field *Ansätze* and finally inspect their energy barriers individually.

7.1 Basic $SU(3)$ Yang-Mills-Higgs theory

We generalize the Higgs field components in the basic Yang-Mills-Higgs theory as follows:

$$\widehat{\Phi}(r,\omega) = \frac{v}{\sqrt{2}}\Bigg[\beta_1(r,\theta)\Big(\Gamma_{\Phi,1}(\omega) + i\Gamma_{\Phi,2}(\omega)\Big)\lambda_3 + \beta_2(r,\theta)\Big(\Gamma_{\Phi,3}(\omega) + i\Gamma_{\Phi,4}(\omega)\Big)2iT_\rho + \beta_3(r,\theta)\Big(\Gamma_{\Phi,5}(\omega) + i\Gamma_{\Phi,6}(\omega)\Big)2iV_\rho\Bigg]\begin{pmatrix}1\\0\\0\end{pmatrix}, \tag{7.10}$$

with real structure functions $\Gamma_{\Phi,i}(\omega)$ $(i = 1, \ldots, 6)$, which are obtained by matching the field's asymptotic behavior at spatial infinity. These structure functions are given explicitly in App. C. The profile functions β_j $(j = 1, 2, 3)$ are those obtained from minimization in the previous section.

We can now simply insert the Yang-Mills and Higgs fields into the basic Yang-Mills-Higgs theory energy functional for any choice of ψ, μ and α, integrate numerically over x, θ and ϕ and obtain the energy value at that point on the NCS.

We will look at three possible gauge-field vacuum to gauge-field vacuum paths through configuration space, each crossing the $\widehat{S}$. On the NCS they are parametrized by fixing two of the three NCS angles to $\pi/2$ and varying the third from 0 to π. Since these paths are orthogonal at the "top" of the NCS[3], this gives us a significant hint at the energy barrier structure. The slice parametrized by α is of particular interest. Due to the axial symmetry (7.4) of configurations on it, it is expected to feature the lowest energy path of the three.

The energy barrier of each of the three slices, is approximated for 250 equally spaced points between 0 and $\pi/2$. Fig. 7.1 shows the obtained energy structure along each of the slices, mirrored on the symmetry axis $\psi/\mu, \alpha = \pi/2$, utilizing (7.5). We can clearly identify a local minimum of the energy at the $\widehat{S}$ configuration in these one dimensional projections.

We also notice an equality of energy barriers for the slices parametrized by ψ and μ. Upon closer inspection we find, that the energy is not only invariant under exchange of ψ and μ, but that there exists a continuous symmetry, which can be well visualized by looking at Figs. 2.1a

[2] All other steps of the minimization procedures remain the same.

[3] This is a consequence of the explicit parametrization of the map U, derived in Section 2.3.

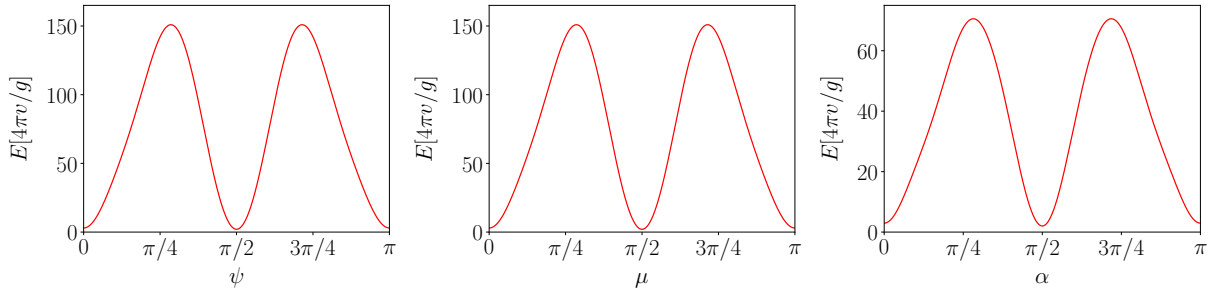

(a) $\mu = \alpha = \pi/2$ (b) $\psi = \alpha = \pi/2$ (c) $\psi = \mu = \pi/2$

Figure 7.1: Numerical approximation of three energy barrier slices connecting the vacuum configuration and the $\widehat{S}$ configuration of the basic Yang-Mills-Higgs theory, obtained from minimization at expansion order cut-offs $(M, N) = (11, 3)$, using $\lambda/g^2 = 0$. Slices for $\psi = \alpha = \pi/2$ and $\mu = \alpha = \pi/2$ are similar. The NCS angles ψ, μ and α are not the angles of the same notation used in Ref. [4] (which are in this work referred to as $\tilde{\psi}$, $\tilde{\mu}$ and $\tilde{\alpha}$), but the coordinates introduced in Section 2.3.

and 2.1b. The energy remains invariant under a rotation around the axis connecting gauge-field vacuum and the NCS "top" on the $\mathbb{S}^2$ obtained from the NCS depicted in Fig. 2.1b for fixed $\alpha = \pi/2$. This rotation is parametrized simply by $\tilde{\alpha}$ of the coordinates used by Klinkhamer and Rupp [4] and the invariance of the energy under this transformation has already previously been found [33]. The structure functions and hence the energy density in these coordinates (both given in the appendix of [33]) feature $\tilde{\alpha}$ and ϕ only in terms of $\sin^n(\phi - \tilde{\alpha})$ and $\cos^n(\phi - \tilde{\alpha})$. As a result, the energy density is not invariant under the rotation[4], but the energy obtained by integration over $\phi \in [0, 2\pi]$ is[5].

Finally, it is important to point out, that the configuration at the bottom of the NCS we have constructed here is merely the gauge-field vacuum ($E_{\text{YM}} = 0$) not the vacuum of the full theory. As a result, the plotted energy slices of configurations of the NCS do not go to $E = 0$.

[4]This explains, why there exists no symmetry such as (7.4) for $\tilde{\alpha}$.

[5]This can easily be seen by substituting $\phi' = \phi - \tilde{\alpha}$ and carrying out the integral over the full circle, which is always independent of $\tilde{\alpha}$.

7.2 Extended $SU(3)$ Yang-Mills-Higgs theory

To determine the barrier structure of the $\widehat{S}$ in the extended Yang-Mills-Higgs theory, we must also generalize the extended *Ansatz*:

$$\begin{aligned}\widehat{\Phi}_1(r,\omega) &= \eta\Bigg[\beta_1(r,\theta)\Big(\Gamma_{\Phi,1}(\omega)+i\Gamma_{\Phi,2}(\omega)\Big)\lambda_3+\beta_2(r,\theta)\Big(\Gamma_{\Phi,3}(\omega)+i\Gamma_{\Phi,4}(\omega)\Big)2iT_\rho \\ &\quad +\beta_3(r,\theta)\Big(\Gamma_{\Phi,5}(\omega)+i\Gamma_{\Phi,6}(\omega)\Big)2iV_\rho\Bigg]\begin{pmatrix}1\\0\\0\end{pmatrix}, \qquad (7.11a)\end{aligned}$$

$$\begin{aligned}\widehat{\Phi}_2(r,\omega) &= \eta\Bigg[\beta_4(r,\theta)\Big(\Gamma_{\Phi,7}(\omega)+i\Gamma_{\Phi,8}(\omega)\Big)\lambda_3+\beta_5(r,\theta)\Big(\Gamma_{\Phi,9}(\omega)+i\Gamma_{\Phi,10}(\omega)\Big)2iT_\rho \\ &\quad +\beta_6(r,\theta)\Big(\Gamma_{\Phi,11}(\omega)+i\Gamma_{\Phi,12}(\omega)\Big)2iV_\rho\Bigg]\begin{pmatrix}1\\0\\0\end{pmatrix}, \qquad (7.11b)\end{aligned}$$

$$\begin{aligned}\widehat{\Phi}_3(r,\omega) &= \eta\Bigg[\beta_7(r,\theta)\Big(\Gamma_{\Phi,13}(\omega)+i\Gamma_{\Phi,14}(\omega)\Big)\lambda_3+\beta_8(r,\theta)\Big(\Gamma_{\Phi,15}(\omega)+i\Gamma_{\Phi,16}(\omega)\Big)2iT_\rho \\ &\quad +\beta_9(r,\theta)\Big(\Gamma_{\Phi,17}(\omega)+i\Gamma_{\Phi,18}(\omega)\Big)2iV_\rho\Bigg]\begin{pmatrix}1\\0\\0\end{pmatrix}, \qquad (7.11c)\end{aligned}$$

with the added real structure functions $\Gamma_{\Phi,i}$, for $i=7,\ldots,18$, given explicitly in App. C. The profile functions $\beta_j(r,\theta)$ $(j=4,5,7,8,9)$ are those obtained from minimization in the parent section. Let us recall, that the boundary conditions of $\beta_6(r,\theta)$ at the "top" of the NCS vanish at the origin and towards infinity and that we have found the numerical solution of the $\widehat{S}$ to have an almost vanishing $\beta_6(r,\theta)$ everywhere (see Section 6.2.1). However, setting $\beta_6(r,\theta)$ to vanish leads to an ill-defined energy density at infinity for many configurations on the NCS. To resolve this problem, we absorb the boundary condition of $\beta_6(r,\theta)$ into the structure functions $\Gamma_{\Phi,11}(\omega)$ and $\Gamma_{\Phi,12}(\omega)$ of the extended *Ansatz* (7.11). The configuration at the "top" of the NCS remains unchanged by this, since $\beta_6(r,\theta)$ was found to vanish there regardless. We are now free to choose an arbitrary $\beta_6(r,\theta)$, which satisfies the new boundary condition $\lim_{r\to\infty}\beta_6(r,\theta)=1$:

$$\beta_6(r,\theta)=\left(\frac{r}{1+r}\right)^2. \qquad (7.12)$$

The rest of the procedure is entirely parallel to that of the basic Yang-Mills-Higgs theory, as outlined in the previous section. Likewise, we depict in Fig. 7.2 the three $\widehat{S}$ energy barrier slices obtained from fixing two NCS angles to $\pi/2$ and varying the third. In contrast to the $\widehat{S}$ in the

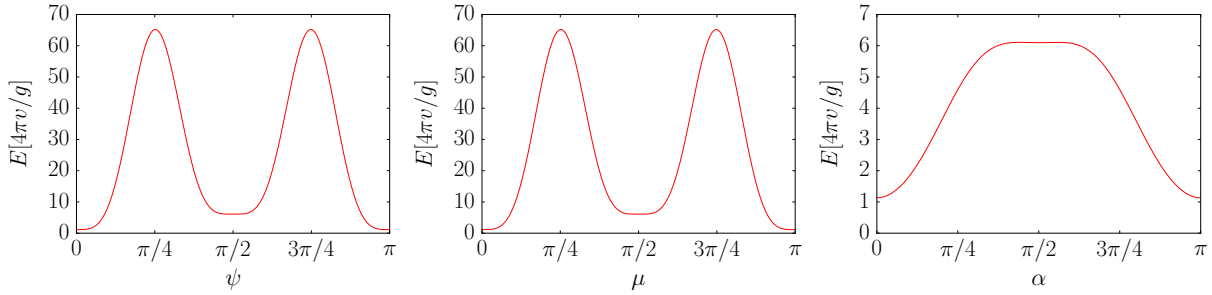

(a) $\mu = \alpha = \pi/2$ (b) $\psi = \alpha = \pi/2$ (c) $\psi = \mu = \pi/2$

Figure 7.2: Numerical approximation of a negative-mode energy barrier slice connecting the vacuum configuration and the $\widehat{S}$ configuration of the extended Yang-Mills-Higgs theory, obtained from minimization at expansion order cut-offs $(M, N) = (11, 3)$, using $\lambda/g^2 = 1$. The NCS angles ψ, μ and α are not the angles of the same notation used in Ref. [4] (which are in this work referred to as $\tilde{\psi}$, $\tilde{\mu}$ and $\tilde{\alpha}$), but the coordinates introduced in Section 2.3.

basic Yang-Mills-Higgs theory, we find that the slice parametrized by α, while fixing $\psi = \mu = \pi/2$, does not feature a "dip".

Hence, we have found a path in configuration space connecting gauge-field vacuum and $\widehat{S}$, with all of its configuration's energies below $E_{\widehat{S}}$, indicating instability of the $\widehat{S}$ in the extended Yang-Mills-Higgs theory.

CHAPTER 8

Conclusion and outlook

The numerical analysis conducted in this thesis has yielded solutions of the reduced field equations of the sphaleron $\widehat{S}$ in $SU(3)$ Yang-Mills-Higgs theories, with both a single and three Higgs triplets. We have determined the behavior of both solutions on all four boundaries analytically and obtained numerical approximations of acceptable precision. As confirmed by our independent calculation, the Yang-Mills-Higgs field equations with the $\widehat{S}$ *Ansatz* inserted, reduce to precisely these reduced field equations, making the obtained solutions solutions of the full Yang-Mills-Higgs equations as well. A significant numerical challenge was the tendency of the basic $\widehat{S}$ gauge fields to approach their asymptotic values at infinity very slowly, most likely due to the massless gauge-field modes.

Both solutions are found to have energies of the same order as the embedded $SU(2) \times U(1)$ sphaleron S. Surprisingly, the energy of the $\widehat{S}$ in the basic Yang-Mills-Higgs theory even lies slightly below that of the embedded $SU(2) \times U(1)$ sphaleron S, perhaps due to the even distribution of the azimuthal and polar gauge fields over the Lie algebra [13]. Indications of an energy below E_S were first obtained in Ref. [19] and later in Refs. [32][33].

We have determined the energy barrier structure of the $\widehat{S}$ in both basic and extended theory and observed a clear discrepancy. The solution in the extended theory is found to have two positive and a single negative mode, is therefore unstable and sphaleron-like. In contrast to this, the obtained $\widehat{S}$ configuration in the basic theory has three positive modes and appears to lie in a local energy minimium of the configuration sub-space of the NCS. This indicates, that the $\widehat{S}$ in the basic theory could perhaps be meta-stable. To determine its stability, a far more elaborate analysis considering the full configuration space around the $\widehat{S}$ would have to be carried out. This could for instance be done by solving the fluctuation equations around the configuration.

The gauge fields of the extended theory $\widehat{S}$ may contribute significantly to the content of QCD glueballs [13]. Defining a "gluon mass" of $m_{\text{gl}} \sim (\text{fm})^{-1} \sim 200\,\text{MeV}$ and a "gluon fine-structure constant" $\alpha_{\text{gl}} \sim \alpha_s(200\,\text{MeV}) \sim 1$, a rough estimate of the $\widehat{S}$ energy in a QCD context can be made [13]: $E_{\widehat{S}} \sim 8.5 \times 200\,\text{MeV} \sim 1.7\,\text{GeV}$. Considering the ratio of energy distribution among gauge and Higgs fields, the $\widehat{S}$ gauge fields, which may contribute to the field content of QCD

glueballs, have an energy of roughly 0.8 GeV.

There is much research that remains to be done on the $\widehat{S}$ solution. An analysis to determine its stability, in essence determining the energy Hessian in configuration space at the $\widehat{S}$, seems to be the logical next step following the conducted barrier analysis. Furthermore, it is certainly of interest to obtain the fermion zero-modes, which could only be determined on the boundary thus far. Finally, the truly challenging task is the $\widehat{S}$ phenomenology, be it in a QCD or a grand-unified-theory context. Perhaps it is even possible to make predictions for heavy ion colliders such as the RHIC or give a more fundamental understanding of certain lattice QCD results and observations in the nonperturbative regime of QCD.

APPENDIX A

Energy density of the $\widehat{S}$ *Ansatz*

A.1 Basic $SU(3)$ Yang-Mills-Higgs theory

The energy density of the generalized *Ansatz* given by Eqs. (5.20) and (5.25) is given below. The gauge has been fixed to radial gauge ($\alpha_9 = \alpha_{10} = \alpha_{11} = 0$). The following is equivalent to the energy density given in the appendix of [4].

$$
\begin{aligned}
e_{YM} = & \frac{1}{2g^2r^2\sin^2\theta}\Big\{ \cos^2\theta\,(\partial_r\alpha_1)^2 + (\partial_r\alpha_2)^2 + \cos^2\theta\,(\partial_r\alpha_3)^2 + (\partial_r\alpha_4)^2 + (\partial_r\alpha_5)^2 \Big\} \\
& + \frac{1}{2g^2r^2}\Big\{ (\partial_r\alpha_6)^2 + \cos^2\theta\,(\partial_r\alpha_7)^2 + (\partial_r\alpha_8)^2 \Big\} \\
& + \frac{1}{2g^2r^4\sin^2\theta}\Bigg\{ \Big[\alpha_6 - \frac{1}{2}\alpha_2\alpha_8 + \alpha_4\alpha_6 - \frac{1}{2}\cos^2\theta\alpha_3\alpha_7 + \partial_\theta\left(\cos\theta\alpha_1\right)\Big]^2 \\
& + \Big[\cos\theta\alpha_7 + \frac{1}{2}\cos\theta\left(\alpha_3\alpha_6 - \alpha_1\alpha_8 - \sqrt{3}\alpha_5\alpha_7 - \alpha_4\alpha_7\right) - \partial_\theta\alpha_2\Big]^2 \\
& + \Big[2\alpha_8 + \frac{1}{2}\alpha_4\alpha_8 - \frac{1}{2}\alpha_2\alpha_6 - \frac{1}{2}\sqrt{3}\alpha_5\alpha_8 - \frac{1}{2}\cos^2\theta\alpha_1\alpha_7 - \partial_\theta\left(\cos\theta\alpha_3\right)\Big]^2 \\
& + \Big[\cos\theta\left(\alpha_1\alpha_6 + \frac{1}{2}\alpha_2\alpha_7 - \frac{1}{2}\alpha_3\alpha_8\right) - \partial_\theta\alpha_4\Big]^2 \\
& + \Big[\frac{\sqrt{3}}{2}\cos\theta\left(\alpha_3\alpha_8 + \alpha_2\alpha_7\right) - \partial_\theta\alpha_5\Big]^2\Bigg\},
\end{aligned}
\tag{A.1}
$$

$$
\begin{aligned}
e_{Hkin} = & \frac{v^2}{2}\Big\{ (\partial_r\beta_1)^2 + \cos^2\theta\,(\partial_r\beta_2)^2 + (\partial_r\beta_3)^2 \Big\} \\
& + \frac{v^2}{2r^2}\Big\{ \Big[\partial_\theta\beta_1 - \frac{1}{2}\cos\theta\,(\alpha_7\beta_3 + \alpha_6\beta_2)\Big]^2 + \Big[\partial_\theta\beta_3 + \frac{1}{2}\cos\theta\,(\alpha_8\beta_2 + \alpha_7\beta_1)\Big]^2 \\
& \qquad + \Big[\partial_\theta\,(\cos\theta\beta_2) + \frac{1}{2}\,(\alpha_6\beta_1 - \alpha_8\beta_3)\Big]^2\Big\} \\
& + \frac{v^2}{8r^2\sin^2\theta}\Big\{ \Big[\alpha_4\beta_1 + \alpha_5\beta_1/\sqrt{3} + \cos^2\theta\alpha_1\beta_2 + \alpha_2\beta_3\Big]^2 \\
& \qquad + \cos^2\theta\,\Big[2\beta_2 - \alpha_1\beta_1 + \alpha_4\beta_2 - \alpha_5\beta_2/\sqrt{3} - \alpha_3\beta_3\Big]^2 \\
& \qquad + \Big[2\beta_3 + \alpha_2\beta_1 - 2\alpha_5\beta_3/\sqrt{3} + \cos^2\theta\alpha_3\beta_2\Big]^2\Big\}, \qquad \text{(A.2)}
\end{aligned}
$$

$$
e_{Hpot} = \lambda\frac{v^4}{4}\Big[\beta_1^2 + \cos^2\theta\beta_2^2 + \beta_3^2 - 1\Big]^2. \qquad \text{(A.3)}
$$

A.2 Extended $SU(3)$ Yang-Mills-Higgs theory

$$
\begin{aligned}
\widehat{e}_{\mathrm{Hkin},2}(r,\theta) = & \eta^2\Big\{ [\partial_r\beta_4]^2 + \cos^2\theta\,[\partial_r\beta_5]^2 + [\partial_r\beta_6]^2 \Big\} \\
& + \frac{\eta^2}{4r^2}\Big\{ [\cos\theta\alpha_7\beta_6]^2 + [\cos\theta\alpha_6\beta_5 - 2\partial_\theta\beta_4]^2 + [\alpha_8\beta_6]^2 + 4\,[\partial_\theta\beta_6]^2 \\
& \qquad + [\alpha_6\beta_4 - 2\sin\theta\beta_5 + 2\cos\theta\partial_\theta\beta_5]^2 + \cos^2\theta\,[\alpha_7\beta_4 + \alpha_8\beta_5]^2\Big\} \\
& + \frac{\eta^2}{12r^2\sin^2\theta}\Big\{ 3\,[\alpha_2\beta_6]^2 + \Big[\sqrt{3}\cos^2\theta\alpha_1\beta_5 + 2\sqrt{3}\beta_4 + \sqrt{3}\alpha_4\beta_4 + \alpha_5\beta_4\Big]^2 \\
& \qquad + \cos^2\theta\,\Big[\sqrt{3}\,(\alpha_1\beta_4 - \alpha_4\beta_5) + \alpha_5\beta_5\Big]^2 + 3\cos^2\theta\,[\alpha_3\beta_6]^2 \\
& \qquad + 4\,[\alpha_5\beta_6]^2 + 3\Big[\alpha_2\beta_4 + \cos^2\theta\alpha_3\beta_5\Big]^2\Big\} \qquad \text{(A.4)}
\end{aligned}
$$

$$\begin{aligned}
\widehat{e}_{\mathrm{Hkin},3}(r,\theta) = \eta^2 \Bigg\{ & \cos^2\theta \left[\partial_r \beta_7\right]^2 + \left[\partial_r \beta_8\right]^2 + \cos^2\theta \left[\partial_r \beta_9\right]^2 \Bigg\} \\
& + \frac{\eta^2}{4r^2} \Bigg\{ \Big[\alpha_6\beta_8 + \cos^2\theta\alpha_7\beta_9 - 2\partial_\theta\left(\cos\theta\beta_7\right)\Big]^2 \\
& \quad + \left[\cos\theta\alpha_6\beta_7 - \cos\theta\alpha_8\beta_9 + 2\partial_\theta\beta_8\right]^2 \\
& \quad + \Big[\alpha_8\beta_8 + \cos^2\theta\alpha_7\beta_7 + 2\partial_\theta\left(\cos\theta\beta_9\right)\Big]^2 \Bigg\} \\
& + \frac{\eta^2}{12r^2\sin^2\theta} \Bigg\{ \cos^2\theta \left[\sqrt{3}\left(\alpha_1\beta_8 + \alpha_2\beta_9\right) + \frac{\beta_7}{\sqrt{3}}\left(3\alpha_4 + \sqrt{3}\alpha_5 - 6\right)\right]^2 \\
& \quad + \left[\cos^2\theta\sqrt{3}\left(\alpha_1\beta_7 + \alpha_3\beta_9\right) - \frac{\beta_8}{\sqrt{3}}\left(3\alpha_4 - \sqrt{3}\alpha_5 + 12\right)\right]^2 \\
& \quad + \cos^2\theta\left[\sqrt{3}\alpha_2\beta_7 + \sqrt{3}\alpha_3\beta_8 - 2\alpha_5\beta_9\right]^2 \Bigg\}
\end{aligned} \tag{A.5}$$

$$\begin{aligned}
\widehat{e}_{\mathrm{Hpot},123}(r,\theta) = \eta^4\lambda \Bigg\{ & \left[\beta_1^2 + \cos^2\theta\beta_2^2 + \beta_3^2 - 1\right]^2 + \left[\beta_4^2 + \cos^2\theta\beta_5^2 + \beta_6^2 - 1\right]^2 \\
& + \left[\cos^2\theta\beta_7^2 + \beta_8^2 + \cos^2\theta\beta_9^2 - 1\right]^2 + \left[\beta_1\beta_4 + \cos^2\theta\beta_2\beta_5\right]^2 \\
& + \left[\beta_3\beta_6\right]^2 + \cos^2\theta\left[\beta_1\beta_7 + \beta_2\beta_8 + \beta_3\beta_9\right]^2 \\
& + \cos^2\theta\left[\beta_4\beta_7 + \beta_5\beta_8\right]^2 + \cos^2\theta\left[\beta_6\beta_9\right]^2 \Bigg\}
\end{aligned} \tag{A.6}$$

APPENDIX B

Reduced field equations in the radial gauge

B.1 Basic $SU(3)$ Yang-Mills-Higgs theory

The reduced field equations listed below are obtained from the radial gauge energy functional, the corresponding energy density being given in App. A, by variation with respect to profile functions α_i for $i = 1, \ldots, 8$ (given by Eqs. (B.1) through (B.8)) and β_i for $i = 1, 2, 3$ (given by Eqs. (B.9), (B.10) and (B.11)).

$$
\begin{aligned}
& r^2 \sin\theta\cos\theta\partial_r^2\alpha_1 + \sin\theta\cos\theta\partial_\theta^2\alpha_1 - \frac{3}{2}\partial_\theta\alpha_1 + \frac{1}{2}\cos 2\theta\ \partial_\theta\alpha_1 - \sin\theta\cos\theta\alpha_1\alpha_6^2 \\
& - \frac{1}{4}\sin\theta\cos^3\theta\alpha_1\alpha_7^2 - \frac{1}{4}\sin\theta\cos\theta\alpha_1\alpha_8^2 - \frac{1}{4}g^2r^2v^2\sin\theta\cos\theta\alpha_1\beta_1^2 \\
& - \frac{1}{4}g^2r^2v^2\sin\theta\cos^3\theta\alpha_1\beta_2^2 - \sin\theta\partial_\theta\alpha_2\alpha_8 - \frac{3}{4}\sin\theta\cos\theta\alpha_2\alpha_6\alpha_7 - \frac{1}{2}\sin\theta\alpha_2\partial_\theta\alpha_8 \\
& + \frac{1}{2}\cos\theta\alpha_2\alpha_8 - \frac{1}{4}g^2r^2v^2\sin\theta\cos\theta\alpha_2\beta_2\beta_3 - \sin\theta\cos^2\theta\partial_\theta\alpha_3\alpha_7 + \frac{3}{4}\sin\theta\cos\theta\alpha_3\alpha_6\alpha_8 \\
& - \frac{1}{2}\sin\theta\cos^2\theta\alpha_3\partial_\theta\alpha_7 + \cos\theta\alpha_3\alpha_7 - \frac{1}{2}\cos 2\theta\ \cos\theta\alpha_3\alpha_7 - \frac{1}{4}g^2r^2v^2\sin\theta\cos\theta\alpha_3\beta_1\beta_3 \\
& + 2\sin\theta\partial_\theta\alpha_4\alpha_6 + \sin\theta\alpha_4\partial_\theta\alpha_6 - \cos\theta\alpha_4\alpha_6 - \frac{1}{2}\sqrt{3}\sin\theta\cos\theta\alpha_5\alpha_7\alpha_8 \\
& - \frac{g^2r^2v^2\sin\theta\cos\theta\alpha_5\beta_1\beta_2}{2\sqrt{3}} + \sin\theta\partial_\theta\alpha_6 - \cos\theta\alpha_6 + \frac{3}{2}\sin\theta\cos\theta\alpha_7\alpha_8 \\
& + \frac{1}{2}g^2r^2v^2\sin\theta\cos\theta\beta_1\beta_2 = 0
\end{aligned}
\tag{B.1}
$$

$$
\begin{aligned}
&r^2\sin\theta\partial_r^2\alpha_2+\sin\theta\partial_\theta^2\alpha_2+\sin\theta\cos\theta\partial_\theta\alpha_1\alpha_8-\frac{3}{4}\sin\theta\cos^2\theta\alpha_1\alpha_6\alpha_7+\frac{1}{2}\sin\theta\cos\theta\alpha_1\partial_\theta\alpha_8\\
&-\frac{3}{4}\alpha_1\alpha_8+\frac{1}{4}\cos 2\theta\ \alpha_1\alpha_8-\frac{1}{4}g^2r^2v^2\sin\theta\cos^2\theta\alpha_1\beta_2\beta_3-\cos\theta\partial_\theta\alpha_2-\frac{1}{4}\sin\theta\alpha_2\alpha_6^2\\
&-\sin\theta\cos^2\theta\alpha_2\alpha_7^2-\frac{1}{4}\sin\theta\alpha_2\alpha_8^2-\frac{1}{4}g^2r^2v^2\sin\theta\alpha_2\beta_1^2-\frac{1}{4}g^2r^2v^2\sin\theta\alpha_2\beta_3^2\\
&-\sin\theta\cos\theta\partial_\theta\alpha_3\alpha_6-\frac{1}{2}\sin\theta\cos\theta\alpha_3\partial_\theta\alpha_6+\frac{1}{2}\alpha_3\alpha_6+\frac{1}{2}\sin^2\theta\alpha_3\alpha_6-\frac{3}{4}\sin\theta\cos^2\theta\alpha_3\alpha_7\alpha_8\\
&-\frac{1}{4}g^2r^2v^2\sin\theta\cos^2\theta\alpha_3\beta_1\beta_2+\sin\theta\cos\theta\partial_\theta\alpha_4\alpha_7+\frac{3}{4}\sin\theta\alpha_4\alpha_6\alpha_8+\frac{1}{2}\sin\theta\cos\theta\alpha_4\partial_\theta\alpha_7\\
&-\frac{1}{2}\alpha_4\alpha_7-\frac{1}{4}g^2r^2v^2\sin\theta\alpha_4\beta_1\beta_3+\sqrt{3}\sin\theta\cos\theta\partial_\theta\alpha_5\alpha_7-\frac{1}{4}\sqrt{3}\sin\theta\alpha_5\alpha_6\alpha_8\\
&+\frac{1}{2}\sqrt{3}\sin\theta\cos\theta\alpha_5\partial_\theta\alpha_7-\frac{1}{2}\sqrt{3}\alpha_5\alpha_7+\frac{g^2r^2v^2\sin\theta\alpha_5\beta_1\beta_3}{4\sqrt{3}}+\frac{3}{2}\sin\theta\alpha_6\alpha_8\\
&-\sin\theta\cos\theta\partial_\theta\alpha_7+\alpha_7-\frac{1}{2}g^2r^2v^2\sin\theta\beta_1\beta_3=0
\end{aligned}
\tag{B.2}
$$

$$
\begin{aligned}
&r^2\sin\theta\cos\theta\partial_r^2\alpha_3+\sin\theta\cos\theta\partial_\theta^2\alpha_3+\sin\theta\cos^2\theta\partial_\theta\alpha_1\alpha_7+\frac{3}{4}\sin\theta\cos\theta\alpha_1\alpha_6\alpha_8\\
&+\frac{1}{2}\sin\theta\cos^2\theta\alpha_1\partial_\theta\alpha_7-\cos\theta\alpha_1\alpha_7+\frac{1}{2}\cos 2\theta\ \cos\theta\alpha_1\alpha_7-\frac{1}{4}g^2r^2v^2\sin\theta\cos\theta\alpha_1\beta_1\beta_3\\
&+\sin\theta\partial_\theta\alpha_2\alpha_6+\frac{1}{2}\sin\theta\alpha_2\partial_\theta\alpha_6-\frac{1}{2}\cos\theta\alpha_2\alpha_6-\frac{3}{4}\sin\theta\cos\theta\alpha_2\alpha_7\alpha_8\\
&-\frac{1}{4}g^2r^2v^2\sin\theta\cos\theta\alpha_2\beta_1\beta_2-\frac{3}{2}\partial_\theta\alpha_3+\frac{1}{2}\cos 2\theta\ \partial_\theta\alpha_3-\frac{1}{4}\sin\theta\cos\theta\alpha_3\alpha_6^2\\
&-\frac{1}{4}\sin\theta\cos^3\theta\alpha_3\alpha_7^2-\sin\theta\cos\theta\alpha_3\alpha_8^2-\frac{1}{4}g^2r^2v^2\sin\theta\cos^3\theta\alpha_3\beta_2^2-\frac{1}{4}g^2r^2v^2\sin\theta\cos\theta\alpha_3\beta_3^2\\
&-\sin\theta\partial_\theta\alpha_4\alpha_8+\frac{3}{4}\sin\theta\cos\theta\alpha_4\alpha_6\alpha_7-\frac{1}{2}\sin\theta\alpha_4\partial_\theta\alpha_8+\frac{1}{2}\cos\theta\alpha_4\alpha_8\\
&+\frac{1}{4}g^2r^2v^2\sin\theta\cos\theta\alpha_4\beta_2\beta_3+\sqrt{3}\sin\theta\partial_\theta\alpha_5\alpha_8+\frac{1}{4}\sqrt{3}\sin\theta\cos\theta\alpha_5\alpha_6\alpha_7+\frac{1}{2}\sqrt{3}\sin\theta\alpha_5\partial_\theta\alpha_8\\
&-\frac{1}{2}\sqrt{3}\cos\theta\alpha_5\alpha_8+\frac{g^2r^2v^2\sin\theta\cos\theta\alpha_5\beta_2\beta_3}{4\sqrt{3}}-2\sin\theta\partial_\theta\alpha_8+2\cos\theta\alpha_8=0
\end{aligned}
\tag{B.3}
$$

$$
\begin{aligned}
&r^2\sin\theta\partial_r^2\alpha_4+\sin\theta\partial_\theta^2\alpha_4-2\sin\theta\cos\theta\partial_\theta\alpha_1\alpha_6-\sin\theta\cos\theta\alpha_1\partial_\theta\alpha_6+\alpha_1\alpha_6\\
&+\sin^2\theta\alpha_1\alpha_6-\sin\theta\cos\theta\partial_\theta\alpha_2\alpha_7+\frac{3}{4}\sin\theta\alpha_2\alpha_6\alpha_8-\frac{1}{2}\sin\theta\cos\theta\alpha_2\partial_\theta\alpha_7\\
&+\frac{1}{2}\alpha_2\alpha_7-\frac{1}{4}g^2r^2v^2\sin\theta\alpha_2\beta_1\beta_3+\sin\theta\cos\theta\partial_\theta\alpha_3\alpha_8+\frac{3}{4}\sin\theta\cos^2\theta\alpha_3\alpha_6\alpha_7\\
&+\frac{1}{2}\sin\theta\cos\theta\alpha_3\partial_\theta\alpha_8-\frac{3}{4}\alpha_3\alpha_8+\frac{1}{4}\cos2\theta\ \alpha_3\alpha_8+\frac{1}{16}g^2r^2v^2\sin\theta\alpha_3\beta_2\beta_3\\
&+\frac{1}{16}g^2r^2v^2\sin3\theta\ \alpha_3\beta_2\beta_3-\cos\theta\partial_\theta\alpha_4-\sin\theta\alpha_4\alpha_6^2-\frac{1}{4}\sin\theta\cos^2\theta\alpha_4\alpha_7^2-\frac{1}{4}\sin\theta\alpha_4\alpha_8^2\\
&-\frac{1}{4}g^2r^2v^2\sin\theta\alpha_4\beta_1^2-\frac{1}{16}g^2r^2v^2\sin\theta\alpha_4\beta_2^2-\frac{1}{16}g^2r^2v^2\sin3\theta\ \alpha_4\beta_2^2-\frac{1}{4}\sqrt{3}\sin\theta\cos^2\theta\alpha_5\alpha_7^2\\
&+\frac{1}{4}\sqrt{3}\sin\theta\alpha_5\alpha_8^2-\frac{g^2r^2v^2\sin\theta\alpha_5\beta_1^2}{4\sqrt{3}}+\frac{g^2r^2v^2\sin\theta\alpha_5\beta_2^2}{16\sqrt{3}}+\frac{g^2r^2v^2\sin3\theta\ \alpha_5\beta_2^2}{16\sqrt{3}}-\sin\theta\alpha_6^2\\
&+\frac{1}{2}\sin\theta\cos^2\theta\alpha_7^2-\sin\theta\alpha_8^2-\frac{1}{8}g^2r^2v^2\sin\theta\beta_2^2-\frac{1}{8}g^2r^2v^2\sin3\theta\ \beta_2^2=0
\end{aligned}
\tag{B.4}
$$

$$
\begin{aligned}
&r^2\sin\theta\partial_r^2\alpha_5+\sin\theta\partial_\theta^2\alpha_5-\frac{1}{2}\sqrt{3}\sin\theta\cos^2\theta\alpha_1\alpha_7\alpha_8-\frac{g^2r^2v^2\sin\theta\cos^2\theta\alpha_1\beta_1\beta_2}{2\sqrt{3}}\\
&-\sqrt{3}\sin\theta\cos\theta\partial_\theta\alpha_2\alpha_7-\frac{1}{4}\sqrt{3}\sin\theta\alpha_2\alpha_6\alpha_8-\frac{1}{2}\sqrt{3}\sin\theta\cos\theta\alpha_2\partial_\theta\alpha_7+\frac{1}{2}\sqrt{3}\alpha_2\alpha_7\\
&+\frac{g^2r^2v^2\sin\theta\alpha_2\beta_1\beta_3}{4\sqrt{3}}-\sqrt{3}\sin\theta\cos\theta\partial_\theta\alpha_3\alpha_8+\frac{1}{4}\sqrt{3}\sin\theta\cos^2\theta\alpha_3\alpha_6\alpha_7\\
&-\frac{1}{2}\sqrt{3}\sin\theta\cos\theta\alpha_3\partial_\theta\alpha_8+\frac{3}{4}\sqrt{3}\alpha_3\alpha_8-\frac{1}{4}\sqrt{3}\cos2\theta\ \alpha_3\alpha_8+\frac{g^2r^2v^2\sin\theta\cos^2\theta\alpha_3\beta_2\beta_3}{4\sqrt{3}}\\
&-\frac{1}{4}\sqrt{3}\sin\theta\cos^2\theta\alpha_4\alpha_7^2+\frac{1}{4}\sqrt{3}\sin\theta\alpha_4\alpha_8^2-\frac{g^2r^2v^2\sin\theta\alpha_4\beta_1^2}{4\sqrt{3}}+\frac{g^2r^2v^2\sin\theta\cos^2\theta\alpha_4\beta_2^2}{4\sqrt{3}}\\
&-\cos\theta\partial_\theta\alpha_5-\frac{3}{4}\sin\theta\cos^2\theta\alpha_5\alpha_7^2-\frac{3}{4}\sin\theta\alpha_5\alpha_8^2-\frac{1}{12}g^2r^2v^2\sin\theta\alpha_5\beta_1^2\\
&-\frac{1}{12}g^2r^2v^2\sin\theta\cos^2\theta\alpha_5\beta_2^2-\frac{1}{3}g^2r^2v^2\sin\theta\alpha_5\beta_3^2+\frac{1}{2}\sqrt{3}\sin\theta\cos^2\theta\alpha_7^2+\sqrt{3}\sin\theta\alpha_8^2\\
&+\frac{g^2r^2v^2\sin\theta\cos^2\theta\beta_2^2}{2\sqrt{3}}+\frac{g^2r^2v^2\sin\theta\beta_3^2}{\sqrt{3}}=0
\end{aligned}
\tag{B.5}
$$

$$
\begin{aligned}
&r^2\sin^2\theta\partial_r^2\alpha_6 - \cos\theta\partial_\theta\alpha_1\alpha_4 - \cos\theta\partial_\theta\alpha_1 - \frac{3}{4}\cos^2\theta\alpha_1\alpha_2\alpha_7 + \frac{3}{4}\cos^2\theta\alpha_1\alpha_3\alpha_8 \\
&+ \cos\theta\alpha_1\partial_\theta\alpha_4 + \sin\theta\alpha_1\alpha_4 - \cos^2\theta\alpha_1^2\alpha_6 + \sin\theta\alpha_1 + \frac{1}{2}\cos\theta\partial_\theta\alpha_2\alpha_3 - \frac{1}{2}\cos\theta\alpha_2\partial_\theta\alpha_3 \\
&+ \frac{1}{2}\sin\theta\alpha_2\alpha_3 + \frac{3}{4}\alpha_2\alpha_4\alpha_8 - \frac{1}{4}\sqrt{3}\alpha_2\alpha_5\alpha_8 - \frac{1}{4}\alpha_2^2\alpha_6 + \frac{3}{2}\alpha_2\alpha_8 + \frac{3}{4}\cos^2\theta\alpha_3\alpha_4\alpha_7 \\
&+ \frac{1}{4}\sqrt{3}\cos^2\theta\alpha_3\alpha_5\alpha_7 - \frac{1}{4}\cos^2\theta\alpha_3^2\alpha_6 - \alpha_4^2\alpha_6 - 2\alpha_4\alpha_6 - \frac{1}{4}g^2r^2v^2\sin^2\theta\alpha_6\beta_1^2 \\
&- \frac{1}{4}g^2r^2v^2\sin^2\theta\cos^2\theta\alpha_6\beta_2^2 - \alpha_6 - \frac{1}{4}g^2r^2v^2\sin^2\theta\cos^2\theta\alpha_7\beta_2\beta_3 + \frac{1}{4}g^2r^2v^2\sin^2\theta\alpha_8\beta_1\beta_3 \\
&+ \frac{1}{2}g^2r^2v^2\sin^2\theta\cos\theta\partial_\theta\beta_1\beta_2 - \frac{1}{2}g^2r^2v^2\sin^2\theta\cos\theta\beta_1\partial_\theta\beta_2 + \frac{1}{2}g^2r^2v^2\sin^3\theta\beta_1\beta_2 = 0
\end{aligned}
\tag{B.6}
$$

$$
\begin{aligned}
&r^2\cos\theta\sin^2\theta\partial_r^2\alpha_7 + \frac{1}{2}\cos^2\theta\partial_\theta\alpha_1\alpha_3 - \frac{3}{4}\cos\theta\alpha_1\alpha_2\alpha_6 - \frac{1}{2}\cos^2\theta\alpha_1\partial_\theta\alpha_3 \\
&- \frac{1}{2}\sqrt{3}\cos\theta\alpha_1\alpha_5\alpha_8 - \frac{1}{4}\cos^3\theta\alpha_1^2\alpha_7 + \frac{3}{2}\cos\theta\alpha_1\alpha_8 - \frac{1}{2}\partial_\theta\alpha_2\alpha_4 - \frac{1}{2}\sqrt{3}\partial_\theta\alpha_2\alpha_5 + \partial_\theta\alpha_2 \\
&- \frac{3}{4}\cos\theta\alpha_2\alpha_3\alpha_8 + \frac{1}{2}\alpha_2\partial_\theta\alpha_4 + \frac{1}{2}\sqrt{3}\alpha_2\partial_\theta\alpha_5 - \cos\theta\alpha_2^2\alpha_7 + \frac{3}{4}\cos\theta\alpha_3\alpha_4\alpha_6 \\
&+ \frac{1}{4}\sqrt{3}\cos\theta\alpha_3\alpha_5\alpha_6 - \frac{1}{4}\cos^3\theta\alpha_3^2\alpha_7 - \frac{1}{2}\sqrt{3}\cos\theta\alpha_4\alpha_5\alpha_7 - \frac{1}{4}\cos\theta\alpha_4^2\alpha_7 + \cos\theta\alpha_4\alpha_7 \\
&- \frac{3}{4}\cos\theta\alpha_5^2\alpha_7 + \sqrt{3}\cos\theta\alpha_5\alpha_7 - \frac{1}{4}g^2r^2v^2\cos\theta\sin^2\theta\alpha_6\beta_2\beta_3 - \frac{1}{4}g^2r^2v^2\cos\theta\sin^2\theta\alpha_7\beta_1^2 \\
&- \frac{1}{4}g^2r^2v^2\cos\theta\sin^2\theta\alpha_7\beta_3^2 - \cos\theta\alpha_7 - \frac{1}{4}g^2r^2v^2\cos\theta\sin^2\theta\alpha_8\beta_1\beta_2 + \frac{1}{4}g^2r^2v^2\partial_\theta\beta_1\beta_3 \\
&- \frac{1}{4}g^2r^2v^2\cos 2\theta\ \partial_\theta\beta_1\beta_3 - \frac{1}{4}g^2r^2v^2\beta_1\partial_\theta\beta_3 + \frac{1}{4}g^2r^2v^2\cos 2\theta\ \beta_1\partial_\theta\beta_3 = 0
\end{aligned}
\tag{B.7}
$$

$$
\begin{aligned}
&r^2\sin^2\theta\partial_r^2\alpha_8+\frac{1}{2}\cos\theta\partial_\theta\alpha_1\alpha_2-\frac{1}{2}\cos\theta\alpha_1\partial_\theta\alpha_2-\frac{1}{2}\sin\theta\alpha_1\alpha_2+\frac{3}{4}\cos^2\theta\alpha_1\alpha_3\alpha_6\\
&-\frac{1}{2}\sqrt{3}\cos^2\theta\alpha_1\alpha_5\alpha_7+\frac{3}{2}\cos^2\theta\alpha_1\alpha_7-\frac{1}{4}\cos^2\theta\alpha_1^2\alpha_8-\frac{3}{4}\cos^2\theta\alpha_2\alpha_3\alpha_7+\frac{3}{4}\alpha_2\alpha_4\alpha_6\\
&-\frac{1}{4}\sqrt{3}\alpha_2\alpha_5\alpha_6+\frac{3}{2}\alpha_2\alpha_6-\frac{1}{4}\alpha_2^2\alpha_8+\frac{1}{2}\cos\theta\partial_\theta\alpha_3\alpha_4-\frac{1}{2}\sqrt{3}\cos\theta\partial_\theta\alpha_3\alpha_5+2\cos\theta\partial_\theta\alpha_3\\
&-\frac{1}{2}\cos\theta\alpha_3\partial_\theta\alpha_4-\frac{1}{2}\sin\theta\alpha_3\alpha_4+\frac{1}{2}\sqrt{3}\cos\theta\alpha_3\partial_\theta\alpha_5+\frac{1}{2}\sqrt{3}\sin\theta\alpha_3\alpha_5-\cos^2\theta\alpha_3^2\alpha_8\\
&-2\sin\theta\alpha_3+\frac{1}{2}\sqrt{3}\alpha_4\alpha_5\alpha_8-\frac{1}{4}\alpha_4^2\alpha_8-2\alpha_4\alpha_8-\frac{3}{4}\alpha_5^2\alpha_8+2\sqrt{3}\alpha_5\alpha_8+\frac{1}{4}g^2r^2v^2\sin^2\theta\alpha_6\beta_1\beta_3\\
&-\frac{1}{4}g^2r^2v^2\sin^2\theta\cos^2\theta\alpha_7\beta_1\beta_2-\frac{1}{4}g^2r^2v^2\sin^2\theta\cos^2\theta\alpha_8\beta_2^2-\frac{1}{4}g^2r^2v^2\sin^2\theta\alpha_8\beta_3^2-4\alpha_8\\
&+\frac{1}{2}g^2r^2v^2\sin^2\theta\cos\theta\partial_\theta\beta_2\beta_3-\frac{1}{2}g^2r^2v^2\sin^2\theta\cos\theta\beta_2\partial_\theta\beta_3-\frac{1}{2}g^2r^2v^2\sin^3\theta\beta_2\beta_3=0
\end{aligned}
\tag{B.8}
$$

$$
\begin{aligned}
&r^2\sin^2\theta\partial_r^2\beta_1+\sin^2\theta\partial_\theta^2\beta_1-\frac{1}{4}\cos^2\theta\alpha_1\alpha_3\beta_3-\frac{\cos^2\theta\alpha_1\alpha_5\beta_2}{2\sqrt{3}}-\frac{1}{4}\cos^2\theta\alpha_1^2\beta_1\\
&+\frac{1}{2}\cos^2\theta\alpha_1\beta_2-\frac{1}{4}\cos^2\theta\alpha_2\alpha_3\beta_2-\frac{1}{4}\alpha_2\alpha_4\beta_3+\frac{\alpha_2\alpha_5\beta_3}{4\sqrt{3}}-\frac{1}{4}\alpha_2^2\beta_1-\frac{1}{2}\alpha_2\beta_3-\frac{\alpha_4\alpha_5\beta_1}{2\sqrt{3}}\\
&-\frac{1}{4}\alpha_4^2\beta_1-\frac{1}{12}\alpha_5^2\beta_1-\frac{1}{2}\sin^2\theta\cos\theta\partial_\theta\alpha_6\beta_2+\frac{1}{4}\sin^2\theta\alpha_6\alpha_8\beta_3-\frac{1}{4}\sin^2\theta\alpha_6^2\beta_1\\
&-\sin^2\theta\cos\theta\alpha_6\partial_\theta\beta_2+\frac{1}{4}\sin\theta\alpha_6\beta_2-\frac{3}{4}\sin\theta\cos2\theta\ \alpha_6\beta_2-\frac{1}{2}\sin^2\theta\cos\theta\partial_\theta\alpha_7\beta_3\\
&-\frac{1}{4}\sin^2\theta\cos^2\theta\alpha_7\alpha_8\beta_2-\frac{1}{4}\sin^2\theta\cos^2\theta\alpha_7^2\beta_1-\sin^2\theta\cos\theta\alpha_7\partial_\theta\beta_3-\frac{1}{2}\sin\theta\cos2\theta\ \alpha_7\beta_3\\
&+2r\sin^2\theta\partial_r\beta_1+\sin\theta\cos\theta\partial_\theta\beta_1-\lambda r^2v^2\sin^2\theta\cos^2\theta\beta_1\beta_2^2-\lambda r^2v^2\sin^2\theta\beta_1\beta_3^2\\
&-\lambda r^2v^2\sin^2\theta\beta_1^3+\lambda r^2v^2\sin^2\theta\beta_1=0
\end{aligned}
\tag{B.9}
$$

$$
\begin{aligned}
&r^2\cos\theta\sin^2\theta\partial_r^2\beta_2+\cos\theta\sin^2\theta\partial_\theta^2\beta_2-\frac{1}{8}\lambda r^2v^2\cos\theta\beta_2^3+\frac{1}{16}\lambda r^2v^2\cos3\theta\ \beta_2^3\\
&+\frac{1}{16}\lambda r^2v^2\cos5\theta\ \beta_2^3+\frac{1}{4}\lambda r^2v^2\cos\theta\beta_2-\frac{3}{16}\alpha_1^2\cos\theta\beta_2-\frac{3}{16}\alpha_3^2\cos\theta\beta_2-\frac{1}{4}\alpha_4^2\cos\theta\beta_2\\
&-\frac{1}{12}\alpha_5^2\cos\theta\beta_2-\frac{1}{16}\alpha_6^2\cos\theta\beta_2-\frac{1}{16}\alpha_8^2\cos\theta\beta_2-\frac{1}{4}\lambda r^2v^2\beta_1^2\cos\theta\beta_2-\frac{1}{4}\lambda r^2v^2\beta_3^2\cos\theta\beta_2\\
&-\alpha_4\cos\theta\beta_2+\frac{\alpha_4\alpha_5\cos\theta\beta_2}{2\sqrt{3}}+\frac{\alpha_5\cos\theta\beta_2}{\sqrt{3}}-\frac{3}{2}\cos\theta\beta_2-\frac{1}{4}\lambda r^2v^2\cos3\theta\ \beta_2\\
&-\frac{1}{16}\alpha_1^2\cos3\theta\ \beta_2-\frac{1}{16}\alpha_3^2\cos3\theta\ \beta_2+\frac{1}{16}\alpha_6^2\cos3\theta\ \beta_2+\frac{1}{16}\alpha_8^2\cos3\theta\ \beta_2\\
&+\frac{1}{4}\lambda r^2v^2\beta_1^2\cos3\theta\ \beta_2+\frac{1}{4}\lambda r^2v^2\beta_3^2\cos3\theta\ \beta_2+\frac{1}{2}\cos3\theta\ \beta_2+\frac{1}{2}\alpha_1\beta_1\cos\theta-\frac{1}{4}\alpha_2\alpha_3\beta_1\cos\theta\\
&-\frac{\alpha_1\alpha_5\beta_1\cos\theta}{2\sqrt{3}}-\frac{1}{4}\alpha_7\alpha_8\beta_1\cos\theta\sin^2\theta-\frac{1}{4}\alpha_1\alpha_2\beta_3\cos\theta+\frac{1}{4}\alpha_3\alpha_4\beta_3\cos\theta+\frac{\alpha_3\alpha_5\beta_3\cos\theta}{4\sqrt{3}}\\
&-\frac{1}{4}\alpha_6\alpha_7\beta_3\cos\theta\sin^2\theta+\frac{1}{4}\alpha_6\beta_1\sin2\theta\ -\frac{1}{4}\alpha_8\beta_3\sin2\theta\ +\frac{1}{4}\beta_1\partial_\theta\alpha_6-\frac{1}{4}\beta_1\cos2\theta\ \partial_\theta\alpha_6\\
&-\frac{1}{4}\beta_3\partial_\theta\alpha_8+\frac{1}{4}\beta_3\cos2\theta\ \partial_\theta\alpha_8+\frac{1}{2}\alpha_6\partial_\theta\beta_1-\frac{1}{2}\alpha_6\cos2\theta\ \partial_\theta\beta_1-\frac{5}{4}\sin\theta\partial_\theta\beta_2\\
&+\frac{3}{4}\sin3\theta\ \partial_\theta\beta_2-\frac{1}{2}\alpha_8\partial_\theta\beta_3+\frac{1}{2}\alpha_8\cos2\theta\ \partial_\theta\beta_3+\frac{1}{2}r\cos\theta\partial_r\beta_2-\frac{1}{2}r\cos3\theta\ \partial_r\beta_2=0
\end{aligned}
\tag{B.10}
$$

$$
\begin{aligned}
&r^2\sin^2\theta\partial_r^2\beta_3+\sin^2\theta\partial_\theta^2\beta_3-\frac{1}{4}\cos^2\theta\alpha_1\alpha_2\beta_2-\frac{1}{4}\cos^2\theta\alpha_1\alpha_3\beta_1-\frac{1}{4}\alpha_2\alpha_4\beta_1+\frac{\alpha_2\alpha_5\beta_1}{4\sqrt{3}}\\
&-\frac{1}{2}\alpha_2\beta_1-\frac{1}{4}\alpha_2^2\beta_3+\frac{1}{4}\cos^2\theta\alpha_3\alpha_4\beta_2+\frac{\cos^2\theta\alpha_3\alpha_5\beta_2}{4\sqrt{3}}-\frac{1}{4}\cos^2\theta\alpha_3^2\beta_3-\frac{1}{3}\alpha_5^2\beta_3+\frac{2\alpha_5\beta_3}{\sqrt{3}}\\
&-\frac{1}{4}\sin^2\theta\cos^2\theta\alpha_6\alpha_7\beta_2+\frac{1}{4}\sin^2\theta\alpha_6\alpha_8\beta_1+\frac{1}{4}\sin\theta\sin2\theta\ \partial_\theta\alpha_7\beta_1+\frac{1}{2}\sin\theta\sin2\theta\ \alpha_7\partial_\theta\beta_1\\
&+\frac{1}{2}\sin\theta\cos2\theta\ \alpha_7\beta_1-\frac{1}{16}\sin^2 2\theta\ \alpha_7^2\beta_3+\frac{1}{4}\sin\theta\sin2\theta\ \partial_\theta\alpha_8\beta_2+\sin^2\theta\cos\theta\alpha_8\partial_\theta\beta_2\\
&-\frac{1}{4}\sin\theta\alpha_8\beta_2+\frac{3}{4}\sin\theta\cos2\theta\ \alpha_8\beta_2-\frac{1}{4}\sin^2\theta\alpha_8^2\beta_3-\lambda r^2v^2\sin^2\theta\beta_1^2\beta_3\\
&-\frac{1}{4}\lambda r^2v^2\sin^2 2\theta\ \beta_2^2\beta_3+2r\sin^2\theta\partial_r\beta_3+\sin\theta\cos\theta\partial_\theta\beta_3-\lambda r^2v^2\sin^2\theta\beta_3^3\\
&+\lambda r^2v^2\sin^2\theta\beta_3-\beta_3=0
\end{aligned}
\tag{B.11}
$$

B.2 Extended $SU(3)$ Yang-Mills-Higgs theory

The reduced field equations listed below are obtained from the radial gauge energy functional, the corresponding energy density being given in App. A.2, by variation with respect to profile functions α_i, for $i = 1, \ldots, 8$, (given by Eqs. (B.12) through (B.19)) and β_i for $i = 1, \ldots, 9$ (given by Eqs. (B.20) through (B.28)).

$$
\begin{aligned}
&r^2 \sin\theta\cos\theta\partial_r^2\alpha_1 + \sin\theta\cos\theta\partial_\theta^2\alpha_1 - \frac{1}{4}\eta^2 g^2\alpha_1\beta_1^2 \sin 2\theta\ r^2 - \frac{1}{8}\eta^2 g^2\alpha_1\beta_2^2 \sin 2\theta\ r^2 \\
&- \frac{1}{4}\eta^2 g^2\alpha_1\beta_4^2 \sin 2\theta\ r^2 - \frac{1}{8}\eta^2 g^2\alpha_1\beta_5^2 \sin 2\theta\ r^2 - \frac{1}{8}\eta^2 g^2\alpha_1\beta_7^2 \sin 2\theta\ r^2 \\
&- \frac{1}{4}\eta^2 g^2\alpha_1\beta_8^2 \sin 2\theta\ r^2 + \frac{1}{2}\eta^2 g^2\beta_1\beta_2 \sin 2\theta\ r^2 - \frac{\eta^2 g^2\alpha_5\beta_1\beta_2 \sin 2\theta\ r^2}{2\sqrt{3}} \\
&- \frac{1}{4}\eta^2 g^2\alpha_3\beta_1\beta_3 \sin 2\theta\ r^2 - \frac{1}{4}\eta^2 g^2\alpha_2\beta_2\beta_3 \sin 2\theta\ r^2 - \frac{1}{2}\eta^2 g^2\beta_4\beta_5 \sin 2\theta\ r^2 \\
&- \frac{\eta^2 g^2\alpha_5\beta_4\beta_5 \sin 2\theta\ r^2}{2\sqrt{3}} + \frac{3}{2}\eta^2 g^2\beta_7\beta_8 \sin 2\theta\ r^2 - \frac{\eta^2 g^2\alpha_5\beta_7\beta_8 \sin 2\theta\ r^2}{2\sqrt{3}} \\
&- \frac{1}{8}\eta^2 g^2\alpha_3\beta_7\beta_9 \sin 2\theta\ r^2 - \frac{1}{4}\eta^2 g^2\alpha_2\beta_8\beta_9 \sin 2\theta\ r^2 - \frac{1}{16}\eta^2 g^2\alpha_1\beta_2^2 \sin(4\theta) r^2 \\
&- \frac{1}{16}\eta^2 g^2\alpha_1\beta_5^2 \sin(4\theta) r^2 - \frac{1}{16}\eta^2 g^2\alpha_1\beta_7^2 \sin(4\theta) r^2 - \frac{1}{16}\eta^2 g^2\alpha_3\beta_7\beta_9 \sin(4\theta) r^2 \\
&- \alpha_4\alpha_6\cos\theta - \alpha_6\cos\theta + \frac{3}{4}\alpha_3\alpha_7\cos\theta + \frac{1}{2}\alpha_2\alpha_8\cos\theta - \frac{1}{4}\alpha_3\alpha_7\cos 3\theta\ - \frac{1}{2}\alpha_1\alpha_6^2 \sin 2\theta \\
&- \frac{1}{16}\alpha_1\alpha_7^2 \sin 2\theta\ - \frac{1}{8}\alpha_1\alpha_8^2 \sin 2\theta\ - \frac{3}{8}\alpha_2\alpha_6\alpha_7 \sin 2\theta\ + \frac{3}{8}\alpha_3\alpha_6\alpha_8 \sin 2\theta \\
&- \frac{1}{4}\sqrt{3}\alpha_5\alpha_7\alpha_8 \sin 2\theta\ + \frac{3}{4}\alpha_7\alpha_8 \sin 2\theta\ - \frac{1}{32}\alpha_1\alpha_7^2 \sin(4\theta) + \frac{1}{2}\cos 2\theta\ \partial_\theta\alpha_1 \\
&- \frac{3}{2}\partial_\theta\alpha_1 - \alpha_8 \sin\theta\partial_\theta\alpha_2 - \frac{1}{4}\alpha_7 \sin\theta\partial_\theta\alpha_3 - \frac{1}{4}\alpha_7 \sin 3\theta\ \partial_\theta\alpha_3 + 2\alpha_6 \sin\theta\partial_\theta\alpha_4 \\
&+ \alpha_4 \sin\theta\partial_\theta\alpha_6 + \sin\theta\partial_\theta\alpha_6 - \frac{1}{8}\alpha_3 \sin\theta\partial_\theta\alpha_7 - \frac{1}{8}\alpha_3 \sin 3\theta\ \partial_\theta\alpha_7 - \frac{1}{2}\alpha_2 \sin\theta\partial_\theta\alpha_8 = 0
\end{aligned}
\tag{B.12}
$$

$$
\begin{aligned}
&r^2 \sin\theta \partial_r^2 \alpha_2 + \sin\theta \partial_\theta^2 \alpha_2 - \frac{1}{2}\eta^2 g^2 \alpha_2 \beta_1^2 \sin\theta r^2 - \frac{1}{2}\eta^2 g^2 \alpha_2 \beta_3^2 \sin\theta r^2 - \frac{1}{2}\eta^2 g^2 \alpha_2 \beta_4^2 \sin\theta r^2 \\
&- \frac{1}{2}\eta^2 g^2 \alpha_2 \beta_6^2 \sin\theta r^2 - \frac{1}{8}\eta^2 g^2 \alpha_2 \beta_7^2 \sin\theta r^2 - \frac{1}{2}\eta^2 g^2 \alpha_2 \beta_9^2 \cos^2\theta \sin\theta r^2 \\
&- \frac{1}{2}\eta^2 g^2 \alpha_3 \beta_1 \beta_2 \cos^2\theta \sin\theta r^2 - \frac{1}{2}\eta^2 g^2 \alpha_3 \beta_4 \beta_5 \cos^2\theta \sin\theta r^2 - \frac{1}{2}\eta^2 g^2 \alpha_3 \beta_7 \beta_8 \cos^2\theta \sin\theta r^2 \\
&+ \eta^2 g^2 \beta_7 \beta_9 \cos^2\theta \sin\theta r^2 - \frac{1}{2}\eta^2 g^2 \alpha_4 \beta_7 \beta_9 \cos^2\theta \sin\theta r^2 + \frac{\eta^2 g^2 \alpha_5 \beta_7 \beta_9 \cos^2\theta \sin\theta r^2}{2\sqrt{3}} \\
&- \frac{1}{2}\eta^2 g^2 \alpha_1 \beta_8 \beta_9 \cos^2\theta \sin\theta r^2 - \eta^2 g^2 \beta_1 \beta_3 \sin\theta r^2 - \frac{1}{2}\eta^2 g^2 \alpha_4 \beta_1 \beta_3 \sin\theta r^2 - \frac{1}{2}\sin 2\theta \ \partial_\theta \alpha_7 \\
&+ \frac{\eta^2 g^2 \alpha_5 \beta_1 \beta_3 \sin\theta r^2}{2\sqrt{3}} - \frac{1}{8}\eta^2 g^2 \alpha_1 \beta_2 \beta_3 \sin\theta r^2 - \frac{1}{8}\eta^2 g^2 \alpha_2 \beta_7^2 \sin 3\theta \ r^2 + \frac{1}{4}\alpha_1 \sin 2\theta \ \partial_\theta \alpha_8 \\
&- \frac{1}{8}\eta^2 g^2 \alpha_1 \beta_2 \beta_3 \sin 3\theta \ r^2 + \frac{3}{4}\alpha_3 \alpha_6 - \frac{1}{2}\alpha_4 \alpha_7 - \frac{1}{2}\sqrt{3}\alpha_5 \alpha_7 + \alpha_7 - \frac{3}{4}\alpha_1 \alpha_8 \\
&- \frac{1}{4}\alpha_3 \alpha_6 \cos 2\theta \ + \frac{1}{4}\alpha_1 \alpha_8 \cos 2\theta \ - \frac{1}{4}\alpha_2 \alpha_6^2 \sin\theta - \frac{1}{4}\alpha_2 \alpha_8^2 \sin\theta - \alpha_2 \alpha_7^2 \cos^2\theta \sin\theta \\
&- \frac{3}{4}\alpha_1 \alpha_6 \alpha_7 \cos^2\theta \sin\theta - \frac{3}{4}\alpha_3 \alpha_7 \alpha_8 \cos^2\theta \sin\theta + \frac{3}{4}\alpha_4 \alpha_6 \alpha_8 \sin\theta - \frac{1}{4}\sqrt{3}\alpha_5 \alpha_6 \alpha_8 \sin\theta \\
&+ \frac{3}{2}\alpha_6 \alpha_8 \sin\theta + \frac{1}{2}\alpha_8 \sin 2\theta \ \partial_\theta \alpha_1 - \cos\theta \partial_\theta \alpha_2 - \frac{1}{2}\alpha_6 \sin 2\theta \ \partial_\theta \alpha_3 + \frac{1}{2}\alpha_7 \sin 2\theta \ \partial_\theta \alpha_4 \\
&+ \frac{1}{2}\sqrt{3}\alpha_7 \sin 2\theta \ \partial_\theta \alpha_5 - \frac{1}{4}\alpha_3 \sin 2\theta \ \partial_\theta \alpha_6 + \frac{1}{4}\alpha_4 \sin 2\theta \ \partial_\theta \alpha_7 + \frac{1}{4}\sqrt{3}\alpha_5 \sin 2\theta \ \partial_\theta \alpha_7 = 0
\end{aligned}
\tag{B.13}
$$

$$
\begin{aligned}
&r^2 \sin\theta\cos\theta\partial_r^2\alpha_3 + \sin\theta\cos\theta\partial_\theta^2\alpha_3 - \frac{1}{8}\eta^2 g^2\alpha_3\beta_2^2 \sin 2\theta\ r^2 - \frac{1}{4}\eta^2 g^2\alpha_3\beta_3^2 \sin 2\theta\ r^2 \\
&- \frac{1}{8}\eta^2 g^2\alpha_3\beta_5^2 \sin 2\theta\ r^2 - \frac{1}{4}\eta^2 g^2\alpha_3\beta_6^2 \sin 2\theta\ r^2 - \frac{1}{4}\eta^2 g^2\alpha_3\beta_8^2 \sin 2\theta\ r^2 - \frac{1}{2}\alpha_2\alpha_6\cos\theta \\
&- \frac{1}{8}\eta^2 g^2\alpha_3\beta_9^2 \sin 2\theta\ r^2 - \frac{1}{4}\eta^2 g^2\alpha_2\beta_1\beta_2 \sin 2\theta\ r^2 - \frac{1}{4}\eta^2 g^2\alpha_1\beta_1\beta_3 \sin 2\theta\ r^2 - \frac{3}{4}\alpha_1\alpha_7\cos\theta \\
&+ \frac{1}{4}\eta^2 g^2\alpha_4\beta_2\beta_3 \sin 2\theta\ r^2 + \frac{\eta^2 g^2\alpha_5\beta_2\beta_3 \sin 2\theta\ r^2}{4\sqrt{3}} - \frac{1}{4}\eta^2 g^2\alpha_2\beta_4\beta_5 \sin 2\theta\ r^2 + \frac{1}{2}\alpha_4\alpha_8\cos\theta \\
&- \frac{1}{4}\eta^2 g^2\alpha_2\beta_7\beta_8 \sin 2\theta\ r^2 - \frac{1}{8}\eta^2 g^2\alpha_1\beta_7\beta_9 \sin 2\theta\ r^2 + \eta^2 g^2\beta_8\beta_9 \sin 2\theta\ r^2 - \frac{1}{2}\sqrt{3}\alpha_5\alpha_8\cos\theta \\
&+ \frac{1}{4}\eta^2 g^2\alpha_4\beta_8\beta_9 \sin 2\theta\ r^2 + \frac{\eta^2 g^2\alpha_5\beta_8\beta_9 \sin 2\theta\ r^2}{4\sqrt{3}} - \frac{1}{16}\eta^2 g^2\alpha_3\beta_2^2 \sin(4\theta) r^2 + 2\alpha_8\cos\theta \\
&- \frac{1}{16}\eta^2 g^2\alpha_3\beta_5^2 \sin(4\theta) r^2 - \frac{1}{16}\eta^2 g^2\alpha_3\beta_9^2 \sin(4\theta) r^2 - \frac{1}{16}\eta^2 g^2\alpha_1\beta_7\beta_9 \sin(4\theta) r^2 \\
&+ \frac{1}{4}\alpha_1\alpha_7\cos 3\theta\ - \frac{1}{8}\alpha_3\alpha_6^2 \sin 2\theta\ - \frac{1}{16}\alpha_3\alpha_7^2 \sin 2\theta\ - \frac{1}{2}\alpha_3\alpha_8^2 \sin 2\theta\ + \frac{3}{8}\alpha_4\alpha_6\alpha_7 \sin 2\theta \\
&+ \frac{1}{8}\sqrt{3}\alpha_5\alpha_6\alpha_7 \sin 2\theta\ + \frac{3}{8}\alpha_1\alpha_6\alpha_8 \sin 2\theta\ - \frac{3}{8}\alpha_2\alpha_7\alpha_8 \sin 2\theta\ - \frac{1}{32}\alpha_3\alpha_7^2 \sin(4\theta) \\
&+ \frac{1}{4}\alpha_7 \sin\theta\partial_\theta\alpha_1 + \frac{1}{4}\alpha_7 \sin 3\theta\ \partial_\theta\alpha_1 + \alpha_6 \sin\theta\partial_\theta\alpha_2 + \frac{1}{2}\cos 2\theta\ \partial_\theta\alpha_3 - \frac{3}{2}\partial_\theta\alpha_3 \\
&- \alpha_8 \sin\theta\partial_\theta\alpha_4 + \sqrt{3}\alpha_8 \sin\theta\partial_\theta\alpha_5 + \frac{1}{2}\alpha_2 \sin\theta\partial_\theta\alpha_6 + \frac{1}{8}\alpha_1 \sin\theta\partial_\theta\alpha_7 \\
&+ \frac{1}{8}\alpha_1 \sin 3\theta\ \partial_\theta\alpha_7 - \frac{1}{2}\alpha_4 \sin\theta\partial_\theta\alpha_8 + \frac{1}{2}\sqrt{3}\alpha_5 \sin\theta\partial_\theta\alpha_8 - 2\sin\theta\partial_\theta\alpha_8 = 0
\end{aligned}
\tag{B.14}
$$

$$
\begin{aligned}
&r^2\sin\theta\partial_r^2\alpha_4+\sin\theta\partial_\theta^2\alpha_4-\frac{1}{2}\eta^2g^2\alpha_4\beta_1^2\sin\theta r^2-\frac{\eta^2g^2\alpha_5\beta_1^2\sin\theta r^2}{2\sqrt{3}}-\frac{1}{4}\eta^2g^2\beta_2^2\sin\theta r^2\\
&-\frac{1}{8}\eta^2g^2\alpha_4\beta_2^2\sin\theta r^2+\frac{\eta^2g^2\alpha_5\beta_2^2\sin\theta r^2}{8\sqrt{3}}-\eta^2g^2\beta_4^2\sin\theta r^2-\frac{1}{2}\eta^2g^2\alpha_4\beta_4^2\sin\theta r^2\\
&-\frac{\eta^2g^2\alpha_5\beta_4^2\sin\theta r^2}{2\sqrt{3}}-\frac{1}{8}\eta^2g^2\alpha_4\beta_5^2\sin\theta r^2+\frac{\eta^2g^2\alpha_5\beta_5^2\sin\theta r^2}{8\sqrt{3}}+\frac{1}{4}\eta^2g^2\beta_7^2\sin\theta r^2\\
&-\frac{1}{8}\eta^2g^2\alpha_4\beta_7^2\sin\theta r^2-\frac{\eta^2g^2\alpha_5\beta_7^2\sin\theta r^2}{8\sqrt{3}}-2\eta^2g^2\beta_8^2\sin\theta r^2-\frac{1}{2}\eta^2g^2\alpha_4\beta_8^2\sin\theta r^2\\
&+\frac{\eta^2g^2\alpha_5\beta_8^2\sin\theta r^2}{2\sqrt{3}}-\frac{1}{2}\eta^2g^2\alpha_2\beta_1\beta_3\sin\theta r^2+\frac{1}{8}\eta^2g^2\alpha_3\beta_2\beta_3\sin\theta r^2-\frac{1}{8}\eta^2g^2\alpha_2\beta_7\beta_9\sin\theta r^2\\
&+\frac{1}{8}\eta^2g^2\alpha_3\beta_8\beta_9\sin\theta r^2-\frac{1}{4}\eta^2g^2\beta_2^2\sin 3\theta\ r^2-\frac{1}{8}\eta^2g^2\alpha_4\beta_2^2\sin 3\theta\ r^2+\frac{\eta^2g^2\alpha_5\beta_2^2\sin 3\theta\ r^2}{8\sqrt{3}}\\
&-\frac{1}{8}\eta^2g^2\alpha_4\beta_5^2\sin 3\theta\ r^2+\frac{\eta^2g^2\alpha_5\beta_5^2\sin 3\theta\ r^2}{8\sqrt{3}}+\frac{1}{4}\eta^2g^2\beta_7^2\sin 3\theta\ r^2-\frac{1}{8}\eta^2g^2\alpha_4\beta_7^2\sin 3\theta\ r^2\\
&-\frac{\eta^2g^2\alpha_5\beta_7^2\sin 3\theta\ r^2}{8\sqrt{3}}+\frac{1}{8}\eta^2g^2\alpha_3\beta_2\beta_3\sin 3\theta\ r^2-\frac{1}{8}\eta^2g^2\alpha_2\beta_7\beta_9\sin 3\theta\ r^2-\alpha_4\alpha_6^2\sin\theta\\
&+\frac{1}{8}\eta^2g^2\alpha_3\beta_8\beta_9\sin 3\theta\ r^2+\frac{3}{2}\alpha_1\alpha_6+\frac{1}{2}\alpha_2\alpha_7-\frac{3}{4}\alpha_3\alpha_8-\frac{1}{2}\alpha_1\alpha_6\cos 2\theta\ +\frac{1}{4}\alpha_3\alpha_8\cos 2\theta\\
&-\alpha_6^2\sin\theta-\frac{1}{16}\alpha_4\alpha_7^2\sin\theta-\frac{1}{16}\sqrt{3}\alpha_5\alpha_7^2\sin\theta+\frac{1}{8}\alpha_7^2\sin\theta-\frac{1}{4}\alpha_4\alpha_8^2\sin\theta+\frac{1}{4}\sqrt{3}\alpha_5\alpha_8^2\sin\theta\\
&-\alpha_8^2\sin\theta+\frac{3}{16}\alpha_3\alpha_6\alpha_7\sin\theta+\frac{3}{4}\alpha_2\alpha_6\alpha_8\sin\theta-\frac{1}{16}\alpha_4\alpha_7^2\sin 3\theta\ -\frac{1}{16}\sqrt{3}\alpha_5\alpha_7^2\sin 3\theta\\
&+\frac{1}{8}\alpha_7^2\sin 3\theta\ +\frac{3}{16}\alpha_3\alpha_6\alpha_7\sin 3\theta\ -\alpha_6\sin 2\theta\ \partial_\theta\alpha_1-\frac{1}{2}\alpha_7\sin 2\theta\ \partial_\theta\alpha_2+\frac{1}{2}\alpha_8\sin 2\theta\ \partial_\theta\alpha_3\\
&-\cos\theta\partial_\theta\alpha_4-\frac{1}{2}\alpha_1\sin 2\theta\ \partial_\theta\alpha_6-\frac{1}{4}\alpha_2\sin 2\theta\ \partial_\theta\alpha_7+\frac{1}{4}\alpha_3\sin 2\theta\ \partial_\theta\alpha_8=0
\end{aligned}
\tag{B.15}
$$

$$
\begin{aligned}
&r^2\sin\theta\partial_r^2\alpha_5+\sin\theta\partial_\theta^2\alpha_5-\frac{\eta^2g^2\alpha_4\beta_1^2\sin\theta r^2}{2\sqrt{3}}-\frac{1}{6}\eta^2g^2\alpha_5\beta_1^2\sin\theta r^2-\frac{1}{24}\eta^2g^2\alpha_5\beta_2^2\sin\theta r^2\\
&+\frac{2\eta^2g^2\beta_3^2\sin\theta r^2}{\sqrt{3}}-\frac{2}{3}\eta^2g^2\alpha_5\beta_3^2\sin\theta r^2-\frac{\eta^2g^2\beta_4^2\sin\theta r^2}{\sqrt{3}}-\frac{\eta^2g^2\alpha_4\beta_4^2\sin\theta r^2}{2\sqrt{3}}\\
&-\frac{1}{6}\eta^2g^2\alpha_5\beta_4^2\sin\theta r^2-\frac{1}{24}\eta^2g^2\alpha_5\beta_5^2\sin\theta r^2-\frac{2}{3}\eta^2g^2\alpha_5\beta_6^2\sin\theta r^2+\frac{\eta^2g^2\beta_7^2\sin\theta r^2}{4\sqrt{3}}\\
&-\frac{1}{24}\eta^2g^2\alpha_5\beta_7^2\sin\theta r^2+\frac{2\eta^2g^2\beta_8^2\sin\theta r^2}{\sqrt{3}}+\frac{\eta^2g^2\alpha_4\beta_8^2\sin\theta r^2}{2\sqrt{3}}-\frac{1}{6}\eta^2g^2\alpha_5\beta_8^2\sin\theta r^2\\
&-\frac{1}{6}\eta^2g^2\alpha_5\beta_9^2\sin\theta r^2+\frac{\eta^2g^2\beta_2^2\cos^2\theta\sin\theta r^2}{\sqrt{3}}+\frac{\eta^2g^2\alpha_4\beta_2^2\cos^2\theta\sin\theta r^2}{2\sqrt{3}}-\frac{1}{4}\sqrt{3}\alpha_3\alpha_8\cos2\theta\\
&+\frac{\eta^2g^2\alpha_4\beta_5^2\cos^2\theta\sin\theta r^2}{2\sqrt{3}}-\frac{\eta^2g^2\alpha_4\beta_7^2\cos^2\theta\sin\theta r^2}{2\sqrt{3}}-\frac{\eta^2g^2\alpha_1\beta_1\beta_2\cos^2\theta\sin\theta r^2}{\sqrt{3}}\\
&+\frac{\eta^2g^2\alpha_3\beta_2\beta_3\cos^2\theta\sin\theta r^2}{2\sqrt{3}}-\frac{\eta^2g^2\alpha_1\beta_4\beta_5\cos^2\theta\sin\theta r^2}{\sqrt{3}}-\frac{\eta^2g^2\alpha_1\beta_7\beta_8\cos^2\theta\sin\theta r^2}{\sqrt{3}}\\
&+\frac{\eta^2g^2\alpha_2\beta_7\beta_9\cos^2\theta\sin\theta r^2}{2\sqrt{3}}+\frac{\eta^2g^2\alpha_2\beta_1\beta_3\sin\theta r^2}{2\sqrt{3}}+\frac{\eta^2g^2\alpha_3\beta_8\beta_9\sin\theta r^2}{8\sqrt{3}}\\
&-\frac{1}{24}\eta^2g^2\alpha_5\beta_2^2\sin3\theta\ r^2-\frac{1}{24}\eta^2g^2\alpha_5\beta_5^2\sin3\theta\ r^2+\frac{\eta^2g^2\beta_7^2\sin3\theta\ r^2}{4\sqrt{3}}+\frac{3}{4}\sqrt{3}\alpha_3\alpha_8\\
&-\frac{1}{24}\eta^2g^2\alpha_5\beta_7^2\sin3\theta\ r^2-\frac{1}{6}\eta^2g^2\alpha_5\beta_9^2\sin3\theta\ r^2+\frac{\eta^2g^2\alpha_3\beta_8\beta_9\sin3\theta\ r^2}{8\sqrt{3}}+\frac{1}{2}\sqrt{3}\alpha_2\alpha_7\\
&+\frac{1}{4}\sqrt{3}\alpha_4\alpha_8^2\sin\theta-\frac{3}{4}\alpha_5\alpha_8^2\sin\theta+\sqrt{3}\alpha_8^2\sin\theta-\frac{1}{4}\sqrt{3}\alpha_4\alpha_7^2\cos^2\theta\sin\theta-\frac{3}{4}\alpha_5\alpha_7^2\cos^2\theta\sin\theta\\
&+\frac{1}{2}\sqrt{3}\alpha_7^2\cos^2\theta\sin\theta+\frac{1}{4}\sqrt{3}\alpha_3\alpha_6\alpha_7\cos^2\theta\sin\theta-\frac{1}{4}\sqrt{3}\alpha_2\alpha_6\alpha_8\sin\theta\\
&-\frac{1}{4}\sqrt{3}\alpha_1\alpha_7\alpha_8\cos\theta\sin2\theta\ -\sqrt{3}\alpha_7\cos\theta\sin\theta\partial_\theta\alpha_2-\frac{1}{2}\sqrt{3}\alpha_8\sin2\theta\ \partial_\theta\alpha_3-\cos\theta\partial_\theta\alpha_5\\
&-\frac{1}{4}\sqrt{3}\alpha_2\sin2\theta\ \partial_\theta\alpha_7-\frac{1}{2}\sqrt{3}\alpha_3\cos\theta\sin\theta\partial_\theta\alpha_8=0
\end{aligned}
\tag{B.16}
$$

$$
\begin{aligned}
& r^2 \sin^2\theta \partial_r^2 \alpha_6 - \frac{1}{2}\eta^2 g^2 \alpha_6 \beta_1^2 \sin^2\theta r^2 - \frac{1}{2}\eta^2 g^2 \alpha_6 \beta_4^2 \sin^2\theta r^2 - \frac{1}{2}\eta^2 g^2 \alpha_6 \beta_8^2 \sin^2\theta r^2 \\
& - \frac{1}{2}\eta^2 g^2 \alpha_6 \beta_2^2 \cos^2\theta \sin^2\theta r^2 - \frac{1}{2}\eta^2 g^2 \alpha_6 \beta_5^2 \cos^2\theta \sin^2\theta r^2 - \frac{1}{2}\eta^2 g^2 \alpha_6 \beta_7^2 \cos^2\theta \sin^2\theta r^2 \\
& + \frac{1}{4}\eta^2 g^2 \alpha_8 \beta_1 \beta_3 r^2 - \frac{1}{16}\eta^2 g^2 \alpha_7 \beta_2 \beta_3 r^2 + \frac{1}{16}\eta^2 g^2 \alpha_8 \beta_7 \beta_9 r^2 - \frac{1}{16}\eta^2 g^2 \alpha_7 \beta_8 \beta_9 r^2 \\
& - \frac{1}{4}\eta^2 g^2 \alpha_8 \beta_1 \beta_3 \cos 2\theta \; r^2 + \frac{1}{16}\eta^2 g^2 \alpha_7 \beta_2 \beta_3 \cos(4\theta) r^2 - \frac{1}{16}\eta^2 g^2 \alpha_8 \beta_7 \beta_9 \cos(4\theta) r^2 \\
& + \frac{1}{16}\eta^2 g^2 \alpha_7 \beta_8 \beta_9 \cos(4\theta) r^2 + \frac{3}{4}\eta^2 g^2 \beta_1 \beta_2 \sin\theta r^2 + \frac{3}{4}\eta^2 g^2 \beta_4 \beta_5 \sin\theta r^2 - \frac{3}{4}\eta^2 g^2 \beta_7 \beta_8 \sin\theta r^2 \\
& - \frac{1}{4}\eta^2 g^2 \beta_1 \beta_2 \sin 3\theta \; r^2 - \frac{1}{4}\eta^2 g^2 \beta_4 \beta_5 \sin 3\theta \; r^2 + \frac{1}{4}\eta^2 g^2 \beta_7 \beta_8 \sin 3\theta \; r^2 - \alpha_4 \cos\theta \partial_\theta \alpha_1 \\
& - \frac{1}{4}\eta^2 g^2 \beta_2 \cos 3\theta \; \partial_\theta \beta_1 r^2 - \frac{1}{4}\eta^2 g^2 \beta_1 \cos\theta \partial_\theta \beta_2 r^2 + \frac{1}{4}\eta^2 g^2 \beta_1 \cos 3\theta \; \partial_\theta \beta_2 r^2 + \alpha_1 \alpha_4 \sin\theta \\
& + \frac{1}{4}\eta^2 g^2 \beta_5 \cos\theta \partial_\theta \beta_4 r^2 - \frac{1}{4}\eta^2 g^2 \beta_5 \cos 3\theta \; \partial_\theta \beta_4 r^2 - \frac{1}{4}\eta^2 g^2 \beta_4 \cos\theta \partial_\theta \beta_5 r^2 - \cos\theta \partial_\theta \alpha_1 \\
& + \frac{1}{4}\eta^2 g^2 \beta_4 \cos 3\theta \; \partial_\theta \beta_5 r^2 + \frac{1}{4}\eta^2 g^2 \beta_8 \cos\theta \partial_\theta \beta_7 r^2 - \frac{1}{4}\alpha_3^2 \alpha_6 \cos^2\theta + \frac{3}{4}\alpha_3 \alpha_4 \alpha_7 \cos^2\theta \\
& - \frac{1}{4}\eta^2 g^2 \beta_8 \cos 3\theta \; \partial_\theta \beta_7 r^2 - \frac{1}{4}\eta^2 g^2 \beta_7 \cos\theta \partial_\theta \beta_8 r^2 + \frac{1}{4}\eta^2 g^2 \beta_7 \cos 3\theta \; \partial_\theta \beta_8 r^2 - \alpha_1^2 \alpha_6 \cos^2\theta \\
& + \frac{1}{4}\sqrt{3}\alpha_3 \alpha_5 \alpha_7 \cos^2\theta + \frac{3}{4}\alpha_1 \alpha_3 \alpha_8 \cos^2\theta - \frac{1}{4}\alpha_2^2 \alpha_6 - \alpha_4^2 \alpha_6 - 2\alpha_4 \alpha_6 - \alpha_6 - \frac{3}{8}\alpha_1 \alpha_2 \alpha_7 \\
& + \frac{3}{2}\alpha_2 \alpha_8 + \frac{3}{4}\alpha_2 \alpha_4 \alpha_8 - \frac{1}{4}\sqrt{3}\alpha_2 \alpha_5 \alpha_8 - \frac{3}{8}\alpha_1 \alpha_2 \alpha_7 \cos 2\theta \; + \alpha_1 \sin\theta + \frac{1}{2}\alpha_2 \alpha_3 \sin\theta \\
& + \frac{1}{2}\alpha_3 \cos\theta \partial_\theta \alpha_2 - \frac{1}{2}\alpha_2 \cos\theta \partial_\theta \alpha_3 + \alpha_1 \cos\theta \partial_\theta \alpha_4 + \frac{1}{4}\eta^2 g^2 \beta_2 \cos\theta \partial_\theta \beta_1 r^2 = 0
\end{aligned}
\tag{B.17}
$$

$$
\begin{aligned}
&r^2\sin^2\theta\cos\theta\partial_r^2\alpha_7 - \frac{1}{4}\alpha_1^2\alpha_7\cos^3\theta - \frac{1}{2}\alpha_1\partial_\theta\alpha_3\cos^2\theta - \frac{1}{8}\eta^2g^2r^2\alpha_7\beta_1^2\cos\theta \\
&- \frac{1}{8}\eta^2g^2r^2\alpha_7\beta_3^2\cos\theta - \frac{1}{8}\eta^2g^2r^2\alpha_7\beta_4^2\cos\theta - \frac{1}{8}\eta^2g^2r^2\alpha_7\beta_6^2\cos\theta - \frac{1}{16}\eta^2g^2r^2\alpha_7\beta_7^2\cos\theta \\
&- \frac{1}{16}\eta^2g^2r^2\alpha_7\beta_9^2\cos\theta - \frac{3}{4}\alpha_1\alpha_2\alpha_6\cos\theta + \frac{3}{4}\alpha_3\alpha_4\alpha_6\cos\theta + \frac{1}{4}\sqrt{3}\alpha_3\alpha_5\alpha_6\cos\theta - \alpha_2^2\alpha_7\cos\theta \\
&- \frac{3}{16}\alpha_3^2\alpha_7\cos\theta - \frac{1}{4}\alpha_4^2\alpha_7\cos\theta - \frac{3}{4}\alpha_5^2\alpha_7\cos\theta + \alpha_4\alpha_7\cos\theta - \frac{1}{2}\sqrt{3}\alpha_4\alpha_5\alpha_7\cos\theta \\
&+ \sqrt{3}\alpha_5\alpha_7\cos\theta - \alpha_7\cos\theta + \frac{3}{2}\alpha_1\alpha_8\cos\theta - \frac{3}{4}\alpha_2\alpha_3\alpha_8\cos\theta - \frac{1}{2}\sqrt{3}\alpha_1\alpha_5\alpha_8\cos\theta \\
&- \frac{1}{8}\eta^2g^2r^2\alpha_8\beta_1\beta_2\cos\theta - \frac{1}{8}\eta^2g^2r^2\alpha_6\beta_2\beta_3\cos\theta - \frac{1}{8}\eta^2g^2r^2\alpha_8\beta_4\beta_5\cos\theta \\
&- \frac{1}{8}\eta^2g^2r^2\alpha_8\beta_7\beta_8\cos\theta - \frac{1}{8}\eta^2g^2r^2\alpha_6\beta_8\beta_9\cos\theta + \frac{1}{8}\eta^2g^2r^2\alpha_7\beta_1^2\cos 3\theta \\
&+ \frac{1}{8}\eta^2g^2r^2\alpha_7\beta_3^2\cos 3\theta + \frac{1}{8}\eta^2g^2r^2\alpha_7\beta_4^2\cos 3\theta + \frac{1}{8}\eta^2g^2r^2\alpha_7\beta_6^2\cos 3\theta + \frac{1}{8}\eta^2g^2r^2\beta_9\partial_\theta\beta_7 \\
&+ \frac{1}{32}\eta^2g^2r^2\alpha_7\beta_7^2\cos 3\theta + \frac{1}{32}\eta^2g^2r^2\alpha_7\beta_9^2\cos 3\theta - \frac{1}{16}\alpha_3^2\alpha_7\cos 3\theta - \frac{1}{8}\eta^2g^2r^2\beta_7\partial_\theta\beta_9 \\
&+ \frac{1}{8}\eta^2g^2r^2\alpha_8\beta_1\beta_2\cos 3\theta + \frac{1}{8}\eta^2g^2r^2\alpha_6\beta_2\beta_3\cos 3\theta + \frac{1}{8}\eta^2g^2r^2\alpha_8\beta_4\beta_5\cos 3\theta \\
&+ \frac{1}{8}\eta^2g^2r^2\alpha_8\beta_7\beta_8\cos 3\theta + \frac{1}{8}\eta^2g^2r^2\alpha_6\beta_8\beta_9\cos 3\theta + \frac{1}{32}\eta^2g^2r^2\alpha_7\beta_7^2\cos(5\theta) \\
&+ \frac{1}{32}\eta^2g^2r^2\alpha_7\beta_9^2\cos(5\theta) + \frac{1}{4}\alpha_3\partial_\theta\alpha_1 + \frac{1}{4}\alpha_3\cos 2\theta\ \partial_\theta\alpha_1 - \frac{1}{2}\alpha_4\partial_\theta\alpha_2 - \frac{1}{2}\sqrt{3}\alpha_5\partial_\theta\alpha_2 + \partial_\theta\alpha_2 \\
&+ \frac{1}{2}\alpha_2\partial_\theta\alpha_4 + \frac{1}{2}\sqrt{3}\alpha_2\partial_\theta\alpha_5 + \frac{1}{2}\eta^2g^2r^2\beta_3\partial_\theta\beta_1 - \frac{1}{2}\eta^2g^2r^2\beta_3\cos 2\theta\ \partial_\theta\beta_1 - \frac{1}{2}\eta^2g^2r^2\beta_1\partial_\theta\beta_3 \\
&+ \frac{1}{2}\eta^2g^2r^2\beta_1\cos 2\theta\ \partial_\theta\beta_3 - \frac{1}{8}\eta^2g^2r^2\beta_9\cos(4\theta)\partial_\theta\beta_7 + \frac{1}{8}\eta^2g^2r^2\beta_7\cos(4\theta)\partial_\theta\beta_9 = 0
\end{aligned}
\tag{B.18}
$$

$$
\begin{aligned}
&r^2\sin^2\theta\partial_r^2\alpha_8 - \frac{1}{2}\eta^2g^2\alpha_8\beta_3^2\sin^2\theta r^2 - \frac{1}{2}\eta^2g^2\alpha_8\beta_6^2\sin^2\theta r^2 - \frac{1}{2}\eta^2g^2\alpha_8\beta_8^2\sin^2\theta r^2 \\
&- \frac{1}{2}\eta^2g^2\alpha_8\beta_2^2\cos^2\theta\sin^2\theta r^2 - \frac{1}{2}\eta^2g^2\alpha_8\beta_5^2\cos^2\theta\sin^2\theta r^2 - \frac{1}{2}\eta^2g^2\alpha_8\beta_9^2\cos^2\theta\sin^2\theta r^2 \\
&- \frac{1}{16}\eta^2g^2\alpha_7\beta_1\beta_2 r^2 + \frac{1}{4}\eta^2g^2\alpha_6\beta_1\beta_3 r^2 - \frac{1}{16}\eta^2g^2\alpha_7\beta_4\beta_5 r^2 - \frac{1}{16}\eta^2g^2\alpha_7\beta_7\beta_8 r^2 \\
&+ \frac{1}{16}\eta^2g^2\alpha_6\beta_7\beta_9 r^2 - \frac{1}{4}\eta^2g^2\alpha_6\beta_1\beta_3\cos 2\theta\ r^2 + \frac{1}{16}\eta^2g^2\alpha_7\beta_1\beta_2\cos(4\theta)r^2 \\
&+ \frac{1}{16}\eta^2g^2\alpha_7\beta_4\beta_5\cos(4\theta)r^2 + \frac{1}{16}\eta^2g^2\alpha_7\beta_7\beta_8\cos(4\theta)r^2 - \frac{1}{16}\eta^2g^2\alpha_6\beta_7\beta_9\cos(4\theta)r^2 \\
&- \frac{3}{4}\eta^2g^2\beta_2\beta_3\sin\theta r^2 + \frac{3}{4}\eta^2g^2\beta_8\beta_9\sin\theta r^2 + \frac{1}{4}\eta^2g^2\beta_2\beta_3\sin 3\theta\ r^2 - \frac{1}{4}\eta^2g^2\beta_8\beta_9\sin 3\theta\ r^2 \\
&+ \frac{1}{4}\eta^2g^2\beta_3\cos\theta\partial_\theta\beta_2 r^2 - \frac{1}{4}\eta^2g^2\beta_3\cos 3\theta\ \partial_\theta\beta_2 r^2 - \frac{1}{4}\eta^2g^2\beta_2\cos\theta\partial_\theta\beta_3 r^2 \\
&+ \frac{1}{4}\eta^2g^2\beta_2\cos 3\theta\ \partial_\theta\beta_3 r^2 + \frac{1}{4}\eta^2g^2\beta_9\cos\theta\partial_\theta\beta_8 r^2 - \frac{1}{4}\eta^2g^2\beta_9\cos 3\theta\ \partial_\theta\beta_8 r^2 \\
&- \frac{1}{4}\eta^2g^2\beta_8\cos\theta\partial_\theta\beta_9 r^2 + \frac{1}{4}\eta^2g^2\beta_8\cos 3\theta\ \partial_\theta\beta_9 r^2 - \frac{3}{4}\alpha_2\alpha_3\alpha_7\cos^2\theta - \frac{1}{4}\alpha_1^2\alpha_8\cos^2\theta \\
&- \alpha_3^2\alpha_8\cos^2\theta + \frac{3}{2}\alpha_2\alpha_6 + \frac{3}{8}\alpha_1\alpha_3\alpha_6 + \frac{3}{4}\alpha_2\alpha_4\alpha_6 - \frac{1}{4}\sqrt{3}\alpha_2\alpha_5\alpha_6 + \frac{3}{4}\alpha_1\alpha_7 - \frac{1}{4}\sqrt{3}\alpha_1\alpha_5\alpha_7 \\
&- \frac{1}{4}\alpha_2^2\alpha_8 - \frac{1}{4}\alpha_4^2\alpha_8 - \frac{3}{4}\alpha_5^2\alpha_8 - 2\alpha_4\alpha_8 + \frac{1}{2}\sqrt{3}\alpha_4\alpha_5\alpha_8 + 2\sqrt{3}\alpha_5\alpha_8 - 4\alpha_8 \\
&+ \frac{3}{4}\alpha_1\alpha_7\cos 2\theta\ - \frac{1}{4}\sqrt{3}\alpha_1\alpha_5\alpha_7\cos 2\theta\ - \frac{1}{2}\alpha_1\alpha_2\sin\theta - 2\alpha_3\sin\theta - \frac{1}{2}\alpha_3\alpha_4\sin\theta \\
&+ \frac{1}{2}\sqrt{3}\alpha_3\alpha_5\sin\theta + \frac{1}{2}\alpha_2\cos\theta\partial_\theta\alpha_1 - \frac{1}{2}\alpha_1\cos\theta\partial_\theta\alpha_2 + \frac{1}{2}\alpha_4\cos\theta\partial_\theta\alpha_3 \\
&- \frac{1}{2}\sqrt{3}\alpha_5\cos\theta\partial_\theta\alpha_3 + 2\cos\theta\partial_\theta\alpha_3 - \frac{1}{2}\alpha_3\cos\theta\partial_\theta\alpha_4 + \frac{1}{2}\sqrt{3}\alpha_3\cos\theta\partial_\theta\alpha_5 \\
&+ \frac{3}{8}\alpha_1\alpha_3\alpha_6\cos 2\theta\ = 0
\end{aligned}
\tag{B.19}
$$

$$
\begin{aligned}
&r^2\sin^2\theta\partial_r^2\beta_1+\sin^2\theta\partial_\theta^2\beta_1-\frac{1}{4}\cos^2\theta\alpha_1\alpha_3\beta_3-\frac{\cos^2\theta\alpha_1\alpha_5\beta_2}{2\sqrt{3}}-\frac{1}{4}\cos^2\theta\alpha_1^2\beta_1\\
&+\frac{1}{2}\cos^2\theta\alpha_1\beta_2-\frac{1}{4}\cos^2\theta\alpha_2\alpha_3\beta_2-\frac{1}{4}\alpha_2\alpha_4\beta_3+\frac{\alpha_2\alpha_5\beta_3}{4\sqrt{3}}-\frac{1}{4}\alpha_2^2\beta_1-\frac{1}{2}\alpha_2\beta_3-\frac{\alpha_4\alpha_5\beta_1}{2\sqrt{3}}\\
&-\frac{1}{4}\alpha_4^2\beta_1-\frac{1}{12}\alpha_5^2\beta_1-\frac{1}{4}\sin\theta\sin2\theta\ \partial_\theta\alpha_6\beta_2+\frac{1}{4}\sin^2\theta\alpha_6\alpha_8\beta_3-\frac{1}{4}\sin^2\theta\alpha_6^2\beta_1\\
&-\frac{1}{2}\sin\theta\sin2\theta\ \alpha_6\partial_\theta\beta_2+\frac{5}{8}\sin\theta\alpha_6\beta_2-\frac{3}{8}\sin3\theta\ \alpha_6\beta_2-\frac{1}{4}\sin\theta\sin2\theta\ \partial_\theta\alpha_7\beta_3\\
&-\frac{1}{16}\sin^2 2\theta\ \alpha_7\alpha_8\beta_2-\frac{1}{4}\sin^2\theta\cos^2\theta\alpha_7^2\beta_1-\frac{1}{2}\sin\theta\sin2\theta\ \alpha_7\partial_\theta\beta_3-\frac{1}{2}\sin\theta\cos2\theta\ \alpha_7\beta_3\\
&+2r\sin^2\theta\partial_r\beta_1+\frac{1}{2}\sin2\theta\ \partial_\theta\beta_1-2\eta^2\lambda r^2\sin^2\theta\cos^2\theta\beta_1\beta_2^2-2\eta^2\lambda r^2\sin^2\theta\beta_1\beta_3^2\\
&-\eta^2\lambda r^2\sin^2\theta\beta_1\beta_4^2-\eta^2\lambda r^2\sin^2\theta\cos^2\theta\beta_1\beta_7^2-2\eta^2\lambda r^2\sin^2\theta\beta_1^3+2\eta^2\lambda r^2\sin^2\theta\beta_1\\
&-\frac{1}{8}\eta^2\lambda r^2\beta_2\beta_4\beta_5+\frac{1}{8}\eta^2\lambda r^2\cos(4\theta)\beta_2\beta_4\beta_5-\frac{1}{8}\eta^2\lambda r^2\beta_2\beta_7\beta_8\\
&+\frac{1}{8}\eta^2\lambda r^2\cos(4\theta)\beta_2\beta_7\beta_8-\frac{1}{8}\eta^2\lambda r^2\beta_3\beta_7\beta_9+\frac{1}{8}\eta^2\lambda r^2\cos(4\theta)\beta_3\beta_7\beta_9=0
\end{aligned}
\tag{B.20}
$$

$$
\begin{aligned}
&r^2\sin^2\theta\cos\theta\partial_r^2\beta_2 - \frac{1}{4}\cos 3\theta\ \partial_\theta^2\beta_2 + \frac{1}{4}\cos\theta\partial_\theta^2\beta_2 - \frac{1}{4}\eta^2\lambda r^2\cos\theta\beta_2^3 + \frac{1}{8}\eta^2\lambda r^2\cos 3\theta\ \beta_2^3 \\
&+ \frac{1}{8}\eta^2\lambda r^2\cos(5\theta)\beta_2^3 + \frac{1}{2}\eta^2\lambda r^2\cos\theta\beta_2 - \frac{3}{16}\alpha_1^2\cos\theta\beta_2 - \frac{3}{16}\alpha_3^2\cos\theta\beta_2 - \frac{1}{4}\alpha_4^2\cos\theta\beta_2 \\
&- \frac{1}{12}\alpha_5^2\cos\theta\beta_2 - \frac{1}{16}\alpha_6^2\cos\theta\beta_2 - \frac{1}{16}\alpha_8^2\cos\theta\beta_2 - \frac{1}{2}\eta^2\lambda r^2\beta_1^2\cos\theta\beta_2 - \frac{1}{2}\eta^2\lambda r^2\beta_3^2\cos\theta\beta_2 \\
&- \frac{1}{8}\eta^2\lambda r^2\beta_5^2\cos\theta\beta_2 - \frac{1}{4}\eta^2\lambda r^2\beta_8^2\cos\theta\beta_2 - \alpha_4\cos\theta\beta_2 + \frac{\alpha_4\alpha_5\cos\theta\beta_2}{2\sqrt{3}} + \frac{\alpha_5\cos\theta\beta_2}{\sqrt{3}} \\
&- \frac{3}{2}\cos\theta\beta_2 - \frac{1}{2}\eta^2\lambda r^2\cos 3\theta\ \beta_2 - \frac{1}{16}\alpha_1^2\cos 3\theta\ \beta_2 - \frac{1}{16}\alpha_3^2\cos 3\theta\ \beta_2 + \frac{1}{16}\alpha_6^2\cos 3\theta\ \beta_2 \\
&+ \frac{1}{16}\alpha_8^2\cos 3\theta\ \beta_2 + \frac{1}{2}\eta^2\lambda r^2\beta_1^2\cos 3\theta\ \beta_2 + \frac{1}{2}\eta^2\lambda r^2\beta_3^2\cos 3\theta\ \beta_2 + \frac{1}{16}\eta^2\lambda r^2\beta_5^2\cos 3\theta\ \beta_2 \\
&+ \frac{1}{4}\eta^2\lambda r^2\beta_8^2\cos 3\theta\ \beta_2 + \frac{1}{2}\cos 3\theta\ \beta_2 + \frac{1}{16}\eta^2\lambda r^2\beta_5^2\cos(5\theta)\beta_2 + \frac{1}{2}\alpha_1\beta_1\cos\theta \\
&- \frac{1}{4}\alpha_2\alpha_3\beta_1\cos\theta - \frac{\alpha_1\alpha_5\beta_1\cos\theta}{2\sqrt{3}} - \frac{1}{16}\alpha_7\alpha_8\beta_1\cos\theta - \frac{1}{4}\alpha_1\alpha_2\beta_3\cos\theta + \frac{1}{4}\alpha_3\alpha_4\beta_3\cos\theta \\
&+ \frac{\alpha_3\alpha_5\beta_3\cos\theta}{4\sqrt{3}} - \frac{1}{16}\alpha_6\alpha_7\beta_3\cos\theta - \frac{1}{4}\eta^2\lambda r^2\beta_1\beta_4\beta_5\cos\theta - \frac{1}{4}\eta^2\lambda r^2\beta_1\beta_7\beta_8\cos\theta \\
&- \frac{1}{4}\eta^2\lambda r^2\beta_3\beta_8\beta_9\cos\theta + \frac{1}{16}\alpha_7\alpha_8\beta_1\cos 3\theta\ + \frac{1}{16}\alpha_6\alpha_7\beta_3\cos 3\theta\ + \frac{1}{4}\eta^2\lambda r^2\beta_1\beta_4\beta_5\cos 3\theta \\
&+ \frac{1}{4}\eta^2\lambda r^2\beta_1\beta_7\beta_8\cos 3\theta\ + \frac{1}{4}\eta^2\lambda r^2\beta_3\beta_8\beta_9\cos 3\theta\ + \frac{1}{4}\alpha_6\beta_1\sin 2\theta\ - \frac{1}{4}\alpha_8\beta_3\sin 2\theta \\
&+ \frac{1}{4}\beta_1\partial_\theta\alpha_6 - \frac{1}{4}\beta_1\cos 2\theta\ \partial_\theta\alpha_6 - \frac{1}{4}\beta_3\partial_\theta\alpha_8 + \frac{1}{4}\beta_3\cos 2\theta\ \partial_\theta\alpha_8 + \frac{1}{2}\alpha_6\partial_\theta\beta_1 \\
&- \frac{1}{2}\alpha_6\cos 2\theta\ \partial_\theta\beta_1 - \frac{5}{4}\sin\theta\partial_\theta\beta_2 + \frac{3}{4}\sin 3\theta\ \partial_\theta\beta_2 - \frac{1}{2}\alpha_8\partial_\theta\beta_3 \\
&+ \frac{1}{2}\alpha_8\cos 2\theta\ \partial_\theta\beta_3 + \frac{1}{2}r\cos\theta\partial_r\beta_2 - \frac{1}{2}r\cos 3\theta\ \partial_r\beta_2 = 0
\end{aligned}
\tag{B.21}
$$

$$
\begin{aligned}
&r^2\sin^2\theta\partial_r^2\beta_3+\sin^2\theta\partial_\theta^2\beta_3-\frac{1}{4}\cos^2\theta\alpha_1\alpha_2\beta_2-\frac{1}{4}\cos^2\theta\alpha_1\alpha_3\beta_1-\frac{1}{4}\alpha_2\alpha_4\beta_1+\frac{\alpha_2\alpha_5\beta_1}{4\sqrt{3}}\\
&-\frac{1}{2}\alpha_2\beta_1-\frac{1}{4}\alpha_2^2\beta_3+\frac{1}{4}\cos^2\theta\alpha_3\alpha_4\beta_2+\frac{\cos^2\theta\alpha_3\alpha_5\beta_2}{4\sqrt{3}}-\frac{1}{4}\cos^2\theta\alpha_3^2\beta_3-\frac{1}{3}\alpha_5^2\beta_3+\frac{2\alpha_5\beta_3}{\sqrt{3}}\\
&-\frac{1}{4}\sin^2\theta\cos^2\theta\alpha_6\alpha_7\beta_2+\frac{1}{4}\sin^2\theta\alpha_6\alpha_8\beta_1+\frac{1}{4}\sin\theta\sin2\theta\ \partial_\theta\alpha_7\beta_1+\frac{1}{2}\sin\theta\sin2\theta\ \alpha_7\partial_\theta\beta_1\\
&+\frac{1}{2}\sin\theta\cos2\theta\ \alpha_7\beta_1-\frac{1}{16}\sin^2 2\theta\ \alpha_7^2\beta_3+\frac{1}{4}\sin\theta\sin2\theta\ \partial_\theta\alpha_8\beta_2+\sin^2\theta\cos\theta\alpha_8\partial_\theta\beta_2\\
&-\frac{1}{4}\sin\theta\alpha_8\beta_2+\frac{3}{4}\sin\theta\cos2\theta\ \alpha_8\beta_2-\frac{1}{4}\sin^2\theta\alpha_8^2\beta_3-2\eta^2\lambda r^2\sin^2\theta\beta_1^2\beta_3\\
&-\eta^2\lambda r^2\sin^2\theta\cos^2\theta\beta_1\beta_7\beta_9-2\eta^2\lambda r^2\sin^2\theta\cos^2\theta\beta_2^2\beta_3-\eta^2\lambda r^2\sin^2\theta\cos^2\theta\beta_2\beta_8\beta_9\\
&+2r\sin^2\theta\partial_r\beta_3+\sin\theta\cos\theta\partial_\theta\beta_3-\eta^2\lambda r^2\sin^2\theta\beta_3\beta_6^2-\eta^2\lambda r^2\sin^2\theta\cos^2\theta\beta_3\beta_9^2\\
&-2\eta^2\lambda r^2\sin^2\theta\beta_3^3+2\eta^2\lambda r^2\sin^2\theta\beta_3-\beta_3=0
\end{aligned}
\tag{B.22}
$$

$$
\begin{aligned}
&r^2\sin^2\theta\partial_r^2\beta_4+\sin^2\theta\partial_\theta^2\beta_4-\frac{\cos^2\theta\alpha_1\alpha_5\beta_5}{2\sqrt{3}}-\frac{1}{4}\cos^2\theta\alpha_1^2\beta_4-\frac{1}{2}\cos^2\theta\alpha_1\beta_5\\
&-\frac{1}{4}\cos^2\theta\alpha_2\alpha_3\beta_5-\frac{1}{4}\alpha_2^2\beta_4-\frac{\alpha_4\alpha_5\beta_4}{2\sqrt{3}}-\frac{1}{4}\alpha_4^2\beta_4-\alpha_4\beta_4-\frac{1}{12}\alpha_5^2\beta_4-\frac{\alpha_5\beta_4}{\sqrt{3}}\\
&-\frac{1}{4}\sin\theta\sin2\theta\ \partial_\theta\alpha_6\beta_5-\frac{1}{4}\sin^2\theta\alpha_6^2\beta_4-\frac{1}{2}\sin\theta\sin2\theta\ \alpha_6\partial_\theta\beta_5+\frac{1}{4}\sin\theta\alpha_6\beta_5\\
&-\frac{3}{4}\sin\theta\cos2\theta\ \alpha_6\beta_5-\frac{1}{4}\sin^2\theta\cos^2\theta\alpha_7\alpha_8\beta_5-\frac{1}{16}\sin^2 2\theta\ \alpha_7^2\beta_4\\
&-\eta^2\lambda r^2\sin^2\theta\cos^2\theta\beta_1\beta_2\beta_5-\eta^2\lambda r^2\sin^2\theta\beta_1^2\beta_4+2r\sin^2\theta\partial_r\beta_4+\sin\theta\cos\theta\partial_\theta\beta_4\\
&-\frac{1}{2}\eta^2\lambda r^2\sin^2 2\theta\ \beta_4\beta_5^2-2\eta^2\lambda r^2\sin^2\theta\beta_4\beta_6^2-\frac{1}{4}\eta^2\lambda r^2\sin^2 2\theta\ \beta_4\beta_7^2-2\eta^2\lambda r^2\sin^2\theta\beta_4^3\\
&+2\eta^2\lambda r^2\sin^2\theta\beta_4-\beta_4-\eta^2\lambda r^2\sin^2\theta\cos^2\theta\beta_5\beta_7\beta_8=0
\end{aligned}
\tag{B.23}
$$

$$
\begin{aligned}
&r^2\sin^2\theta\cos\theta\partial_r^2\beta_5+\sin^2\theta\cos\theta\partial_\theta^2\beta_5-\frac{1}{4}\eta^2\lambda r^2\cos\theta\beta_5^3+\frac{1}{8}\eta^2\lambda r^2\cos 3\theta\ \beta_5^3\\
&+\frac{1}{8}\eta^2\lambda r^2\cos(5\theta)\beta_5^3-\frac{1}{4}\alpha_1^2\cos^3\theta\beta_5+\frac{1}{2}\eta^2\lambda r^2\cos\theta\beta_5-\frac{3}{16}\alpha_3^2\cos\theta\beta_5-\frac{1}{4}\alpha_4^2\cos\theta\beta_5\\
&-\frac{1}{12}\alpha_5^2\cos\theta\beta_5-\frac{1}{16}\alpha_6^2\cos\theta\beta_5-\frac{1}{16}\alpha_8^2\cos\theta\beta_5-\frac{1}{8}\eta^2\lambda r^2\beta_2^2\cos\theta\beta_5-\frac{1}{2}\eta^2\lambda r^2\beta_4^2\cos\theta\beta_5\\
&-\frac{1}{2}\eta^2\lambda r^2\beta_6^2\cos\theta\beta_5-\frac{1}{4}\eta^2\lambda r^2\beta_8^2\cos\theta\beta_5+\frac{\alpha_4\alpha_5\cos\theta\beta_5}{2\sqrt{3}}-\frac{1}{2}\cos\theta\beta_5-\frac{1}{2}\eta^2\lambda r^2\cos 3\theta\ \beta_5\\
&-\frac{1}{16}\alpha_3^2\cos 3\theta\ \beta_5+\frac{1}{16}\alpha_6^2\cos 3\theta\ \beta_5+\frac{1}{16}\alpha_8^2\cos 3\theta\ \beta_5+\frac{1}{16}\eta^2\lambda r^2\beta_2^2\cos 3\theta\ \beta_5\\
&+\frac{1}{2}\eta^2\lambda r^2\beta_4^2\cos 3\theta\ \beta_5+\frac{1}{2}\eta^2\lambda r^2\beta_6^2\cos 3\theta\ \beta_5+\frac{1}{4}\eta^2\lambda r^2\beta_8^2\cos 3\theta\ \beta_5+\frac{1}{2}\cos 3\theta\ \beta_5\\
&+\frac{1}{16}\eta^2\lambda r^2\beta_2^2\cos(5\theta)\beta_5-\frac{1}{2}\alpha_1\beta_4\cos\theta-\frac{1}{4}\alpha_2\alpha_3\beta_4\cos\theta-\frac{\alpha_1\alpha_5\beta_4\cos\theta}{2\sqrt{3}}-\frac{1}{16}\alpha_7\alpha_8\beta_4\cos\theta\\
&-\frac{1}{4}\eta^2\lambda r^2\beta_1\beta_2\beta_4\cos\theta-\frac{1}{4}\eta^2\lambda r^2\beta_4\beta_7\beta_8\cos\theta+\frac{1}{16}\alpha_7\alpha_8\beta_4\cos 3\theta\ +\frac{1}{4}\eta^2\lambda r^2\beta_1\beta_2\beta_4\cos 3\theta\\
&+\frac{1}{4}\eta^2\lambda r^2\beta_4\beta_7\beta_8\cos 3\theta\ +\frac{1}{4}\alpha_6\beta_4\sin 2\theta\ +\frac{1}{4}\beta_4\partial_\theta\alpha_6-\frac{1}{4}\beta_4\cos 2\theta\ \partial_\theta\alpha_6+\frac{1}{2}\alpha_6\partial_\theta\beta_4\\
&-\frac{1}{2}\alpha_6\cos 2\theta\ \partial_\theta\beta_4-\frac{5}{4}\sin\theta\partial_\theta\beta_5+\frac{3}{4}\sin 3\theta\ \partial_\theta\beta_5+\frac{1}{2}r\cos\theta\partial_r\beta_5-\frac{1}{2}r\cos 3\theta\ \partial_r\beta_5=0
\end{aligned}
\tag{B.24}
$$

$$
\begin{aligned}
&r^2\sin^2\theta\partial_r^2\beta_6+\sin^2\theta\partial_\theta^2\beta_6-\frac{1}{4}\alpha_2^2\beta_6-\frac{1}{4}\cos^2\theta\alpha_3^2\beta_6-\frac{1}{3}\alpha_5^2\beta_6-\frac{1}{32}\alpha_7^2\beta_6+\frac{1}{32}\cos(4\theta)\alpha_7^2\beta_6\\
&-\frac{1}{4}\sin^2\theta\alpha_8^2\beta_6-\eta^2\lambda r^2\sin^2\theta\beta_3^2\beta_6-2\eta^2\lambda r^2\sin^2\theta\beta_4^2\beta_6-2\eta^2\lambda r^2\sin^2\theta\cos^2\theta\beta_5^2\beta_6\\
&+2r\sin^2\theta\partial_r\beta_6+\sin\theta\cos\theta\partial_\theta\beta_6-\eta^2\lambda r^2\sin^2\theta\cos^2\theta\beta_6\beta_9^2-2\eta^2\lambda r^2\sin^2\theta\beta_6^3\\
&+2\eta^2\lambda r^2\sin^2\theta\beta_6=0
\end{aligned}
\tag{B.25}
$$

$$
\begin{aligned}
&r^2 \sin^2\theta \cos\theta \partial_r^2 \beta_7 + \frac{1}{2}\sin\theta \sin 2\theta\ \partial_\theta^2 \beta_7 - \frac{1}{4}\cos^3\theta \alpha_1\alpha_3\beta_9 - \frac{\cos\theta \alpha_1\alpha_5\beta_8}{2\sqrt{3}} - \frac{1}{4}\cos^3\theta \alpha_1^2\beta_7 \\
&+ \frac{3}{2}\cos\theta\alpha_1\beta_8 - \frac{1}{4}\cos\theta\alpha_2\alpha_3\beta_8 - \frac{1}{4}\cos\theta\alpha_2\alpha_4\beta_9 + \frac{\cos\theta\alpha_2\alpha_5\beta_9}{4\sqrt{3}} - \frac{1}{4}\cos\theta\alpha_2^2\beta_7 \\
&+ \frac{1}{2}\cos\theta\alpha_2\beta_9 - \frac{\cos\theta\alpha_4\alpha_5\beta_7}{2\sqrt{3}} - \frac{1}{4}\cos\theta\alpha_4^2\beta_7 + \cos\theta\alpha_4\beta_7 - \frac{1}{12}\cos\theta\alpha_5^2\beta_7 + \frac{\cos\theta\alpha_5\beta_7}{\sqrt{3}} \\
&- \frac{1}{2}\sin^2\theta\partial_\theta\alpha_6\beta_8 + \frac{1}{8}\sin\theta\sin 2\theta\ \alpha_6\alpha_8\beta_9 - \frac{1}{4}\sin^2\theta\cos\theta\alpha_6^2\beta_7 - \sin^2\theta\alpha_6\partial_\theta\beta_8 \\
&- \frac{1}{2}\sin\theta\cos\theta\alpha_6\beta_8 - \frac{1}{8}\sin^2\theta\partial_\theta\alpha_7\beta_9 - \frac{1}{8}\sin\theta\sin 3\theta\ \partial_\theta\alpha_7\beta_9 - \frac{1}{4}\sin^2\theta\cos\theta\alpha_7\alpha_8\beta_8 \\
&- \frac{1}{32}\cos\theta\alpha_7^2\beta_7 + \frac{1}{32}\cos(4\theta)\cos\theta\alpha_7^2\beta_7 - \frac{1}{4}\sin^2 2\theta\ \alpha_7\partial_\theta\beta_9 + \sin\theta\cos\theta\alpha_7\beta_9 \\
&- \frac{1}{2}\sin 3\theta\ \cos\theta\alpha_7\beta_9 - \frac{1}{2}\eta^2\lambda r^2\sin\theta\sin 2\theta\ \beta_1\beta_2\beta_8 - \frac{1}{2}\eta^2\lambda r^2\sin\theta\sin 2\theta\ \beta_1\beta_3\beta_9 \\
&- \eta^2\lambda r^2\sin^2\theta\cos\theta\beta_1^2\beta_7 - \frac{1}{2}\eta^2\lambda r^2\sin\theta\sin 2\theta\ \beta_4\beta_5\beta_8 - \eta^2\lambda r^2\sin^2\theta\cos\theta\beta_4^2\beta_7 \\
&- \frac{1}{2}\sin\theta\partial_\theta\beta_7 + r\sin\theta\sin 2\theta\ \partial_r\beta_7 + \frac{3}{2}\sin\theta\cos 2\theta\ \partial_\theta\beta_7 - 2\eta^2\lambda r^2\sin^2\theta\cos\theta\beta_7\beta_8^2 \\
&- 2\eta^2\lambda r^2\sin^2\theta\cos^3\theta\beta_7\beta_9^2 - 2\eta^2\lambda r^2\sin^2\theta\cos^3\theta\beta_7^3 + 2\eta^2\lambda r^2\sin^2\theta\cos\theta\beta_7 \\
&- 2\cos\theta\beta_7 + \cos 2\theta\ \cos\theta\beta_7 = 0
\end{aligned}
\tag{B.26}
$$

$$
\begin{aligned}
&r^2\sin^2\theta\partial_r^2\beta_8+\sin^2\theta\partial_\theta^2\beta_8-\frac{1}{4}\cos^2\theta\alpha_1\alpha_2\beta_9-\frac{\cos^2\theta\alpha_1\alpha_5\beta_7}{2\sqrt{3}}+\frac{3}{2}\cos^2\theta\alpha_1\beta_7\\
&-\frac{1}{4}\cos^2\theta\alpha_1^2\beta_8-\frac{1}{4}\cos^2\theta\alpha_2\alpha_3\beta_7+\frac{1}{4}\cos^2\theta\alpha_3\alpha_4\beta_9+\frac{\cos^2\theta\alpha_3\alpha_5\beta_9}{4\sqrt{3}}-\frac{1}{4}\cos^2\theta\alpha_3^2\beta_8\\
&+\cos^2\theta\alpha_3\beta_9+\frac{\alpha_4\alpha_5\beta_8}{2\sqrt{3}}-\frac{1}{4}\alpha_4^2\beta_8-2\alpha_4\beta_8-\frac{1}{12}\alpha_5^2\beta_8+\frac{2\alpha_5\beta_8}{\sqrt{3}}+\frac{1}{4}\sin\theta\sin2\theta\ \partial_\theta\alpha_6\beta_7\\
&-\frac{1}{4}\sin^2\theta\cos^2\theta\alpha_6\alpha_7\beta_9+\frac{1}{2}\sin\theta\sin2\theta\ \alpha_6\partial_\theta\beta_7-\frac{1}{4}\sin\theta\alpha_6\beta_7+\frac{3}{4}\sin\theta\cos2\theta\ \alpha_6\beta_7\\
&-\frac{1}{4}\sin^2\theta\alpha_6^2\beta_8-\frac{1}{4}\sin^2\theta\cos^2\theta\alpha_7\alpha_8\beta_7-\frac{1}{4}\sin\theta\sin2\theta\ \partial_\theta\alpha_8\beta_9-\frac{1}{4}\sin^2\theta\alpha_8^2\beta_8\\
&-\frac{1}{2}\sin\theta\sin2\theta\ \alpha_8\partial_\theta\beta_9+\frac{1}{4}\sin\theta\alpha_8\beta_9-\frac{3}{4}\sin\theta\cos2\theta\ \alpha_8\beta_9-\frac{1}{4}\eta^2\lambda r^2\sin^2\theta\beta_1\beta_2\beta_7\\
&-\frac{1}{4}\eta^2\lambda r^2\sin\theta\sin3\theta\ \beta_1\beta_2\beta_7-\frac{1}{4}\eta^2\lambda r^2\sin^2\theta\beta_2\beta_3\beta_9-\frac{1}{4}\eta^2\lambda r^2\sin\theta\sin3\theta\ \beta_2\beta_3\beta_9\\
&-\frac{1}{4}\eta^2\lambda r^2\sin^2 2\theta\ \beta_2^2\beta_8-\frac{1}{4}\eta^2\lambda r^2\sin^2\theta\beta_4\beta_5\beta_7-\frac{1}{4}\eta^2\lambda r^2\sin\theta\sin3\theta\ \beta_4\beta_5\beta_7\\
&-\frac{1}{4}\eta^2\lambda r^2\sin^2 2\theta\ \beta_5^2\beta_8-\frac{1}{2}\eta^2\lambda r^2\sin^2 2\theta\ \beta_7^2\beta_8+2r\sin^2\theta\partial_r\beta_8+\frac{1}{2}\sin2\theta\ \partial_\theta\beta_8\\
&-\frac{1}{2}\eta^2\lambda r^2\sin^2 2\theta\ \beta_8\beta_9^2-2\eta^2\lambda r^2\sin^2\theta\beta_8^3+2\eta^2\lambda r^2\sin^2\theta\beta_8-4\beta_8=0
\end{aligned}
\tag{B.27}
$$

$$
\begin{aligned}
&r^2\sin^2\theta\cos\theta\partial_r^2\beta_9+\frac{1}{4}\cos\theta\partial_\theta^2\beta_9-\frac{1}{4}\cos 3\theta\ \partial_\theta^2\beta_9-\frac{1}{4}\eta^2\lambda r^2\cos\theta\beta_9^3\\
&+\frac{1}{8}\eta^2\lambda r^2\cos 3\theta\ \beta_9^3+\frac{1}{8}\eta^2\lambda r^2\cos(5\theta)\beta_9^3+\frac{1}{2}\eta^2\lambda r^2\cos\theta\beta_9-\frac{1}{4}\alpha_2^2\cos\theta\beta_9-\frac{3}{16}\alpha_3^2\cos\theta\beta_9\\
&-\frac{1}{3}\alpha_5^2\cos\theta\beta_9-\frac{1}{32}\alpha_7^2\cos\theta\beta_9-\frac{1}{16}\alpha_8^2\cos\theta\beta_9-\frac{1}{4}\eta^2\lambda r^2\beta_3^2\cos\theta\beta_9-\frac{1}{4}\eta^2\lambda r^2\beta_6^2\cos\theta\beta_9\\
&-\frac{1}{4}\eta^2\lambda r^2\beta_7^2\cos\theta\beta_9-\frac{1}{2}\eta^2\lambda r^2\beta_8^2\cos\theta\beta_9-\frac{1}{2}\cos\theta\beta_9-\frac{1}{2}\eta^2\lambda r^2\cos 3\theta\ \beta_9-\frac{1}{16}\alpha_3^2\cos 3\theta\ \beta_9\\
&+\frac{1}{64}\alpha_7^2\cos 3\theta\ \beta_9+\frac{1}{16}\alpha_8^2\cos 3\theta\ \beta_9+\frac{1}{4}\eta^2\lambda r^2\beta_3^2\cos 3\theta\ \beta_9+\frac{1}{4}\eta^2\lambda r^2\beta_6^2\cos 3\theta\ \beta_9\\
&+\frac{1}{8}\eta^2\lambda r^2\beta_7^2\cos 3\theta\ \beta_9+\frac{1}{2}\eta^2\lambda r^2\beta_8^2\cos 3\theta\ \beta_9+\frac{1}{2}\cos 3\theta\ \beta_9+\frac{1}{64}\alpha_7^2\cos(5\theta)\beta_9\\
&+\frac{1}{8}\eta^2\lambda r^2\beta_7^2\cos(5\theta)\beta_9+\frac{1}{4}\alpha_6\alpha_8\beta_7\cos\theta\sin^2\theta-\frac{1}{4}\alpha_6\alpha_7\beta_8\cos\theta\sin^2\theta+\frac{1}{2}\alpha_2\beta_7\cos\theta\\
&-\frac{3}{16}\alpha_1\alpha_3\beta_7\cos\theta-\frac{1}{4}\alpha_2\alpha_4\beta_7\cos\theta+\frac{\alpha_2\alpha_5\beta_7\cos\theta}{4\sqrt{3}}-\frac{1}{4}\eta^2\lambda r^2\beta_1\beta_3\beta_7\cos\theta\\
&+\alpha_3\beta_8\cos\theta+\frac{1}{4}\alpha_3\alpha_4\beta_8\cos\theta+\frac{\alpha_3\alpha_5\beta_8\cos\theta}{4\sqrt{3}}-\frac{1}{4}\eta^2\lambda r^2\beta_2\beta_3\beta_8\cos\theta-\frac{1}{16}\alpha_1\alpha_3\beta_7\cos 3\theta\\
&+\frac{1}{4}\eta^2\lambda r^2\beta_1\beta_3\beta_7\cos 3\theta\ +\frac{1}{4}\eta^2\lambda r^2\beta_2\beta_3\beta_8\cos 3\theta\ -\frac{1}{4}\alpha_7\beta_7\sin 2\theta\ +\frac{1}{4}\alpha_8\beta_8\sin 2\theta\\
&+\frac{1}{4}\alpha_7\beta_7\sin(4\theta)+\frac{1}{16}\beta_7\partial_\theta\alpha_7-\frac{1}{16}\beta_7\cos(4\theta)\partial_\theta\alpha_7+\frac{1}{4}\beta_8\partial_\theta\alpha_8-\frac{1}{4}\beta_8\cos 2\theta\ \partial_\theta\alpha_8\\
&+\frac{1}{8}\alpha_7\partial_\theta\beta_7-\frac{1}{8}\alpha_7\cos(4\theta)\partial_\theta\beta_7+\frac{1}{2}\alpha_8\partial_\theta\beta_8-\frac{1}{2}\alpha_8\cos 2\theta\ \partial_\theta\beta_8-\frac{5}{4}\sin\theta\partial_\theta\beta_9\\
&+\frac{3}{4}\sin 3\theta\ \partial_\theta\beta_9+\frac{1}{2}r\cos\theta\partial_r\beta_9-\frac{1}{2}r\cos 3\theta\ \partial_r\beta_9-\frac{1}{4}\alpha_1\alpha_2\beta_8\cos\theta=0
\end{aligned}
\tag{B.28}
$$

APPENDIX C

Energy-barrier structure functions

In this appendix we will give a detailed derivation of the structure functions $\Gamma_{A_\phi,i}$ and $\Gamma_{A_\theta,i}$, for $i = 1, \ldots, 8$, as well as $\Gamma_{\Phi,j}(\omega)$, for $j = 1, \ldots, 18$, which we introduced in Chapter 7.

The gauge-field structure functions can be obtained by requiring, that the *Ansatz* (7.6) is asymptotically ($r \to \infty$) equivalent to the pure gauge (7.1). Explicitly, this involves replacing the profile functions $\alpha_i(r, \theta)$ in Eq. (7.6) with their asymptotic values and solving the resulting matrix equations

$$\begin{aligned}
-\partial_\phi U(\omega)\, U^{-1}(\omega) &= \Gamma_{A_\phi,1}(\omega) T_\phi - 2\sin\theta(1+\sin^2\theta)\,\Gamma_{A_\phi,2}(\omega) T_\rho + \Gamma_{A_\phi,3}(\omega) V_\phi \\
&+ 2\sin\theta\,\Gamma_{A_\phi,4}(\omega) V_\rho + \Gamma_{A_\phi,5}(\omega) U_\phi - 2\sin^2\theta\,\Gamma_{A_\phi,6}(\omega) U_\rho \\
&- \sin^2\theta(1+2\sin^2\theta)\,\Gamma_{A_\phi,7}(\omega)\frac{\lambda_3}{2i} + \sqrt{3}\sin^2\theta\,\Gamma_{A_\phi,8}(\omega)\frac{\lambda_8}{2i}, \qquad \text{(C.1a)} \\
-\partial_\theta U(\omega)\, U^{-1}(\omega) &= 2\,\Gamma_{A_\theta,1}(\omega) T_\phi + \Gamma_{A_\theta,2}(\omega) T_\rho + 2\,\Gamma_{A_\theta,3}(\omega) V_\phi \\
&+ \Gamma_{A_\theta,4}(\omega) V_\rho - 2\sin\theta\,\Gamma_{A_\theta,5}(\omega) U_\phi + \Gamma_{A_\theta,6}(\omega) U_\rho \\
&+ \Gamma_{A_\theta,7}(\omega)\frac{\lambda_3}{2i} + \Gamma_{A_\theta,8}(\omega)\frac{\lambda_8}{2i}, \qquad \text{(C.1b)}
\end{aligned}$$

with the short-hand notation $\omega = \{\psi, \mu, \alpha, \theta, \phi\}$. The map U is given by Eq. (2.8) with parametrization (2.49) and the matrices T_ϕ, T_ρ, V_ϕ, V_ρ, U_ϕ and U_ρ by Eq. (5.19). The resulting structure functions are too long to be given here explicitly.

To derive the Higgs structure functions we proceed in a similar manner. We require, that the fields of the *Ansatz* (7.11) take the asymptotic form (7.3) towards infinity. Inserting the

asymptotic values of profile functions $\beta_j(r,\theta)$, we obtain

$$U(\omega)\begin{pmatrix}1\\0\\0\end{pmatrix} = \Big[\Big(\Gamma_{\Phi,1}(\omega)+i\Gamma_{\Phi,2}(\omega)\Big)\lambda_3 - \sin\theta\Big(\Gamma_{\Phi,3}(\omega)+i\Gamma_{\Phi,4}(\omega)\Big)2iT_\rho - \sin\theta\Big(\Gamma_{\Phi,5}(\omega)+i\Gamma_{\Phi,6}(\omega)\Big)2iV_\rho\Big]\begin{pmatrix}1\\0\\0\end{pmatrix}, \tag{C.2a}$$

$$U(\omega)\begin{pmatrix}0\\0\\-1\end{pmatrix} = \Big[-\sin\theta\Big(\Gamma_{\Phi,7}(\omega)+i\Gamma_{\Phi,8}(\omega)\Big)\lambda_3 - \Big(\Gamma_{\Phi,9}(\omega)+i\Gamma_{\Phi,10}(\omega)\Big)2iT_\rho + \Big(\Gamma_{\Phi,11}(\omega)+i\Gamma_{\Phi,12}(\omega)\Big)2iV_\rho\Big]\begin{pmatrix}1\\0\\0\end{pmatrix}, \tag{C.2b}$$

$$U(\omega)\begin{pmatrix}0\\1\\0\end{pmatrix} = \Big[-\sin\theta\Big(\Gamma_{\Phi,13}(\omega)+i\Gamma_{\Phi,14}(\omega)\Big)\lambda_3 + \sin^2\theta\Big(\Gamma_{\Phi,15}(\omega)+i\Gamma_{\Phi,16}(\omega)\Big)2iT_\rho - \Big(\Gamma_{\Phi,17}(\omega)+i\Gamma_{\Phi,18}(\omega)\Big)2iV_\rho\Big]\begin{pmatrix}1\\0\\0\end{pmatrix}. \tag{C.2c}$$

Solving these equations yields the structure functions given below.

$$\begin{aligned}\Gamma_{\Phi,1}(\omega) =& 2\sin^2\mu\cos^2\mu\left(\sin^2\psi\left(\sin^2\alpha\cos\theta+\cos^2\alpha\right)+\cos^2\psi\right)+\cos^4\mu \\ &+\sin^4\mu\Big\{2\sin^2\psi\cos^2\psi\left(\sin^2\alpha\cos\theta+\cos^2\alpha\right)+\cos^4\psi \\ &+\sin^4\psi\left(\sin^4\alpha\cos^2\theta-\frac{1}{2}\sin^2\alpha\cos^2\alpha(-8\cos\theta+\cos 2\theta\ +3)+\cos^4\alpha\right)\Big\}\end{aligned} \tag{C.3}$$

$$\begin{aligned}\Gamma_{\Phi,2}(\omega) =& -2\sin\alpha\cos\alpha\sin^2\mu\sin^2\psi(\cos\theta-1) \\ &\times\Big\{\sin^2\mu\left(\sin^2\psi\left(\sin^2\alpha\cos\theta+\cos^2\alpha\right)+\cos^2\psi\right)+\cos^2\mu\Big\}\end{aligned} \tag{C.4}$$

$$\begin{aligned}\Gamma_{\Phi,3}(\omega) =& \frac{1}{-\sin\theta}\Big[-\sin\alpha\sin\mu\sin\psi\Big\{\sin\theta\Big(\sin^2\mu\left(\sin^2\psi\left(\sin^2\alpha\cos\theta+\cos^2\alpha\right)+\cos^2\psi\right)\\ &+\cos^2\mu\Big) - 2\sin\mu\cos\phi\cos\psi\sin^2\frac{\theta}{2} - \cos\mu\sin\phi(\cos\theta-1)\Big\}\Big]\end{aligned} \tag{C.5}$$

$$\begin{aligned}\Gamma_{\Phi,4}(\omega) =& \frac{1}{-\sin\theta}\Big[\sin\alpha\sin\mu\sin\psi(\cos\theta-1)\\ &\times\left(\sin\mu\left(\sin\alpha\cos\alpha\sin\mu\sin^2\psi\sin\theta+\sin\phi\cos\psi\right)+\cos\mu\cos\phi\right)\Big]\end{aligned} \tag{C.6}$$

$$\begin{aligned}\Gamma_{\Phi,5}(\omega) =& \frac{1}{-\sin\theta}\Big[-\sin\alpha\sin\mu\sin\psi\Big\{2\sin\mu\sin^2\frac{\theta}{2}\Big(\cos^2\mu\cos\phi\cos\psi\\ &-\sin\mu\cos\mu\sin\phi\Big(\sin^2\alpha\Big(\sin^2\psi\cos\theta+\cos^2\psi\Big)+\cos^2\alpha\Big)+\sin^2\mu\cos\psi\\ &\times\Big(\sin^2\psi\Big(\sin\alpha\cos\theta\sin(\alpha+\phi)+\cos\alpha\cos(\alpha+\phi)\Big)+\cos\phi\cos^2\psi\Big)\Big)\\ &-2\sin 2\alpha\ \sin^2\mu\cos\mu\cos\phi\sin^2\psi\sin^4\frac{\theta}{2}+\cos^3\mu\sin\phi(\cos\theta-1)+\sin\theta\Big\}\Big]\end{aligned} \tag{C.7}$$

$$\begin{aligned}\Gamma_{\Phi,6}(\omega) =& \frac{1}{-\sin\theta}\Big[-\sin\alpha\sin\mu\sin\psi\Big\{2\sin^2\mu\cos\mu\sin^2\frac{\theta}{2}\Big(-\sin 2\alpha\ \sin\phi\sin^2\psi\sin^2\frac{\theta}{2}\\ &+\cos\phi\left(\sin^2\alpha\left(\sin^2\psi\cos\theta+\cos^2\psi\right)+\cos^2\alpha\right)\Big)+2\sin^3\mu\cos\psi\sin^2\frac{\theta}{2}\\ &\times\Big(\sin^2\psi\Big(\cos\alpha\sin(\alpha+\phi)-\sin\alpha\cos\theta\cos(\alpha+\phi)\Big)+\sin\phi\cos^2\psi\Big)\\ &+2\sin\mu\cos^2\mu\sin\phi\cos\psi\sin^2\frac{\theta}{2}+\cos^3\mu(-\cos\phi)(\cos\theta-1)\Big\}\Big]\end{aligned} \tag{C.8}$$

$$\Gamma_{\Phi,7}(\omega) = \frac{1}{-\sin\theta}\Big[\sin\alpha\sin\mu\sin\psi\Big\{2\sin\mu\sin^2\frac{\theta}{2}\Big(-2\sin\alpha\cos\alpha\sin\mu\cos\mu\sin^2\psi\sin^2\frac{\theta}{2}$$
$$+\cos\psi\left(\sin^2\mu\left(\sin^2\psi\left(\sin^2\alpha\cos\theta+\cos^2\alpha\right)+\cos^2\psi\right)+\cos^2\mu\right)\Big) \tag{C.9}$$
$$-\cos\phi\sin\theta\Big\}\Big]$$

$$\Gamma_{\Phi,8}(\omega) = \frac{1}{-\sin\theta}\Big[\frac{1}{2}\sin\alpha\sin\mu\sin\psi\Big\{\sin\mu\sin^2\frac{\theta}{2}\Big(2\sin^2\alpha\sin 2\mu\ \left(\sin^2\psi\cos\theta+\cos^2\psi\right)$$
$$-4\sin\alpha\cos\alpha\sin^2\mu\sin^2\psi\cos\psi\cos\theta+\sin 2\alpha\ \sin^2\mu\sin\psi\sin 2\psi \tag{C.10}$$
$$+4\cos^2\alpha\sin\mu\cos\mu\Big)-2\cos^3\mu(\cos\theta-1)+2\sin\phi\sin\theta\Big\}\Big]$$

$$\Gamma_{\Phi,9}(\omega) = -\Big[-\cos^2\mu\cos\phi-\frac{1}{4}\sin^2\mu\Big\{\cos(2\alpha+\phi)+3\cos\phi$$
$$+2\sin\alpha\Big(4\sin\alpha\sin\mu\sin^2\psi\cos\psi\sin\theta\sin^2\frac{\theta}{2} \tag{C.11}$$
$$+\sin(\alpha+\phi)\left(2\sin^2\psi\cos\theta+\cos 2\psi\ \right)\Big)\Big\}\Big]$$

$$\Gamma_{\Phi,10}(\omega) = -\Big[\sin^2\mu\left(\sin^2\psi\Big(\cos\alpha\sin(\alpha+\phi)-\sin\alpha\cos\theta\cos(\alpha+\phi)\Big)+\sin\phi\cos^2\psi\right)$$
$$-2\sin^2\alpha\sin^2\mu\cos\mu\sin^2\psi\sin^2\left(\frac{\theta}{2}\right)\sin\theta+\cos^2\mu\sin\phi\Big] \tag{C.12}$$

$$\Gamma_{\Phi,11}(\omega) = 4\sin^2\alpha\sin^2\mu\sin^2\psi\sin^4\frac{\theta}{2}$$
$$\times\left(\cos\phi\left(\cos^2\mu-\sin^2\mu\cos^2\psi\right)+\sin 2\mu\ \sin\phi\cos\psi\right) \tag{C.13}$$

$$\Gamma_{\Phi,12}(\omega) = -4\sin^2\alpha\sin^2\mu\sin^2\psi\sin^4\frac{\theta}{2}$$
$$\times\left(\sin\phi\left(\sin^2\mu\cos^2\psi-\cos^2\mu\right)+\sin 2\mu\ \cos\phi\cos\psi\right) \tag{C.14}$$

$$\Gamma_{\Phi,13}(\omega) = \frac{1}{-\sin\theta}\Big[-\sin\alpha\sin\mu\sin\psi\Big\{\cos^2\mu\cos\phi\sin\theta + \sin\mu\Big(\sin\mu\sin\theta\Big(\cos\phi\cos^2\psi + \sin^2\psi\Big(\sin\alpha\cos\theta\sin(\alpha+\phi) + \cos\alpha\cos(\alpha+\phi)\Big)\Big) - \cos\psi(\cos\theta-1)\Big)\Big\}\Big] \tag{C.15}$$

$$\Gamma_{\Phi,14}(\omega) = \frac{1}{-\sin\theta}\Big[\sin\alpha\sin\mu\sin\psi\Big\{\cos^2\mu(-\sin\phi)\sin\theta - \cos\mu(\cos\theta-1) - \sin^2\mu\sin\theta\Big(\sin^2\psi\Big(\cos\alpha\sin(\alpha+\phi) - \sin\alpha\cos\theta\cos(\alpha+\phi)\Big) + \sin\phi\cos^2\psi\Big)\Big\}\Big] \tag{C.16}$$

$$\Gamma_{\Phi,15}(\omega) = \frac{1}{\sin^2\theta}\Big[\sin^2\alpha\sin^2\mu\cos\phi\sin^2\psi\sin^2\theta\Big] \tag{C.17}$$

$$\Gamma_{\Phi,16}(\omega) = \frac{1}{\sin^2\theta}\Big[\sin^2\alpha\sin^2\mu\sin\phi\sin^2\psi\sin^2\theta\Big] \tag{C.18}$$

$$\begin{aligned}\Gamma_{\Phi,17}(\omega) = -\Big[\sin^2\mu\Big\{&4\sin^2\alpha\sin\mu\cos^2\phi\sin^2\psi\cos\psi\sin^3\frac{\theta}{2}\cos\frac{\theta}{2} \\ &- \sin\alpha\sin\phi\sin^2\psi\left(2\sin\alpha\sin\mu\sin\phi\cos\psi\sin\theta\sin^2\frac{\theta}{2} - \cos\alpha\cos\theta + \cos\alpha\right) \\ &- \cos\phi\left(\sin^2\psi\left(\sin^2\alpha\cos\theta + \cos^2\alpha\right) + \cos^2\psi\right)\Big\} \\ &- 4\sin^2\alpha\sin^2\mu\cos\mu\sin\phi\cos\phi\sin^2\psi\sin^2\frac{\theta}{2}\sin\theta - \cos^2\mu\cos\phi\Big]\end{aligned} \tag{C.19}$$

$$\Gamma_{\Phi,18}(\omega) = -\Big[\sin^2\mu\Big\{-\sin^2\psi\Big(-\cos\phi\sin^2\frac{\theta}{2}\Big(4\sin^2\alpha\sin\mu\sin\phi\cos\psi\sin\theta+\sin 2\alpha\Big)$$

$$+\sin^2\alpha\sin\phi\cos\theta+\cos^2\alpha\sin\phi\Big)-\sin\phi\cos^2\psi\Big\} \tag{C.20}$$

$$+4\sin^2\alpha\sin^2\mu\cos\mu\cos 2\phi\ \ \sin^2\psi\sin^3\frac{\theta}{2}\cos\frac{\theta}{2}-\cos^2\mu\sin\phi\Big]$$

Bibliography

[1] A. A. Belavin, A. M. Polyakov, A. S. Schwartz, and Y. S. Tyupkin, "Pseudoparticle solutions of the Yang-Mills equations," *Phys. Lett. B* **59** (1975) 85–87.

[2] T. Schäfer and E. V. Shuryak, "Instantons in QCD," *Rev. Mod. Phys.* **70** (1998) 323–425.

[3] F. R. Klinkhamer and N. S. Manton, "A saddle point solution in the Weinberg-Salam theory," *Phys. Rev. D* **30** (1984) 2212–2220.

[4] F. R. Klinkhamer and C. Rupp, "A sphaleron for the non-Abelian anomaly," *Nucl. Phys. B* **709** (2005) 171–191, `arXiv:hep-th/0410195`.

[5] R. F. Dashen, B. Hasslacher, and A. Neveu, "Nonperturbative methods and extended-hadron models in field theory," *Phys. Rev. D* **10** (1974) 4138–4142.

[6] N. S. Manton, "Topology in the Weinberg-Salam theory," *Phys. Rev. D* **28** (1983) 2019–2026.

[7] S. L. Adler, "Axial-vector vertex in spinor electrodynamics," *Phys. Rev.* **177** (1969) 2426–2438.

[8] J. S. Bell and R. Jackiw, "A PCAC puzzle: $\pi_0 \to \gamma\gamma$ in the σ-model," *Il Nuovo Cimento A* **60** (1969) 47–61.

[9] F. R. Klinkhamer, "Construction of a new electroweak sphaleron," *Nucl. Phys. B* **410** (1993) 343–354, `arXiv:hep-ph/9306295`.

[10] E. Witten, "An SU(2) anomaly," *Phys. Lett. B* **117** (1982) 324–328.

[11] W. A. Bardeen, "Anomalous Ward identities in spinor field theories," *Phys. Rev.* **184** (1969) 1848–1859.

[12] F. R. Klinkhamer, "Z-string global gauge anomaly and Lorentz non-invariance," *Nucl. Phys. B* **535** (1998) 233–241.

[13] F. R. Klinkhamer, private communication, 2017.

[14] F. R. Klinkhamer and C. Rupp, "Sphalerons, spectral flow and anomalies," *J. Math. Phys.* **44** (2003) 3619–3639, `arXiv:hep-th/0304167`.

[15] Y. Brihaye, "On axially symmetric solutions in the electroweak theory," *Phys. Rev. D* **50** (1994) 4175–4182, `arXiv:hep-ph/9403392`.

[16] B. Kleihaus, J. Kunz, and M. Leißner, "Sphalerons, antisphalerons and vortex rings," *Phys. Lett. B* **663** (2008) 438–444.

[17] R. Ibadov, B. Kleihaus, J. Kunz, and M. Leissner, "Properties of charged rotating electroweak sphaleron-antisphaleron systems," *Phys. Rev. D* **82** (2010) 125037.

[18] T. Püttmann and A. Rigas, "Presentations of the first homotopy groups of the unitary groups," *Commentarii Mathematici Helvetici* **78** (2003) 648–662, `arXiv:math/0301192`.

[19] M. Haberichter, "Untersuchungen des SU(3) Sphalerons," Diplomarbeit, Universität Karlsruhe (TH), 2009.

[20] E. Cech, "Höherdimensionale Homotopiegruppen," in *Verhandlungen des Internationalen Mathematikerkongress*. Zürich, 1932.

[21] R. Bott, "The stable homotopy of the classical groups," in *Proceedings of the National Academy of Sciences of the United States of America*, vol. 43, pp. 933–935. 1957.

[22] J.-P. Serre, "Homologie singuliere des espaces fibres," *Annals of Mathematics* **54** (1951) 425–505.

[23] A. Abanov, "Homotopy groups used in physics." Lecture notes on topolocial terms in condensed matter physics (PHY 680), 2009.

[24] B. Eckmann, "Huritz-Radon matrices revisited: From effective solution of the Hurwitz matrix equations to Bott periodicity," in *The Hilton symposium 1993*, pp. 23–35. American Mathematical Society, 1994.

[25] B. Eckmann, "Hurwitz-Radon matrices and periodicity modulo 8," *Enseign. Math.* **35** (1989) 77–91.

[26] A. Fomenko, *Variational principles of topology. Multidimensional minimal surface theory*, vol. 42. Kluwer, Dordrecht, 1990.

[27] N. E. Steenrod, *The Topology of Fibre Bundles*. Princeton University Press, 1951.

[28] E. H. Spanier, *Algebraic Topology*. Mc-Graw-Hill, 1966.

[29] J. Boguta, "Can nuclear interactions be long ranged?," *Phys. Rev. Lett.* **50** (1983) 148–152.

[30] F. R. Klinkhamer and R. Laterveer, "The sphaleron at finite mixing angle," *Z. Phys. C* **53** (1992) 247–251.

[31] J. Kunz, B. Kleihaus, and Y. Brihaye, "Sphalerons at finite mixing angle," *Phys. Rev. D* **46** (1992) 3587–3600.

[32] M. Schuh, "Weitere Untersuchungen des SU(3) Sphalerons $\widehat{S}$," Diplomarbeit, Karlsruhe Institute of Technology, 2014.

[33] P. Nagel, "Energy and structure analysis of the SU(3) sphaleron," Diplomarbeit, Karlsruhe Institute of Technology, 2014.

[34] S. Kirkpatrick, C. D. Gelatt, and M. P. Vecchi, "Optimization by simulated annealing," *Science* **220** (1983) 671–680.

[35] N. Metropolis, A. W. Rosenbluth, M. N. Rosenbluth, A. H. Teller, and E. Teller, "Equation of state calculations by fast computing machines," *Journal of Chemical Physics* **21** (1953) 1087–1092.

[36] D. Kraft, "A software package for sequential quadratic programming," tech. rep., Institut für Dynamik der Flugsysteme, Oberpfaffenhofen, 1988.

[37] C. G. Broyden, "The convergence of a class of double-rank minimization algorithms," *Journal of the Institute of Mathematics and Its Applications* **6** (1970) 76–90.

[38] R. Fletcher, "A new approach to variable metric algorithms," *Computer Journal* **13** (1970) 317–322.

[39] D. Goldfarb, "A family of variable metric updates derived by variational means," *Mathematics of Computation* **24** (1970) 23–26.

[40] D. F. Shanno, "Conditioning of quasi-Newton methods for function minimization," *Mathematics of Computation* **24** (1970) 647–656.

[41] E. Jones, T. Oliphant, and P. P. et al., "SciPy: Open source scientific tools for Python," 2001–. `http://www.scipy.org`.

[42] W. Schiesser, *The Numerical Method of Lines: Integration of Partial Differential Equations*. Academic Press, 1991.

[43] J. Moré, "The Levenberg-Marquardt algorithm: implementation and theory," in *Numerical analysis*, pp. 105–116. Springer, 1978.

[44] C. D. T. Runge, "Über empirische Funktionen und die Interpolation zwischen äquidistanten Ordinaten," *Zeitschrift für Mathematik und Physik* **46** (1901) 224–243.

[45] Y. Brihaye, B. Kleihaus, and J. Kunz, "Sphalerons at finite mixing angle and singular gauges," *Phys. Rev. D* **47** (1993) 1664–1667.